

**An ATC-63 Study in Support of the
Proposed System Performance
Factors for AISI S110 Standard for
Seismic Design of Cold-Formed
Steel Structures: Special Bolted
Moment Frames**

RESEARCH REPORT RP08-8

OCTOBER 2008

Committee on Specifications
for the Design of Cold-Formed
Steel Structural Members



American Iron and Steel Institute

The material contained herein has been developed by researchers based on their research findings. The material has also been reviewed by the American Iron and Steel Institute Committee on Specifications for the Design of Cold-Formed Steel Structural Members. The Committee acknowledges and is grateful for the contributions of such researchers.

The material herein is for general information only. The information in it should not be used without first securing competent advice with respect to its suitability for any given application. The publication of the information is not intended as a representation or warranty on the part of the American Iron and Steel Institute, or of any other person named herein, that the information is suitable for any general or particular use or of freedom from infringement of any patent or patents. Anyone making use of the information assumes all liability arising from such use.



**STRUCTURAL SYSTEMS
RESEARCH PROJECT**

Report No.
SSRP-2008/10

**An ATC-63 Study in Support of the
Proposed System Performance Factors
for AISI S110 Standard for Seismic Design
of Cold-Formed Steel Structures:
Special Bolted Moment Frames**

by

Atsushi Sato

Chia-Ming Uang

Final Report to the American Iron and Steel Institute

December 2008

Department of Structural Engineering
University of California, San Diego
La Jolla, California 92093-0085

University of California, San Diego
Department of Structural Engineering
Structural Systems Research Project

Report No. SSRP-2008/10

**An ATC-63 Study in Support of the Proposed System
Performance Factors for AISI S110 Standard for
Seismic Design of Cold-Formed Steel Structures
Special Bolted Moment Frames**

by

Atsushi Sato

Assistant Professor, Kyoto University

Chia-Ming Uang

Professor of Structural Engineering

Final Report to the American Iron and Steel Institute

Department of Structural Engineering
University of California, San Diego
La Jolla, California 92093-0085

December 2008

ACKNOWLEDGEMENTS

Funding for this project was provided by the American Iron and Steel Institute. Design of the archetype frames was provided by Mr. Ken Wood. Messrs. Ken Wood (Chair), Victor Azzi, Roger Brokenbrough, and Clarkson Pinkham served on the Peer Review Panel for this project.

ABSTRACT

The objective of this study was to verify the adequacy of the proposed Seismic Performance Factors (SPFs) for the newly developed AISI S110 *Seismic Standard on Cold-Formed Steel–Special Bolted Moment Frame* (CFS-SBMF) in accordance with the ATC-63 Methodology, “*Qualification of Building Seismic Performance Factors.*” This type of one-story framing system is usually composed of cold-formed Hollow Structural Section (HSS) columns and double-channel beams connected by snug-tight high-strength bolts.

Following the ATC-63 Methodology, a total of 13 archetype designs representing two seismicities (high and low) and two gravity load levels (high and low), i.e., a total of 4 performance groups, were designed and analyzed. The archetype frames were designed based on ASCE 7-05 and AISI S110. Expecting inelastic action to occur in the bolted moment connections only, a nonlinear spring element was developed for the nonlinear static and dynamic analyses. Beam and column modeling allowed for yielding, but not buckling. Therefore, both upper bound and lower bound approaches were used to compute collapse margins.

The upper bound approach showed that all 13 individual archetype designs and 4 performance groups met the ATC-63 acceptance criteria by a large margin. By defining 6% story drift ratio as the collapse limit state, the lower bound approach also showed that all individual archetypes and 4 performance groups met the acceptance criteria. Therefore, it was concluded that the proposed Seismic Performance Factors ($R = 3.5$, $C_d = 3.5$, and $\Omega_o = 3$ but with an alternate procedure in AISI S110 permitted to explicitly calculate the seismic load effects with overstrength) were acceptable and would provide a satisfactory margin against collapse under the Maximum Considered Earthquake ground motions.

TABLE OF CONTENT

ACKNOWLEDGEMENTS.....	i
ABSTRACT.....	ii
TABLE OF CONTENT.....	iii
LIST OF TABLES.....	v
LIST OF FIGURES.....	vi
1. INTRODUCTION.....	1
1.1 Statement of Problem.....	1
1.2 Objective.....	1
2. STRUCTURAL SYSTEM INFORMATION.....	4
2.1 Quality Rating.....	4
2.2 Identification of SBMF Archetype Configuration.....	4
2.3 Archetype Structural Design.....	5
2.4 Development of Nonlinear Structural Archetype Model.....	5
3. Nonlinear Static Analyses.....	11
3.1 Introduction.....	11
3.2 Global Response.....	12
3.3 System Overstrength and Ductility Capacity.....	12
4. Nonlinear Dynamic Analyses.....	16
4.1 Incremental Dynamic Analysis.....	16
4.1.1 Ground Motion.....	16
4.1.2 Maximum Considered Earthquake.....	16
4.2 Global Response at Design Basis Earthquake.....	16
4.3 Incremental Dynamic Analysis.....	17
5. EVALUATION OF COLLAPSE MARGIN AND ACCEPTANCE CRITERIA.....	22
5.1 Median Collapse Intensity and Collapse Margin Ratio.....	22
5.2 Adjusted Collapse Margin Ratio.....	23
5.3 Evaluation of Collapse Margin and Acceptance Criteria.....	23
6. CONCLUSIONS.....	33
REFERENCES.....	34

APPENDIX A: Nonlinear Static Analysis Results.....	35
APPENDIX B: Global Response at DBE Level.....	40
APPENDIX C: Incremental Dynamic Analyses Results.....	67
APPENDIX D: Collapse Probability	107

LIST OF TABLES

Table 1.1 Seismic Performance Factors.....	2
Table 2.1 Archetype Structural Design Properties	7
Table 2.2 Archetype Structure Model Sizes	8
Table 2.3 Bolt Configurations.....	8
Table 3.1 Structural Properties	13
Table 4.1 Earthquake Event and PEER-NGA Database for the Far-Field Record Set.....	18
Table 4.2 Normalized Ground Motions for the Far-Field Record Set.....	19
Table 5.1 Summary of Collapse Results for Archetype Designs (Upper Bound)	25
Table 5.2 Summary of Collapse Results for Archetype Designs (Lower Bound).....	26
Table 5.3 Final Collapse Margins and Acceptance Criteria (Upper Bound).....	27
Table 5.4 Final Collapse Margins and Acceptance Criteria (Lower Bound, 6% Drift) ...	28
Table 5.5 Total System Collapse Uncertainty, β_{TOT}	29
Table 5.6 Acceptable Value of Adjusted Collapse Margin Ratio.....	29

LIST OF FIGURES

Figure 1.1 Typical CFS-SBMF.....	3
Figure 2.1 Archetype Analysis Model for SBMF.....	9
Figure 2.2 Sample Correlation of Bolted Moment Connection Response.....	10
Figure 3.1 Idealized Nonlinear Pushover Curve (FEMA 2008).....	14
Figure 3.2 General Response of SBMF (AISI 2007).....	14
Figure 3.3 Sample Nonlinear Static Analysis Results	15
Figure 4.1 Nonlinear Dynamic Analysis (GM1, Component 2, Design Basis Earthquake)	20
Figure 4.2 Sample Incremental Dynamic Analysis Results (Total 44 Ground Motion Records)	21
Figure 5.1 Story Drift Capacity from Full-Scale Testing (Hong and Uang 2004)	30
Figure 5.2 Sample IDA Results and Collapse Probability (Upper Bound)	31
Figure 5.3 Sample IDA Results and Collapse Probability (Lower Bound).....	32

1. INTRODUCTION

1.1 Statement of Problem

The American Iron and Steel Institute (AISI) recently released S110 (AISI 2007), which is a standard for seismic design of cold-formed steel structural systems. The first lateral load-resisting system introduced in this standard is termed the Special Bolted Moment Frame (SBMF). This type of framing system is intended to be used for free standing mezzanines (light storage), elevated office support platforms, equipment support platforms, and small buildings in all seismic areas. SBFM is usually composed of cold-formed Hollow Structural Section (HSS) columns and double-channel beams connected by snug-tight high-strength bolts (see Figure 1.1). Currently S110 limits the SBFM to one story with a height limit to 35ft.

The design provisions for the SBFM in S110 were based on the results of full-scale testing of 9 beam-column subassemblies (Hong et al. 2004) and the associated analytical studies. Testing showed that the bolted moment connection provided a reliable source of energy dissipation through bolt friction and bearing; beams and columns should be designed by the capacity design principles to remain elastic. A numerical model that can properly simulate the cyclic response of the moment connection was developed (Uang et al. 2008). With this numerical model, a seismic design procedure was proposed (Sato and Uang 2008), which forms the basis for the development of AISI S110, “*Standard for Seismic Design of Cold-Formed Steel Structural Systems–Special Bolted Moment Frames.*” For adoption by model codes, the proposed Seismic Performance Factors (SPFs) for the SBFM are listed in Table 1.1.

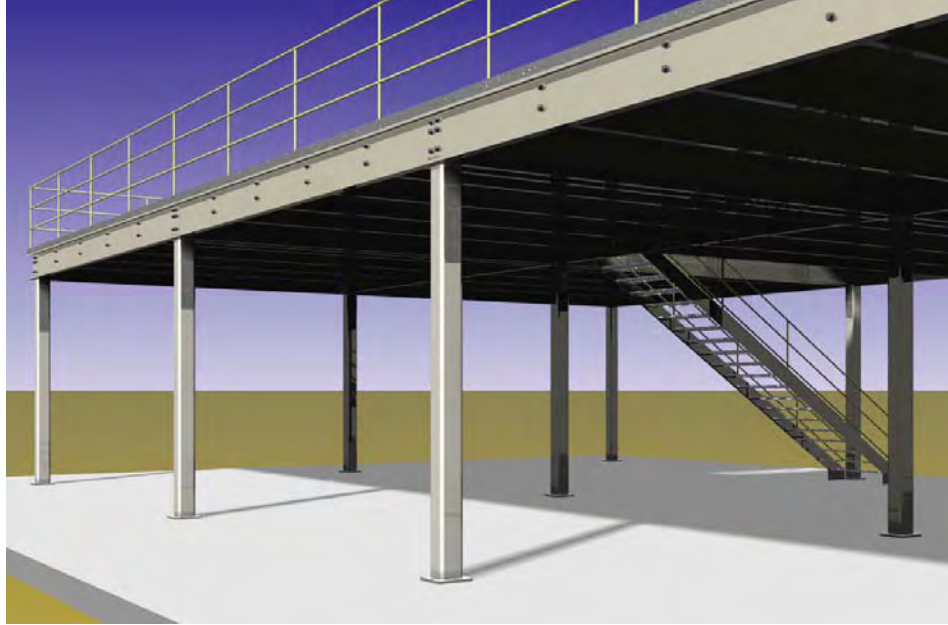
1.2 Objective

The objective of this study was to evaluate if the proposed SPFs are acceptable and would provide a satisfactory margin against collapse under the Maximum Considered Earthquake ground motions. The evaluation procedure developed by the ATC-63 project (FEMA 2008) was used for this purpose.

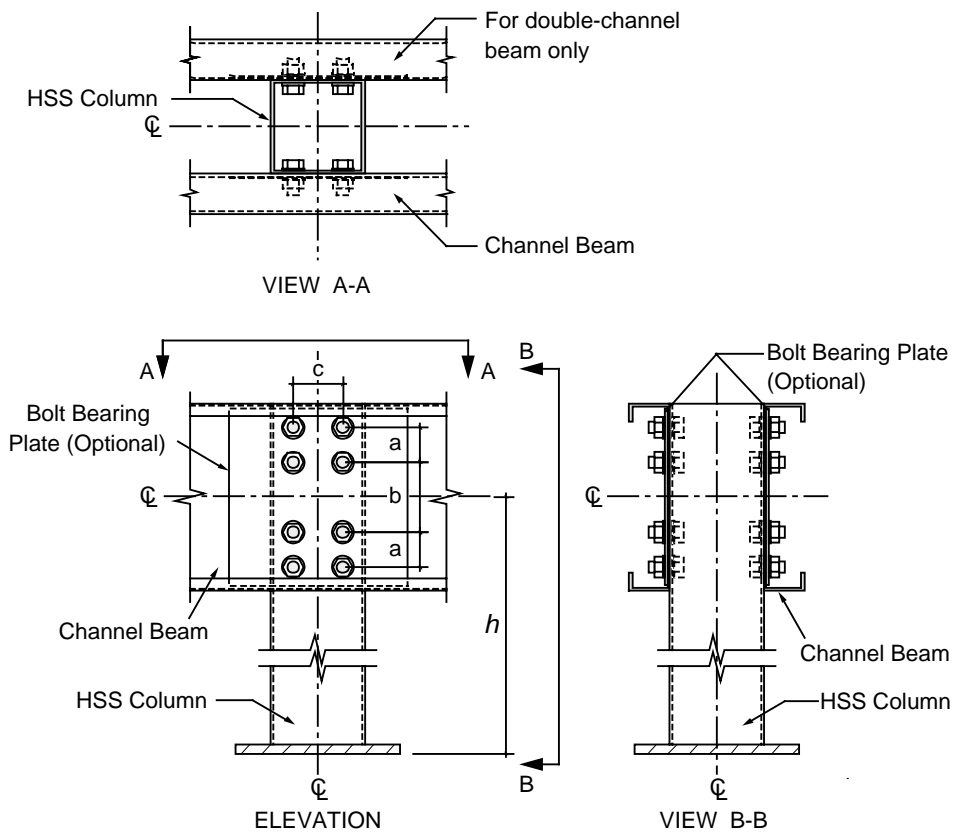
Table 1.1 Seismic Performance Factors

ASCE 7 Section where Detailing Requirements are Specified	Response Modification Coefficient, R	System Overstrength Factor, Ω_o	Deflection Amplification Factor, C_d	Structural System Limitations and Building Height (ft) Limit				
				B	C	D	E	F
14.1	3.5	3.0 ^a	3.5	35	35	35	35	35

^a Alternatively, the seismic load effects with overstrength, E_m , can be calculated based on the procedure in AISI S110.



(a) CFS-SBMF



(b) Typical Bolted Moment Connection Detail

Figure 1.1 Typical CFS-SBMF

2. STRUCTURAL SYSTEM INFORMATION

2.1 Quality Rating

The archetype models were designed based on ASCE 7-05 (ASCE 2005) and AISI S110 (AISI 2007). For the purpose of assessing uncertainty, the AISI S110 design requirements were categorized as “B-Good” per the ATC-63 Methodology since the numerical simulation showed that the experimental cyclic response of SBMF bolted moment connections could be reliably predicted by using the concept of instantaneous center of rotation of an eccentrically loaded bolt group (Uang et al. 2008.) Cyclic test results of 9 full-scale beam-column subassemblies formed the basis for the development of the AISI S110 Seismic Standard. Test specimens included different beam and column member sizes, width-thickness ratios, and bolt configurations (Hong and Uang 2004.) For the purpose of assessing uncertainty, this test data set was categorized as “A-Superior.”

The modeling was conservatively rated as “B-Good.” See Section 2.4 for further information.

2.2 Identification of SBMF Archetype Configuration

Figure 2.1 shows the two-dimensional frame geometry that was used to model the one-story SBMF structures; both one-span and two-span frames were considered. With this configuration, a set of archetype designs was developed to represent the archetype design space. This set of designs was organized into four performance groups that represented the ranges of design ground motion intensities and gravity loading conditions:

- Maximum Seismic (D_{max}) and Low Gravity Loading,
- Maximum Seismic (D_{max}) and High Gravity Loading,
- Minimum Seismic (D_{min}) and Low Gravity Loading, and
- Minimum Seismic (D_{min}) and High Gravity Loading.

2.3 Archetype Structural Design

According to the ATC-63 Methodology, the archetype models were designed based on the following seismic load combinations:

$$1.2D + 1.0E + 0.5L \quad (2-1a)$$

$$0.9D + 1.0E \quad (2-1b)$$

where D is the structural self weight and superimposed dead loads, and L is the live load (see Table 2.2.) E is the earthquake load effect computed as

$$E = \rho Q_E \pm 0.2S_{DS}D \quad (2-2)$$

where Q_E is the effect of horizontal seismic forces, ρ is the redundancy factor ($\rho = 1$ in accordance with the ATC-63 Methodology.) S_{DS} is the design spectral acceleration at short periods.

Table 2.1 shows the design data of each archetype design. The high and low seismic demands were represented by the maximum and minimum demands possible in Seismic Design Category (SDC) D . The archetypes were designed for a Site Class D (soft soil) condition with $S_{DS} = 1.0g$ and $S_{D1} = 0.6g$ for SDC D_{max} and $S_{DS} = 0.5g$ and $S_{D1} = 0.2g$ for SDC D_{min} . The corresponding Maximum Considered Earthquake (MCE) hazard spectral values were equal to 1.5 times of these design spectral values.

The beams were specified to be ASTM A653 galvanized cold-formed steel C-section members with the nominal yield stress (F_y) and ultimate strength (F_u) of 50 and 70 ksi. ASTM A500 Grade B HSS members with the F_y and F_u values of 46 and 70 ksi, respectively, were used for the columns. The above seismic load combinations resulted in the member and connection designs summarized in Table 2.2 and Table 2.3.

2.4 Development of Nonlinear Structural Archetype Model

The model shown in Figure 2.1 included beam and column elements as well as a zero-length rotational spring to simulate the nonlinear behavior of the beam-to-column bolted moment connections. Energy dissipation was confined in the moment connection region. A zero-length nonlinear spring was developed to simulate the cyclic behavior (Uang et al. 2008.) Sample results based on the proposed hysteresis rule for the nonlinear

spring are shown in Figure 2.2. Fiber element was used to model the yielding of beams and columns; no buckling was considered in the analysis. See Section 5.1 on the treatment of strength degradation due to buckling.

According to the ATC-63 Methodology, the expected material properties can be used for the analysis. Therefore, the expected yield stress ($= R_y F_y$) and the expected tensile strength ($= R_t F_u$) were used to compute the member strengths and bolt bearing strength, where $R_y = R_t = 1.1$ for the beams and $R_y = 1.4$ and $R_t = 1.3$ for the columns (AISI 2007.)

For either nonlinear static or dynamic analysis, the ATC-63 Methodology requires that the following expected gravity loads be imposed to the model structure:

$$1.05D + 0.25L \quad (2-3)$$

The nonlinear analyses were performed by using the software OpenSees (Open System for Earthquake Engineering Simulation), developed by Pacific Earthquake Engineering Research Center (PEER). A 5% damping was assumed for the models. The P-Delta effect was also included in the analysis.

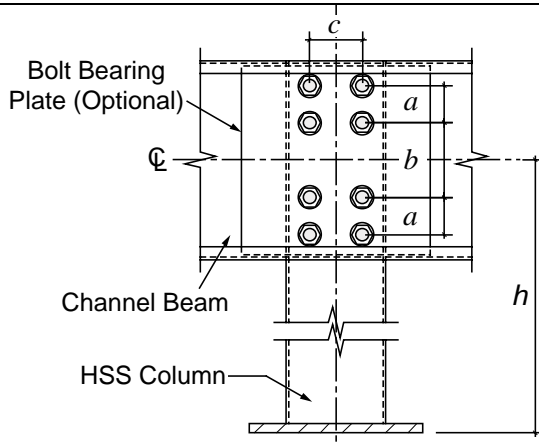
Table 2.1 Archetype Structural Design Properties

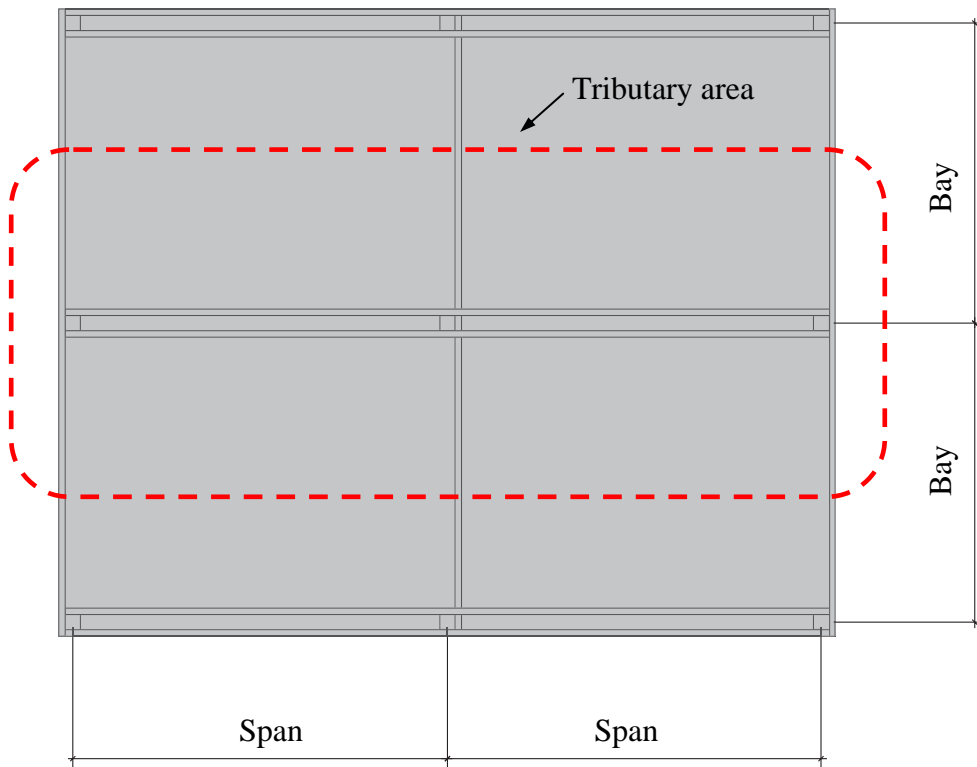
Archetype Design ID Number	Number of Span	Span (ft)	Bay (ft)	Height (ft)	Key Archetype Design Parameters			
					Seismic Design Criteria			S_{MT} [T] g
					SDC	R	T (sec)	
Maximum Seismic (D_{max}) and Low Gravity Designs								
3	1	20.0	16	16	D_{max}	3.5	0.87	1.04
5	2	21.4	20	10.25	D_{max}	3.5	0.51	1.50
10	2	23.375	20	16	D_{max}	3.5	0.77	1.16
13	2	21.4	12	30	D_{max}	3.5	1.36	0.66
Maximum Seismic (D_{max}) and High Gravity Designs								
1	2	21.4	16	16	D_{max}	3.5	0.82	1.10
2	1	20.0	16	16	D_{max}	3.5	0.73	1.24
8	2	21.4	14	24	D_{max}	3.5	1.08	0.84
12	1	22.29	16	11	D_{max}	3.5	0.57	1.50
Minimum Seismic (D_{min}) and Low Gravity Designs								
4	1	22.0	20	8.5	D_{min}	3.5	0.43	0.71
7	2	20.0	17	12	D_{min}	3.5	0.95	0.32
11	2	24.0	14	16	D_{min}	3.5	1.10	0.27
Minimum Seismic (D_{min}) and High Gravity Designs								
6	2	24.2	12	18	D_{min}	3.5	0.90	0.33
9	1	22.0	14	9.5	D_{min}	3.5	0.46	0.66

Table 2.2 Archetype Structure Model Sizes

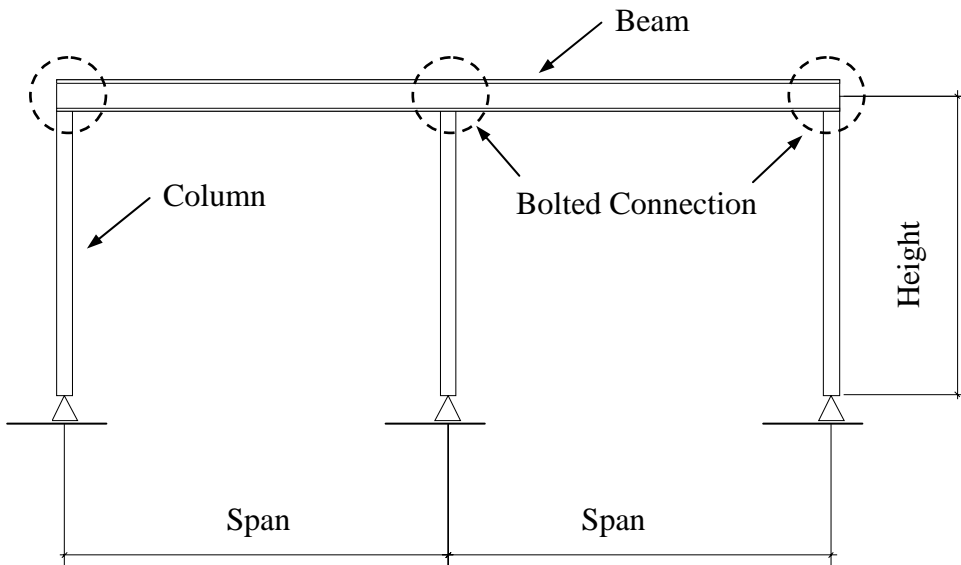
Archetype Design ID	Beam (in)	Column (in)	Live Load, L (psf)	Dead Load, D (psf)
1	2C20×3.5×10Ga	HSS10×10×1/4	125	12
2	2C16×3.5×10Ga	HSS10×10×1/4	125	12
3	2C20×3.5×10Ga	HSS10×10×1/4	50	55
4	2C12×3.5×12Ga	HSS8×8×1/4	50	12
5	2C16×3.5×10Ga	HSS8×8×1/4	50	12
6	2C20×3.5×10Ga	HSS10×10×1/4	125	12
7	2C16×3.5×10Ga	HSS8×8×1/4	50	55
8	2C20×3.5×10Ga	HSS12×12×1/4	125	12
9	2C16×3.5×10Ga	HSS8×8×1/4	125	12
10	2C16×3.5×10Ga	HSS10×10×1/4	50	12
11	2C16×3.5×10Ga	HSS10×10×1/4	50	55
12	2C20×3.5×10Ga	HSS8×8×1/4	125	12
13	2C20×3.5×10Ga	HSS12×12×1/4	125	12

Table 2.3 Bolt Configurations

Archetype Design ID	a (in)	b (in)	c (in)	
1	3	10	6¼	 <p>1-in. snug-tight high-strength bolt, Slip coefficient $k = 0.33$, Bolt tension force = 10 kips.</p>
2	3	6	6¼	
3	3	10	6¼	
4	2½	3	4¼	
5	3	6	4¼	
6	3	10	6¼	
7	3	6	4¼	
8	3	10	8¼	
9	3	6	4¼	
10	3	6	6¼	
11	3	6	6¼	
12	3	10	4¼	
13	3	10	8¼	



(a) Plan

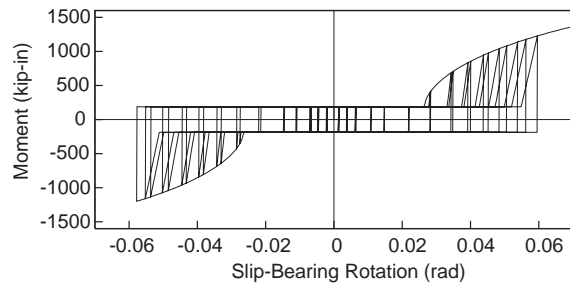
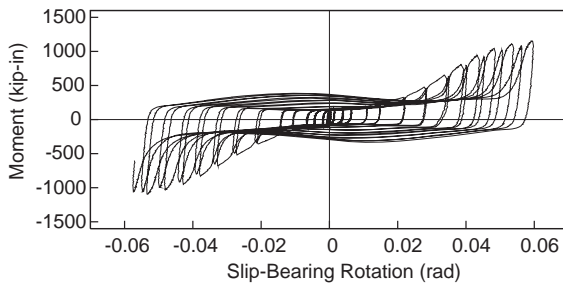


(b) Elevation

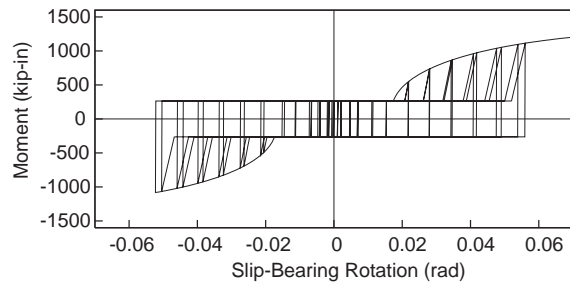
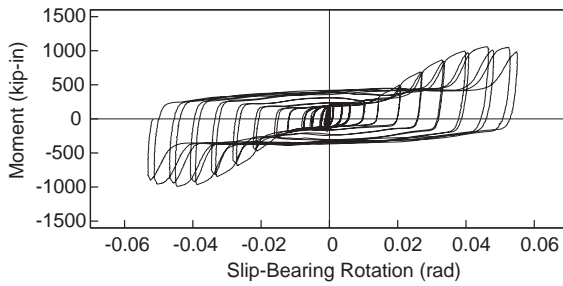
Figure 2.1 Archetype Analysis Model for SBMF

Test

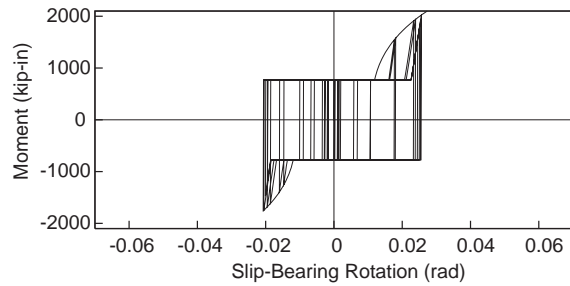
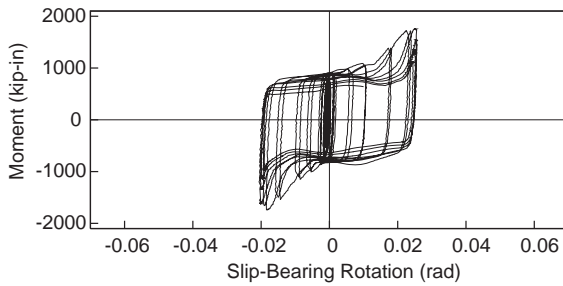
Simulated



(a) Specimen 1: Beam: $2C12 \times 3.5 \times 0.105$, Column: $HSS8 \times 8 \times 1/4$



(b) Specimen 2: Beam: $2C16 \times 3.5 \times 0.105$, Column: $HSS8 \times 8 \times 1/4$



(c) Specimen 9: Beam: $2C20 \times 3\frac{1}{2} \times 0.135$, Column: $HSS10 \times 10 \times 1/4$

Figure 2.2 Sample Correlation of Bolted Moment Connection Response

3. Nonlinear Static Analyses

3.1 Introduction

Nonlinear static (or pushover) analyses were conducted in accordance with the ATC-63 Methodology to help validate the behavior of models and to provide statistical data on the system overstrength, Ω , and the ductility capacity μ_c :

$$\mu_c = \frac{\Delta_{ult}}{\Delta_y} \quad (3-1)$$

and

$$\Omega = \frac{V_{max}}{V} \quad (3-2)$$

See Figure 3.1 for the definition of Δ_{ult} , Δ_y , and V_{max} ; V is the design base shear. Note from this figure that the Methodology assumes that the maximum strength of the system will be reached before it degrades to 80% of the peak strength. This assumed response envelope, however, is very different from that expected for a properly designed SBMF. Figure 3.2 shows that an SBMF will continue to strain harden at a large story drift, implying that the ductility capacity can be very large. Since AISI S110 limits the design story drift to 5% of the story height, h , the ductility capacity can be conservatively defined as follows.

$$\mu_c = \frac{0.05h}{\Delta_y} \quad (3-3)$$

It is also difficult to implement the system overstrength definition (Eq. 3-2) to SBMF because, within the story drift range of practical interest, a properly designed SBMF usually does not reach the peak strength and then degrade. Instead, the lateral strength of the frame continues to increase with the story drift. Note that AISI S110 provides a design procedure to calculate the maximum base shear for a given design story drift (Sato and Uang 2008). Since this procedure explicitly calculates the seismic load effect with overstrength, E_m , the system overstrength factor is not needed. Nonetheless, the Ω as defined below is calculated in this chapter:

$$\Omega = \frac{V_{0.05}}{V} \quad (3-4)$$

where $V_{0.05}$ is the base shear at 5% story drift ratio. The Ω value thus calculated can be very conservative and should be interpreted with caution.

3.2 Global Response

Figure 3.3 shows some sample pushover analysis results. The pseudo-yielding base shear nV_S and the corresponding elastic deformation Δ_y ($= nV_S / K$, where K is the lateral stiffness) are summarized in Table 3.1. Appendix A provides the pushover curves of all archetypes.

3.3 System Overstrength and Ductility Capacity

From pushover curves, key parameters that are used to calculate Ω and μ_c values are listed in Table 3.1. The average value of μ_c ranges from 6.33 to 7.60, with an average value of 7.19. The average Ω value varies from 3.82 to 4.00 for maximum seismic performance groups and is much higher for minimum seismic performance groups. As was explained earlier, the calculated Ω value can be highly conservative and should be interpreted with caution.

Table 3.1 Archetype Structural Properties

ID	h (ft)	K (kips/in)	nV_S (kips)	V (kips)	$V_{0.05}$ (kips)	Δ_y (in.)	$\Delta_{0.05}$ (in.)	Ω	μ_c
Maximum Seismic (D_{max}) and Low Gravity Designs									
3	16	3.07	3.97	4.45	16.2	1.29	9.6	3.64	7.42
5	10.25	8.35	6.44	6.14	22.8	0.77	6.15	3.71	7.97
10	16	4.02	4.57	5.21	17.1	1.14	9.6	3.29	8.44
13	30	1.24	3.40	2.83	13.1	2.75	18.0	4.62	6.55
mean								3.82	7.60
Maximum Seismic (D_{max}) and High Gravity Designs									
1	16	4.61	5.96	6.31	24.2	1.29	9.6	3.84	7.42
2	16	2.71	3.05	3.31	11.6	1.12	9.6	3.51	8.55
8	24	2.32	4.25	4.18	18.1	1.84	14.4	4.34	7.84
12	11	4.94	5.43	4.47	19.3	1.10	6.6	4.32	60
mean								4.00	7.45
Minimum Seismic (D_{min}) and Low Gravity Designs									
4	8.5	7.29	3.91	1.49	9.33	0.54	5.1	6.27	9.50
7	12	5.45	5.51	2.88	18.3	1.01	7.2	6.34	7.12
11	16	3.99	4.57	2.45	17.0	1.15	9.6	6.93	8.38
mean								6.51	6.33
Minimum Seismic (D_{min}) and High Gravity Designs									
6	18	3.24	5.30	1.62	20.1	1.64	10.8	12.4	6.60
9	9.5	6.65	4.63	1.69	16.7	0.70	5.0	9.88	8.18
mean								11.1	7.39

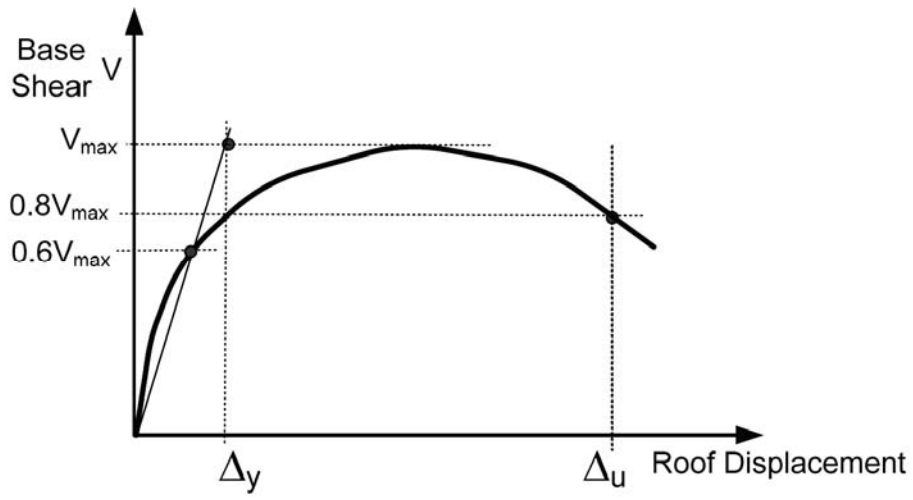


Figure 3.1 Idealized Nonlinear Pushover Curve (FEMA 2008)

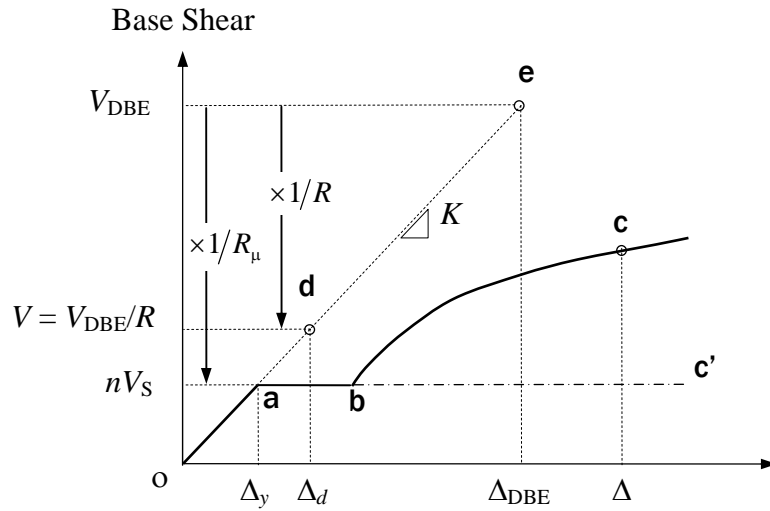
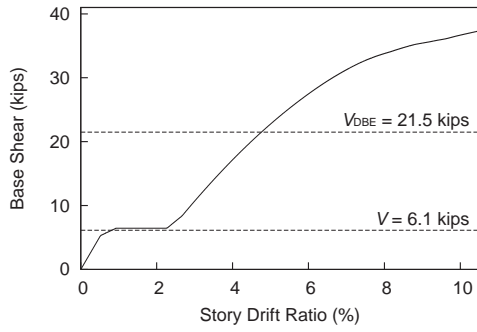
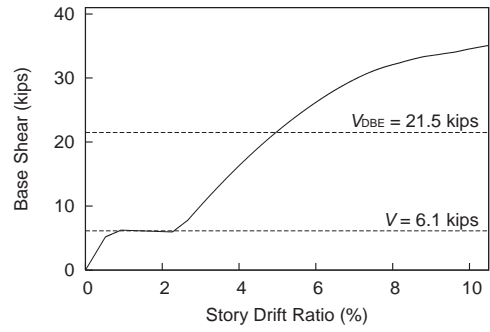


Figure 3.2 General Response of SBMF (AISI 2007)

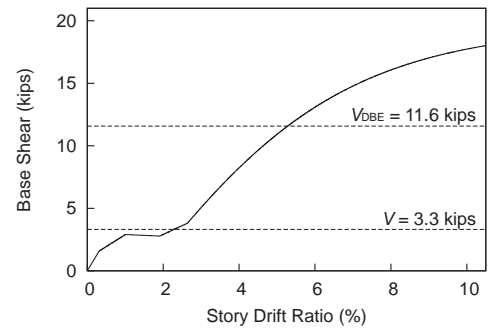
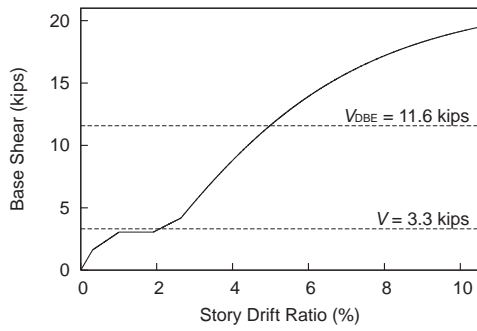
without P-Delta Effects



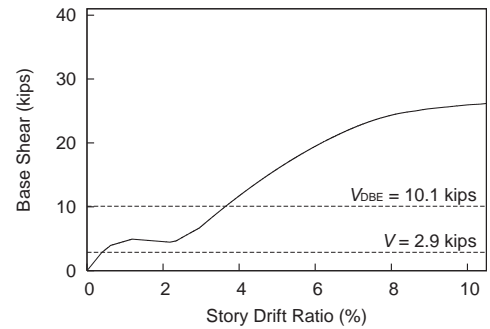
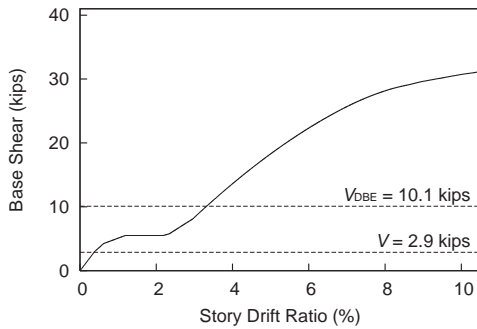
with P-Delta Effects



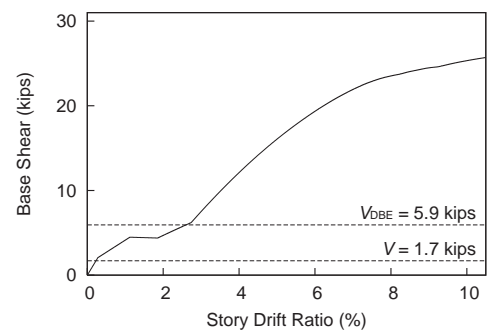
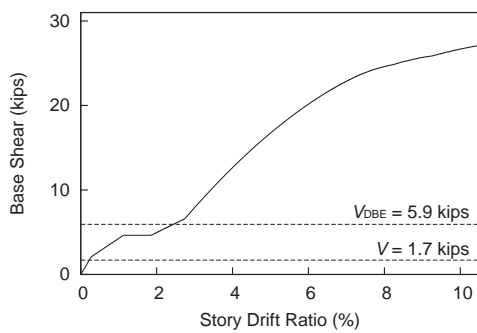
(a) Archetype 5



(b) Archetype 2



(c) Archetype 7



(d) Archetype 9

Figure 3.3 Sample Nonlinear Static Analysis Results

4. Nonlinear Dynamic Analyses

4.1 Incremental Dynamic Analysis

Nonlinear response for each of the archetype models was evaluated for a set of pre-defined earthquake ground motions. The ATC-63 procedure for conducting nonlinear dynamic analyses was based on the concept of incremental dynamic analysis (IDA), in which each ground motion was scaled to increasing intensities until the structure reaches a collapse point. The objective of the analyses was to establish the median collapse capacity and collapse margin ratio for each of the models.

4.1.1 Ground Motion

Twenty-two earthquake ground motion record pairs from sites located greater than or equal to 10 km from the fault rupture, referred to as the “Far-Field” record set, were used for the collapse assessment (FEMA 2008). Table 4.1 and Table 4.2 summarize key information of these ground motion records.

4.1.2 Maximum Considered Earthquake

For each archetype model, the Maximum Considered Earthquake (MCE) spectral acceleration, S_{MT} , corresponding to the fundamental period of the model is summarized in Table 2.1. These MCE values are equal to 1.5 times those of the Design Basis Earthquake (DBE).

4.2 Global Response at Design Basis Earthquake

Although not required by the ATC-63 Methodology, global responses of all archetype models produced by the Design Basis Earthquake ground motions are presented in Appendix B. Figure 4.1 shows sample responses of a few archetypes

produced by the second component of Ground Motion 1 (1994 Northridge, NORTH/MUL279).

4.3 Incremental Dynamic Analysis

Sample results from the incremental dynamic analysis are shown in Figure 4.2. The ground motion intensity, S_T , is defined as the spectral acceleration measured at the fundamental period of the structure. Each point in the figure was produced from a single nonlinear dynamic analysis of one index archetype model subjected to one ground motion record scaled to one intensity level. Each curve in the figure was produced by repeating the same process by scaling the same ground motion record to the full range of intensity values. Appendix C contains the IDA results for all archetype models.

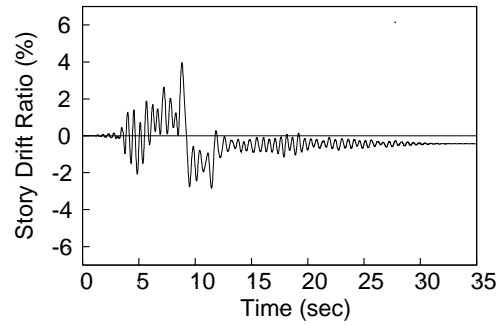
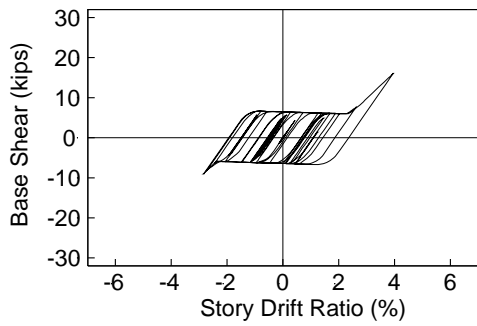
Table 4.1 Earthquake Event and PEER-NGA Database for the Far-Field Record Set

GM ID	Earthquake					Peak Motion *	
	M	Year	Name	Component 1	Component 2	PGA (g)	PGV (cm/sec)
1	6.7	1994	Northridge	NORTH/MUL009	NORTH/MUL279	0.52	63
2	6.7	1994	Northridge	NORTH/LOS000	NORTH/LOS270	0.48	45
3	7.1	1999	Duzce, Turkey	DUZCE/BOL000	DUZCE/BOL090	0.82	62
4	7.1	1999	Hector Mine	HECTOR/HEC000	HECTOR/HEC090	0.34	42
5	6.5	1979	Imperial Valley	IMPVAL/H-DLT262	IMPVAL/H-DLT352	0.35	33
6	6.5	1979	Imperial Valley	IMPVAL/H-E11140	IMPVAL/H-E11230	0.38	42
7	6.9	1995	Kobe, Japan	KOBE/NIS000	KOBE/NIS090	0.51	37
8	6.9	1995	Kobe, Japan	KOBE/SHI000	KOBE/SHI090	0.24	38
9	7.5	1999	Kocaeli, Turkey	KOCAELI/DZC180	KOCAELI/DZC270	0.36	59
10	7.5	1999	Kocaeli, Turkey	KOCAELI/ARC000	KOCAELI/ARC090	0.22	40
11	7.3	1992	Landers	LANDERS/YER279	LANDERS/YER360	0.24	52
12	7.3	1992	Landers	LANDERS/CLW-LN	LANDERS/CLW-TR	0.42	42
13	6.9	1989	Loma Prieta	LOMA/CAP000	LOMA/CAP090	0.53	35
14	6.9	1989	Loma Prieta	LOMA/G03000	LOMA/G03090	0.56	45
15	7.4	1990	Manjil, Iran	MANJIL/ABBAR--L	MANJIL/ABBAR--T	0.51	54
16	6.5	1987	Superstition Hills	SUPERST/B-ICC000	SUPERST/B-ICC090	0.36	46
17	6.5	1987	Superstition Hills	SUPERST/B-POE270	SUPERST/B-POE360	0.45	36
18	7.0	1992	Cape Mendocino	CAPEMEND/RIO270	CAPEMEND/RIO270	0.55	44
19	7.6	1999	Chi-Chi, Taiwan	CHICHI/CHY101-E	CHICHI/CHY101-N	0.44	115
20	7.6	1999	Chi-Chi, Taiwan	CHICHI/TCU045-E	CHICHI/TCU045-N	0.51	39
21	6.6	1971	San Fernando	SFERN/PEL090	SFERN/PEL180	0.21	19
22	6.5	1976	Friuli, Italy	FRIULIA/A-TMZ000	FRIULIA/A-TMZ270	0.35	31

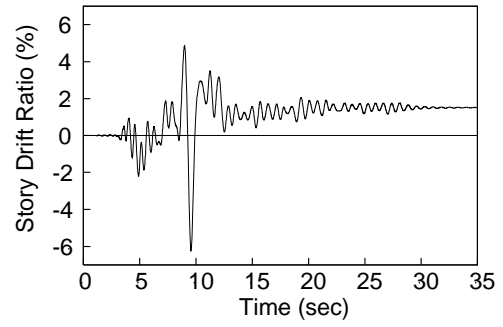
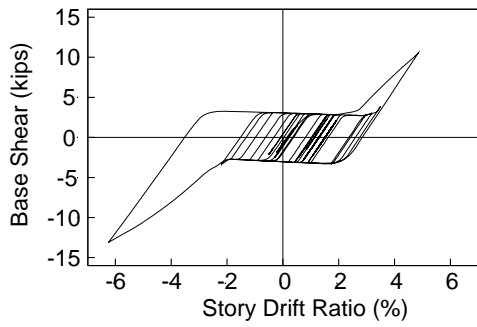
* The larger value of two components is reported.

Table 4.2 Normalized Ground Motions for the Far-Field Record Set

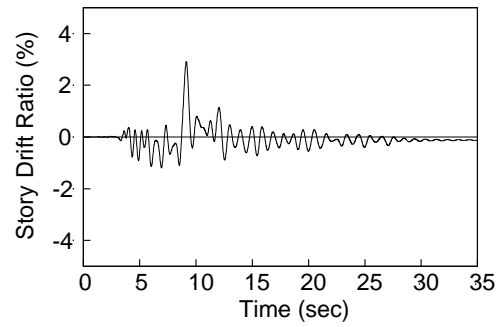
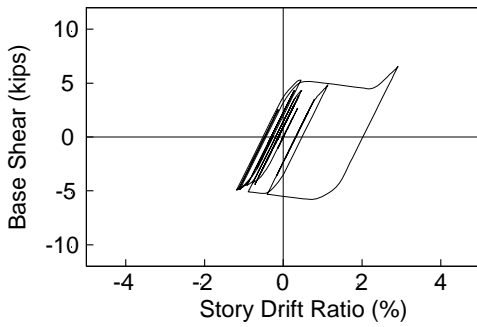
GM ID	Normalized Factor	Normalized Peak Motion*	
		<i>PGA</i> (g)	<i>PGV</i> (cm/sec)
1	0.65	0.34	41
2	0.83	0.40	38
3	0.63	0.52	39
4	1.09	0.37	46
5	1.31	0.46	43
6	1.01	0.39	43
7	1.03	0.53	39
8	1.10	0.26	42
9	0.69	0.25	41
10	1.36	0.30	54
11	0.99	0.24	51
12	1.15	0.48	49
13	1.09	0.58	38
14	0.88	0.49	39
15	0.79	0.40	43
16	0.87	0.31	40
17	1.17	0.53	42
18	0.82	0.45	36
19	0.41	0.18	47
20	0.96	0.49	38
21	2.10	0.44	40
22	1.44	0.50	44



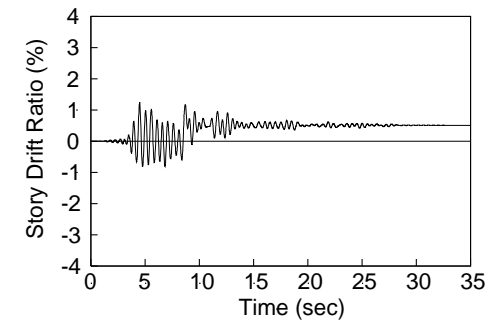
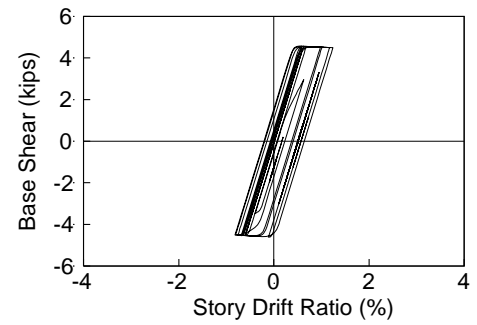
(a) Archetype 5



(b) Archetype 2

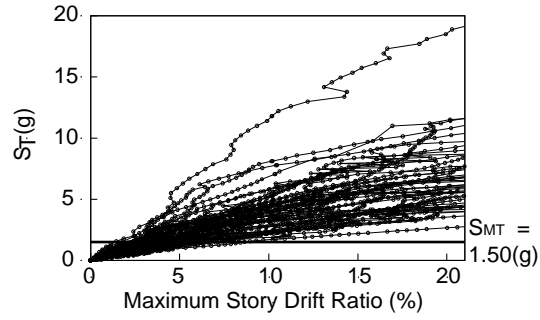


(c) Archetype 7

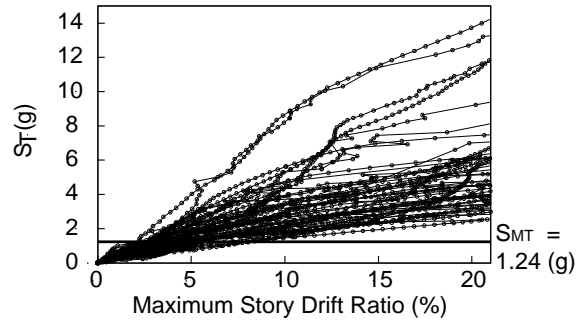


(d) Archetype 9

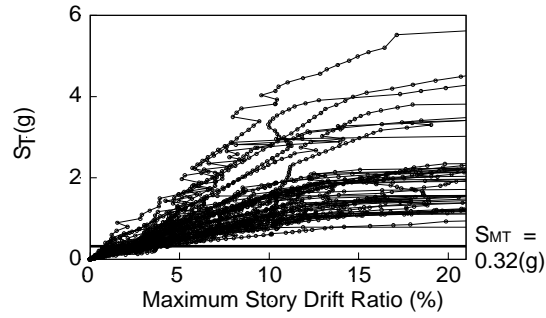
Figure 4.1 Nonlinear Dynamic Analysis (GM1, Component 2, Design Basis Earthquake)



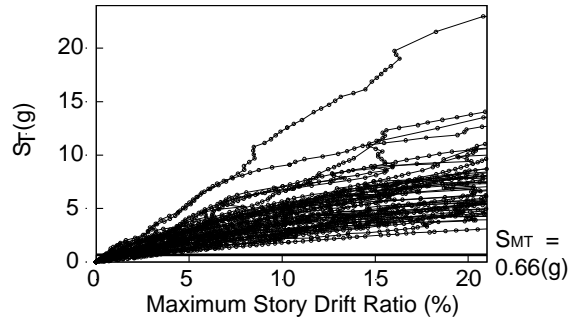
(a) Archetype 5



(b) Archetype 2



(c) Archetype 7



(d) Archetype 9

Figure 4.2 Sample Incremental Dynamic Analysis Results (Total 44 Ground Motion Records)

5. EVALUATION OF COLLAPSE MARGIN AND ACCEPTANCE CRITERIA

5.1 Median Collapse Intensity and Collapse Margin Ratio

For each archetype model, the spectral acceleration at collapse, S_{CT} , was computed for each of the 44 ground motions, from which the median collapse intensity, \hat{S}_{CT} , was computed. \hat{S}_{CT} was obtained by scaling all the records in the Far-Field record set to the MCE intensity, S_{MT} , and then by increasing the intensity until one-half of the scaled ground motion records caused collapse. The MCE intensity, S_{MT} , was obtained from the response spectrum of MCE ground motions at the fundamental period, T , of the structure (see Table 2.1). The ratio between the median collapse intensity, \hat{S}_{CT} , and the MCE intensity, S_{MT} , is the collapse margin ratio (*CMR*).

$$CMR = \frac{\hat{S}_{CT}}{S_{MT}} \quad (5-1)$$

The IDA results presented in Chapter 4 were based on the assumption that the beam and column could yield, but would not buckle. The collapse was defined as that when the story drift ratio exceeds 0.2 radians. Therefore, the predicted *CMR* represents the upper bound value. Since strength degradation due to potential buckling in the beams and columns were not modeled in the analysis, a lower bound value was also calculated. Based on the test results of 9 full-scale beam-column subassemblies (Hong and Uang 2004), the mean and standard deviation of the story drift capacity are 0.077 and 0.019 radians, respectively (see Figure 5.1). Stringent width-thickness ratios were also established from the test results and incorporated in AISI S110. Since the beam and column of all the archetypes satisfied the S110 seismic compactness requirements, it was judged that a story drift capacity of 0.06 radians was a reasonable value to define the lower bound collapse limit state.

Figure 5.2 shows the sample IDA analysis results for the upper bound *CMR* values, while Figure 5.3 shows those for the lower bound values. Results of IDA and

collapse probability for all archetypes are provided in Appendix D. The upper and lower bound \hat{S}_{CT} and CMR values obtained from the collapse assessment are summarized in Table 5.1 and Table 5.2.

5.2 Adjusted Collapse Margin Ratio

The collapse capacity and the calculation of the collapse margin ratio can be significantly influenced by the frequency content (spectral shape) of the ground motion record set. To account for the effects of spectral shape, the modified collapse margin ratio, $ACMR$, was computed.

$$ACMR = SSF \times CMR \quad (5-2)$$

where SSF is the spectral shape factor.

According to the ATC-63 Methodology, SSF is a function of the fundamental period T , the ductility capacity μ_c , and the seismic criteria used for the design of the index archetype as defined by Seismic Design Category. SSF and $ACMR$ for each archetype are listed in Table 5.3 and Table 5.4 for the upper and lower bound approaches, respectively. The mean $ACMR$ value for each performance group is also provided.

5.3 Evaluation of Collapse Margin and Acceptance Criteria

The quality of test data was classified as "A-Superior" and the quality of design requirements was classified as "B-Good." Classifying the model quality as "B-Good," the total system collapse uncertainty (β_{TOT}) was equal to 0.60 (see Table 5.5).

The ATC-63 Methodology provides the acceptable values of the adjusted collapse margin ratios, $ACMR10\%$ and $ACMR20\%$, based on the total system collapse uncertainty and the values of acceptable collapse probability, taken as 10% and 20%, respectively. With $\beta_{TOT} = 0.60$, the values of $ACMR10\%$ and $ACMR20\%$ were 2.16 and 1.66, respectively (see Table 5.6).

Acceptable performance is achieved when, for each performance group, the adjusted collapse margin ratio, $ACMR$, for each index archetype meets the following criteria:

- the average value of the adjusted collapse margin ratio for each performance group exceeds $ACMR10\%$:

$$\overline{ACMR} \geq ACMR10\% \quad (5-3)$$

- individual values of the adjusted collapse margin ratio for each index archetype within a performance group exceeds $ACMR20\%$:

$$ACMR \geq ACMR20\% \quad (5-4)$$

Based on a summary of the upper bound collapse analysis results of all 13 archetype designs and 4 performance groups in Table 5.3, a comparison with the acceptable $ACMR$ values shows that the acceptance criteria were met by a significant margin. When the 6% story drift was used to define the lower bound collapse limit state, Table 5.4 also indicates that the acceptance criteria were met.

Table 5.1 Summary of Collapse Results for Archetype Designs (Upper Bound)

Archetype Design ID Number	Design Configuration		IDA Analysis Results		
	No. of Span	SDC	$S_{MT} [T], g$	$\hat{S}_{CT} [T], g$	CMR
Maximum Seismic (D_{max}) and Low Gravity Designs					
3	1	D_{max}	1.04	3.48	3.35
5	2	D_{max}	1.50	63	4.02
10	2	D_{max}	1.16	4.21	3.63
13	2	D_{max}	0.66	3.24	4.91
Maximum Seismic (D_{max}) and High Gravity Designs					
1	2	D_{max}	1.10	3.86	3.51
2	1	D_{max}	1.24	4.61	3.72
8	2	D_{max}	0.84	3.69	4.39
12	1	D_{max}	1.50	5.08	3.39
Minimum Seismic (D_{min}) and Low Gravity Designs					
4	1	D_{min}	0.71	5.83	8.21
7	2	D_{min}	0.32	1.93	63
11	2	D_{min}	0.27	2.18	8.07
Minimum Seismic (D_{min}) and High Gravity Designs					
6	2	D_{min}	0.33	3.92	11.8
9	1	D_{min}	0.66	6.83	10.3

Table 5.2 Summary of Collapse Results for Archetype Designs (Lower Bound)

Archetype Design ID Number	Design Configuration		IDA Analysis Results		
	No. of Span	SDC	$S_{MT} [T], g$	$\hat{S}_{CT} [T], g$	CMR
Maximum Seismic (D_{max}) and Low Gravity Designs					
3	1	D_{max}	1.04	1.35	1.30
5	2	D_{max}	1.50	2.38	1.59
10	2	D_{max}	1.16	1.67	1.44
13	2	D_{max}	0.66	1.17	1.77
Maximum Seismic (D_{max}) and High Gravity Designs					
1	2	D_{max}	1.10	1.54	1.40
2	1	D_{max}	1.24	1.95	1.57
8	2	D_{max}	0.84	1.31	1.56
12	1	D_{max}	1.50	2.35	1.57
Minimum Seismic (D_{min}) and Low Gravity Designs					
4	1	D_{min}	0.71	2.29	3.23
7	2	D_{min}	0.32	0.84	2.63
11	2	D_{min}	0.27	0.85	3.15
Minimum Seismic (D_{min}) and High Gravity Designs					
6	2	D_{min}	0.33	1.43	4.33
9	1	D_{min}	0.66	2.66	4.03

Table 5.3 Final Collapse Margins and Acceptance Criteria (Upper Bound)

Archetype Design ID Number	Design Configuration		Computed Collapse Margin				Acceptance Check	
	No. of Span	SDC	CMR	μ_c	SSF	$ACMR$	Accept. $ACMR$	Pass/ Fail
Maximum Seismic (D_{max}) and Low Gravity Designs								
3	1	D_{max}	3.35	29.7	1.44	4.82	1.66	Pass
5	2	D_{max}	4.02	31.9	1.34	5.39	1.66	Pass
10	2	D_{max}	3.63	33.8	1.41	5.12	1.66	Pass
13	2	D_{max}	4.91	26.2	1.58	7.76	1.66	Pass
Mean						5.77	2.16	Pass
Maximum Seismic (D_{max}) and High Gravity Designs								
1	2	D_{max}	3.51	29.7	1.43	5.02	1.66	Pass
2	1	D_{max}	3.72	34.2	1.40	5.21	1.66	Pass
8	2	D_{max}	4.39	31.4	1.49	6.54	1.66	Pass
12	1	D_{max}	3.39	24.0	1.34	4.54	1.66	Pass
Mean						5.33	2.16	Pass
Minimum Seismic (D_{min}) and Low Gravity Designs								
4	1	D_{min}	8.21	38.0	1.14	9.36	1.66	Pass
7	2	D_{min}	63	28.5	1.24	7.48	1.66	Pass
11	2	D_{min}	8.07	33.5	1.28	10.3	1.66	Pass
Mean						9.05	2.16	Pass
Minimum Seismic (D_{min}) and High Gravity Designs								
6	2	D_{min}	11.8	26.4	1.23	14.5	1.66	Pass
9	1	D_{min}	10.3	32.7	1.15	11.8	1.66	Pass
Mean						13.2	2.16	Pass

Table 5.4 Final Collapse Margins and Acceptance Criteria (Lower Bound, 6% Drift)

Archetype Design ID Number	Design Configuration		Computed Collapse Margin				Acceptance Check	
	No. of Span	SDC	CMR	μ_c	SSF	$ACMR$	Accept. $ACMR$	Pass/ Fail
Maximum Seismic (D_{max}) and Low Gravity Designs								
3	1	D_{max}	1.30	8.9	1.44	1.82	1.66	Pass
5	2	D_{max}	1.59	9.6	1.34	2.13	1.66	Pass
10	2	D_{max}	1.44	10.1	1.41	2.03	1.66	Pass
13	2	D_{max}	1.77	7.9	1.58	2.80	1.66	Pass
Mean						2.20	2.16	Pass
Maximum Seismic (D_{max}) and High Gravity Designs								
1	2	D_{max}	1.40	8.9	1.43	2.00	1.66	Pass
2	1	D_{max}	1.57	10.3	1.40	2.20	1.66	Pass
8	2	D_{max}	1.56	9.4	1.49	2.32	1.66	Pass
12	1	D_{max}	1.57	7.2	1.34	2.10	1.66	Pass
Mean						2.16	2.16	Pass
Minimum Seismic (D_{min}) and Low Gravity Designs								
4	1	D_{min}	3.23	11.4	1.14	3.68	1.66	Pass
7	2	D_{min}	2.63	8.5	1.24	3.26	1.66	Pass
11	2	D_{min}	3.15	10.1	1.28	4.03	1.66	Pass
Mean						3.66	2.16	Pass
Minimum Seismic (D_{min}) and High Gravity Designs								
6	2	D_{min}	4.33	7.9	1.23	5.33	1.66	Pass
9	1	D_{min}	4.03	9.8	1.15	4.63	1.66	Pass
Mean						4.98	2.16	Pass

Table 5.5 Total System Collapse Uncertainty, β_{TOT}

Quality of Test Data	Quality of Design Requirements			
	A- Superior	B-Good	C-Fair	D-Poor
(A) Superior	0.55	0.60	0.70	0.85
(B) Good	0.60	0.65	0.75	0.85
(C) Fair	0.70	0.75	0.80	0.95
(D) Poor	0.85	0.85	0.95	1.05

Table 5.6 Acceptable Value of Adjusted Collapse Margin Ratio
($ACMR10\%$ and $ACMR20\%$)

Total System Collapse Uncertainty β_{TOT}	Collapse Probability				
	5%	10%	15%	20%	25%
		$ACMR10\%$		$ACMR20\%$	
0.55	2.47	2.02	1.77	1.59	1.45
0.60	2.68	2.16	1.86	1.66	1.50
0.65	2.91	2.30	1.96	1.73	1.55

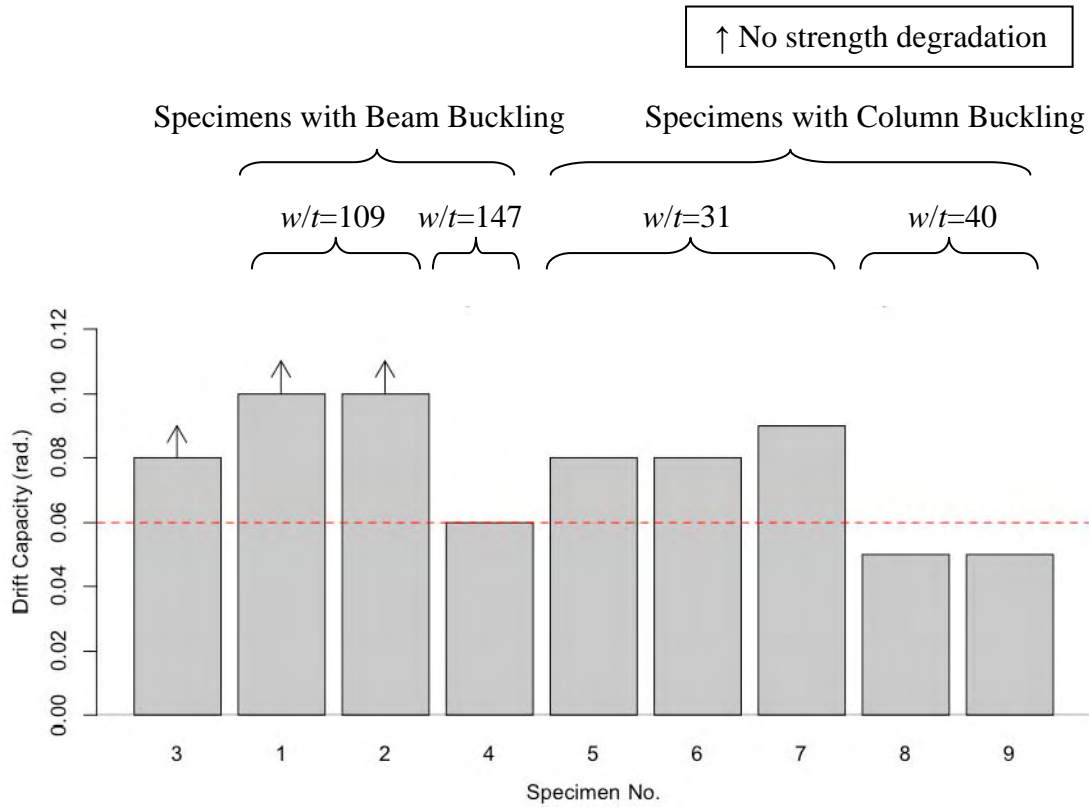
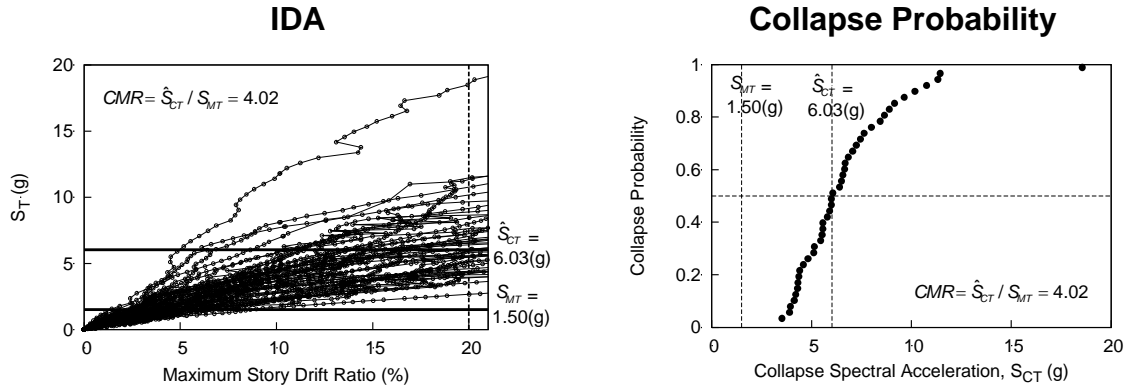
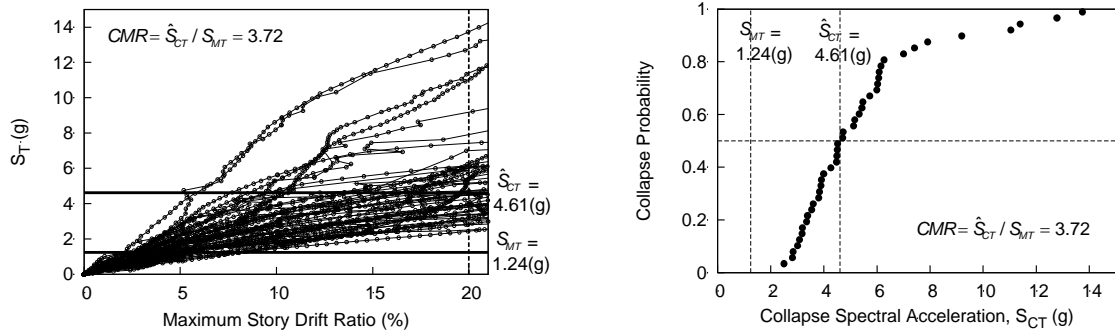


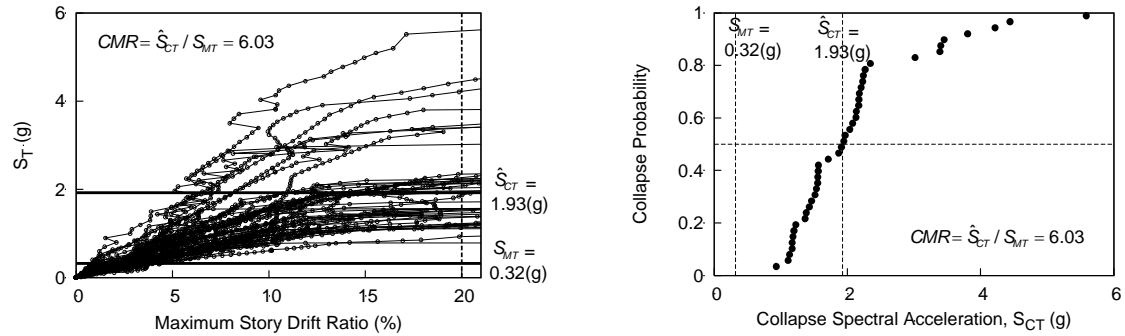
Figure 5.1 Story Drift Capacity from Full-Scale Testing (Hong and Uang 2004)



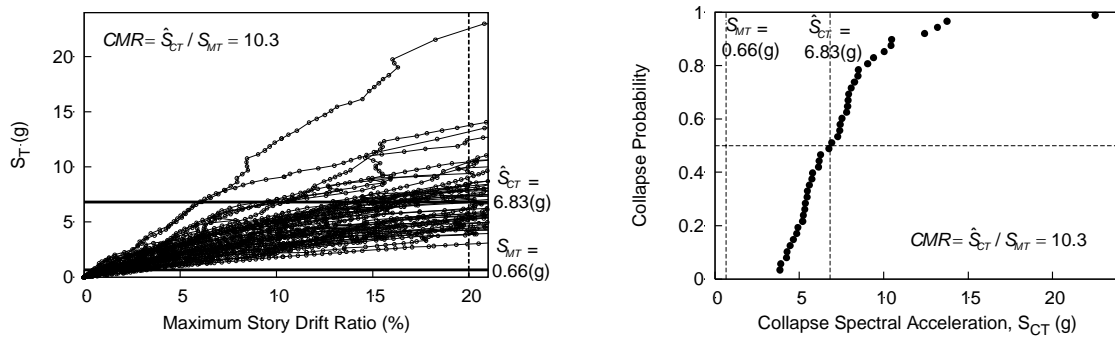
(a) Archetype 5



(b) Archetype 2

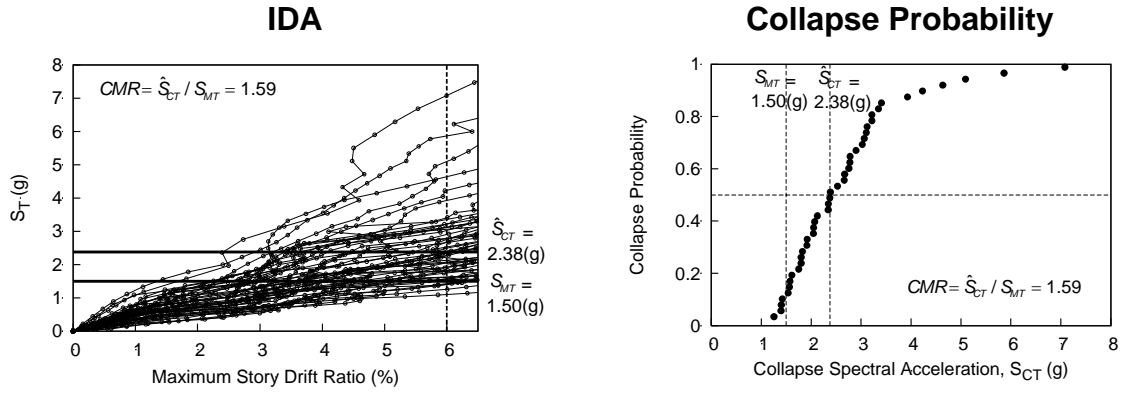


(c) Archetype 7

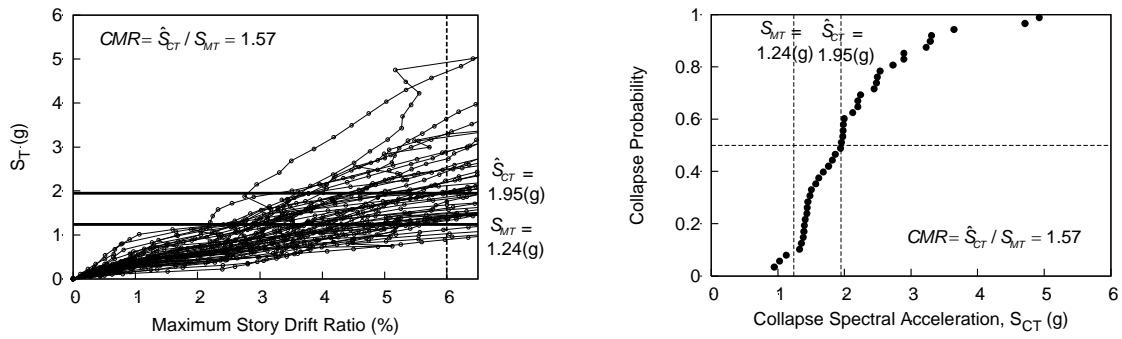


(d) Archetype 9

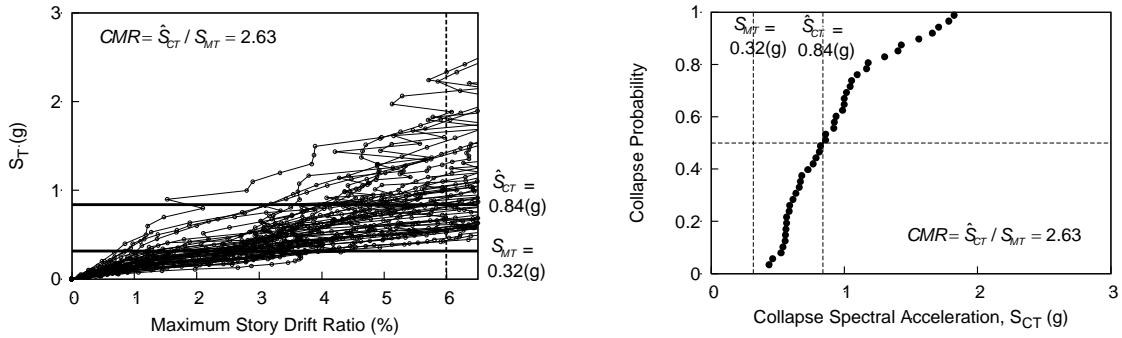
Figure 5.2 Sample IDA Results and Collapse Probability (Upper Bound)



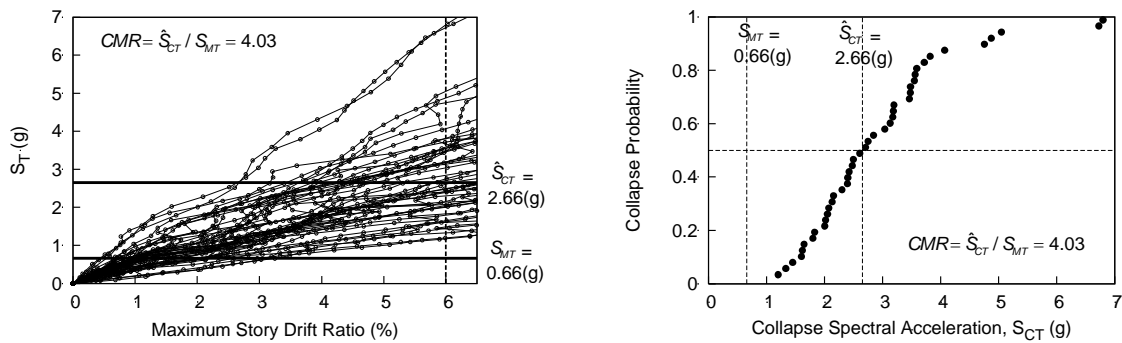
(a) Archetype 5



(b) Archetype 2



(c) Archetype 7



(d) Archetype 9

Figure 5.3 Sample IDA Results and Collapse Probability (Lower Bound)

6. CONCLUSIONS

Following the ATC-63 Methodology, a total of 13 Cold-Formed Steel Special Bolted Moment Frame archetype designs representing two seismicities (high and low) and two gravity load levels (high and low) were designed and analyzed. Expecting inelastic action to occur in the bolted moment connections only, a nonlinear spring element was developed and used in the nonlinear static and dynamic analyses. Although beam and column modeling allowed for yielding, buckling was not modeled in the analyses. Therefore, both upper bound and lower bound approach were used to compute the collapse margins.

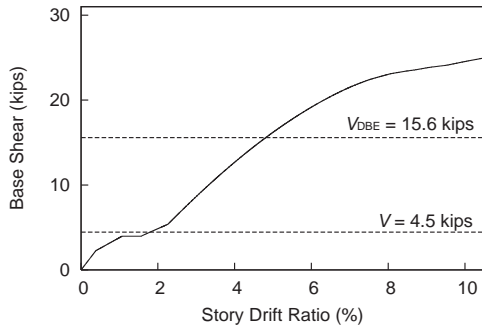
The upper bound approach showed that all 13 individual archetype designs and 4 performance groups met the ATC-63 acceptance criteria by a large margin. The lower bound approach assumed that the collapse limit state was reached when the story drift ratio exceeded 6%. This approach also showed that all individual archetypes and performance groups met the acceptance criteria. Therefore, it was concluded that the Seismic Performance Factors proposed in Table 1.1 were acceptable and would provide a satisfactory margin against collapse under the Maximum Considered Earthquake ground motions.

REFERENCES

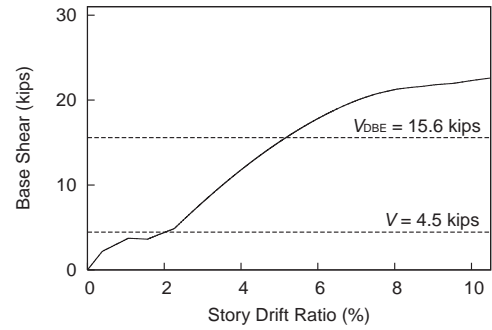
- (1) AISI (2007), *Standard for Seismic Design of Cold-Formed Steel Structural Systems–Special Bolted Moment Frames*, S110, American Iron and Steel Institute, Washington, DC.
- (2) ASCE (2005), *Minimum Design Loads for Buildings and Other Structures*, ASCE/SEI 7-05, American Society of Civil Engineering, Reston, VA.
- (3) FEMA (2008), *Quantification of Building Seismic Performance Factors*, FEMA P695 (90% Draft), Federal Emergency Management Agency, Washington, DC.
- (4) Hong, J.K. and C.M. Uang (2004), “Cyclic Testing of Cold-Formed Steel Moment Connection for Pre-Fabricated Mezzanines,” *Report No. TR-04/03*, University of California, San Diego, La Jolla, CA.
- (5) OpenSees, “Open System for Earthquake Engineering Simulation,” <http://opensees.berkeley.edu/>, Pacific Earthquake Engineering Center (PEER), University of California, Berkeley, CA.
- (6) Sato, A. and Uang, C.M. (2008), “Cold-Formed Steel Special Bolted Moment Frames: Capacity Design Requirements,” *Proceedings*, Nineteenth International Specialty Conference on Cold-Formed Steel Design and Construction, St. Louis, MO, pp. 577-589.
- (7) Uang, C.M., Hong, J.K., Sato, A., and Wood, K. (2008), “Cold-Formed Steel Special Bolted Moment Frames: Cyclic Testing and Numerical Modeling of Moment Connections,” *Proceedings*, Nineteenth International Specialty Conference Cold-Formed Steel Design and Construction, St. Louis, MO, pp. 563-575.

APPENDIX A: Nonlinear Static Analysis Results

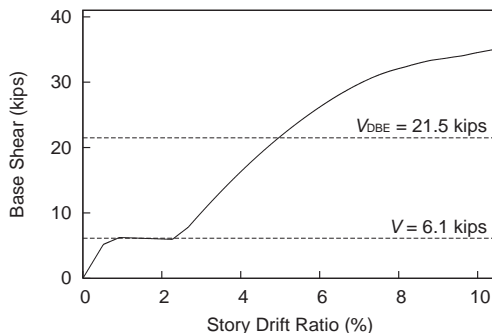
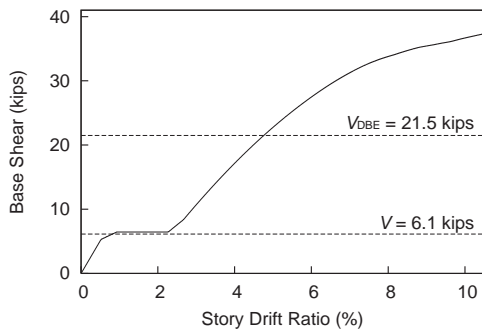
Without P-Delta Effects



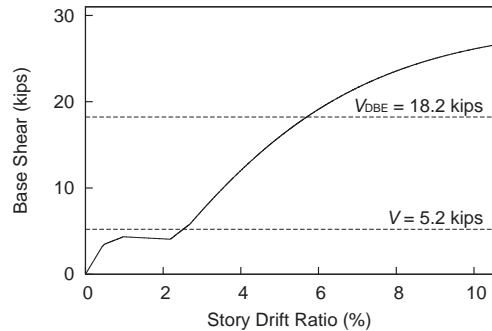
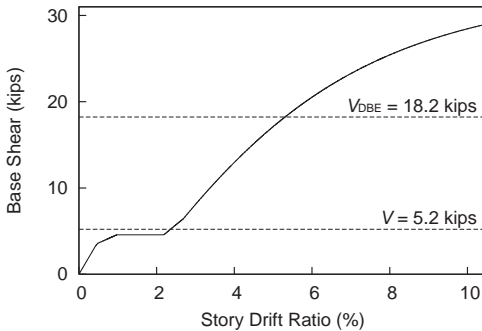
With P-Delta Effects



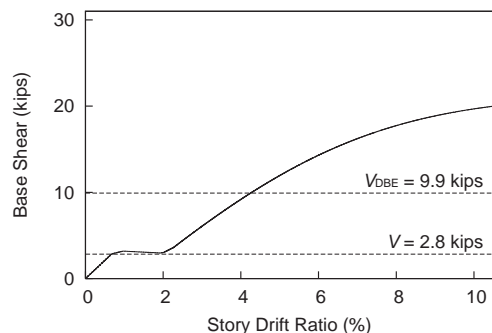
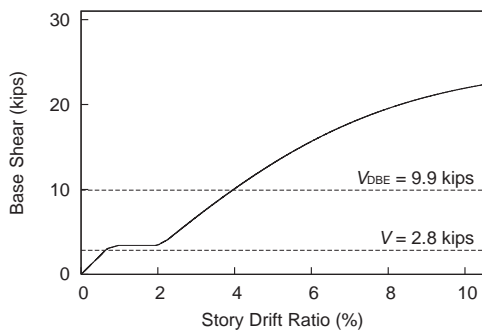
(a) Archetype 3



(b) Archetype 5



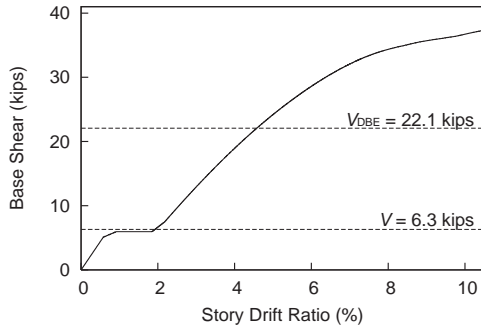
(c) Archetype 10



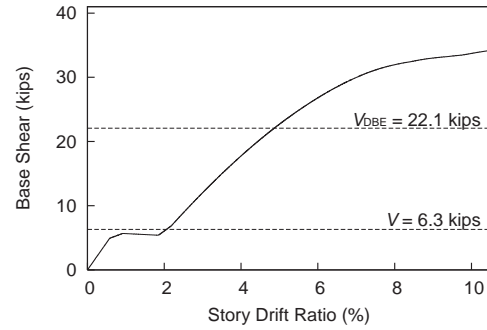
(d) Archetype 13

Figure A.1 Maximum Seismic (D_{max}) and Low Gravity Designs

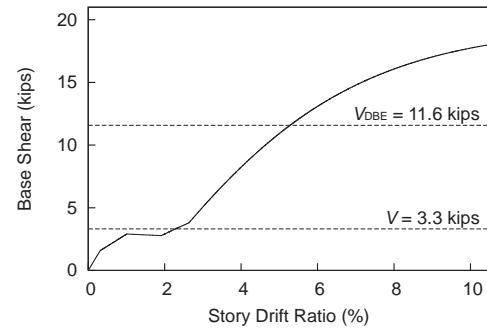
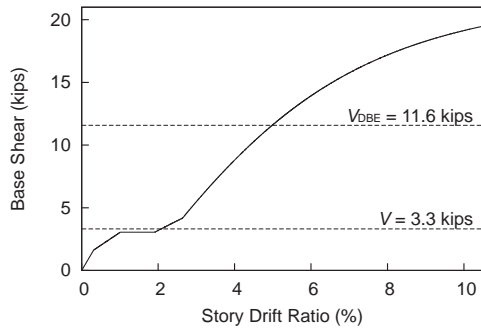
Without P-Delta Effects



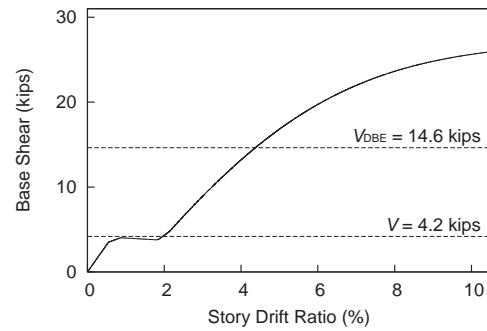
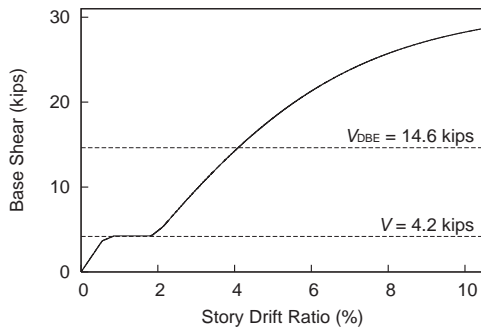
With P-Delta Effects



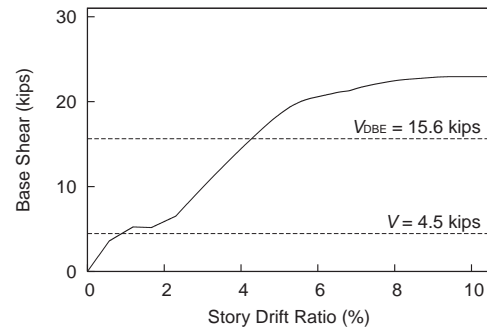
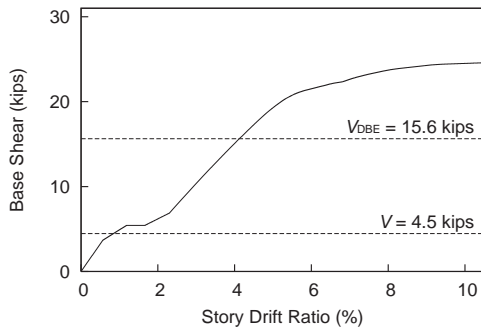
(a) Archetype 1



(b) Archetype 2



(c) Archetype 8

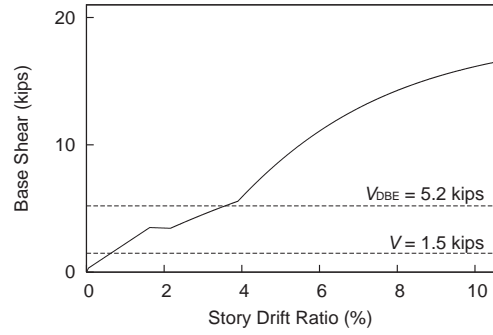
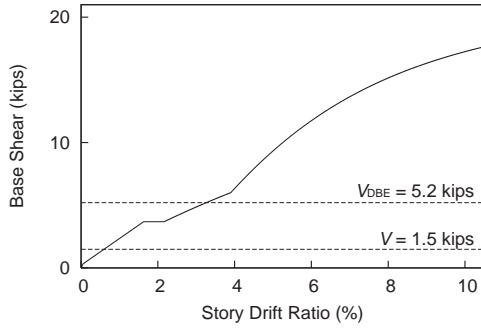


(d) Archetype 12

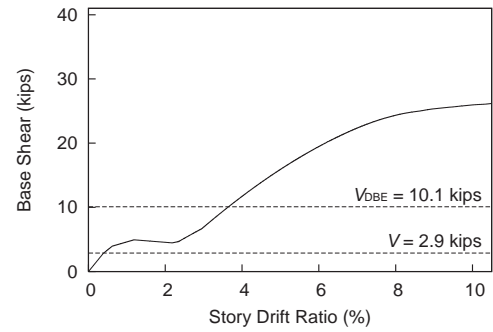
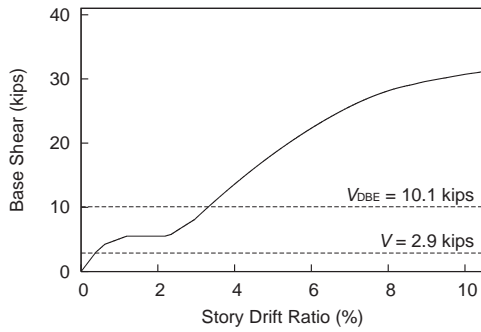
Figure A.2 Maximum Seismic (D_{max}) and High Gravity Designs

Without P-Delta Effects

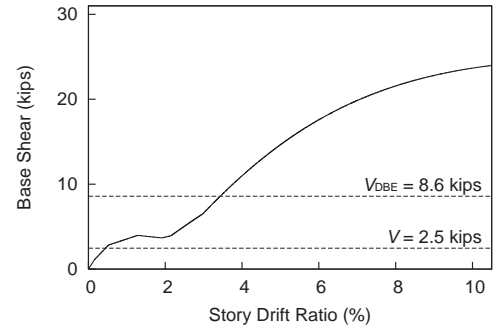
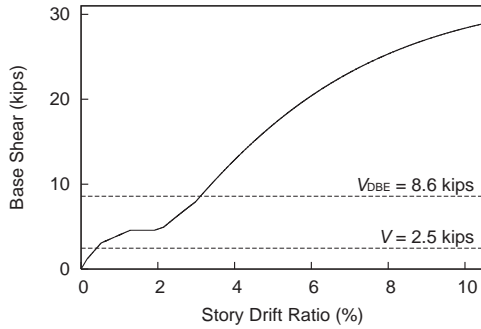
With P-Delta Effects



(a) Archetype 4



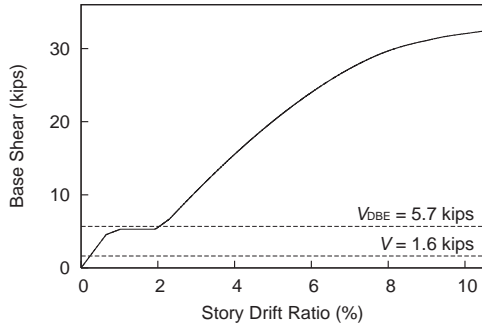
(b) Archetype 7



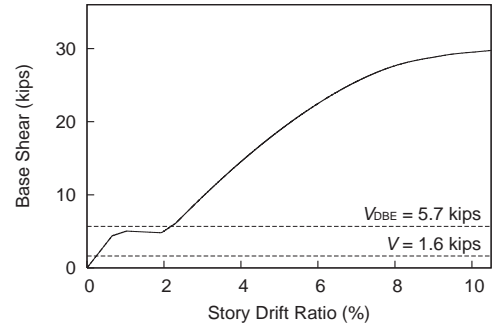
(c) Archetype 11

Figure A.3 Minimum Seismic (D_{min}) and Low Gravity Designs

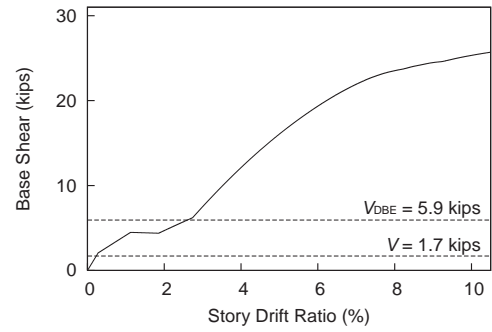
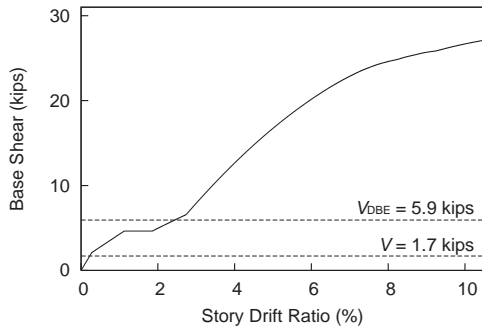
Without P-Delta Effects



With P-Delta Effects



(a) Archetype 6



(b) Archetype 9

Figure A.4 Minimum Seismic (D_{min}) and High Gravity Designs

APPENDIX B: Global Response at DBE Level

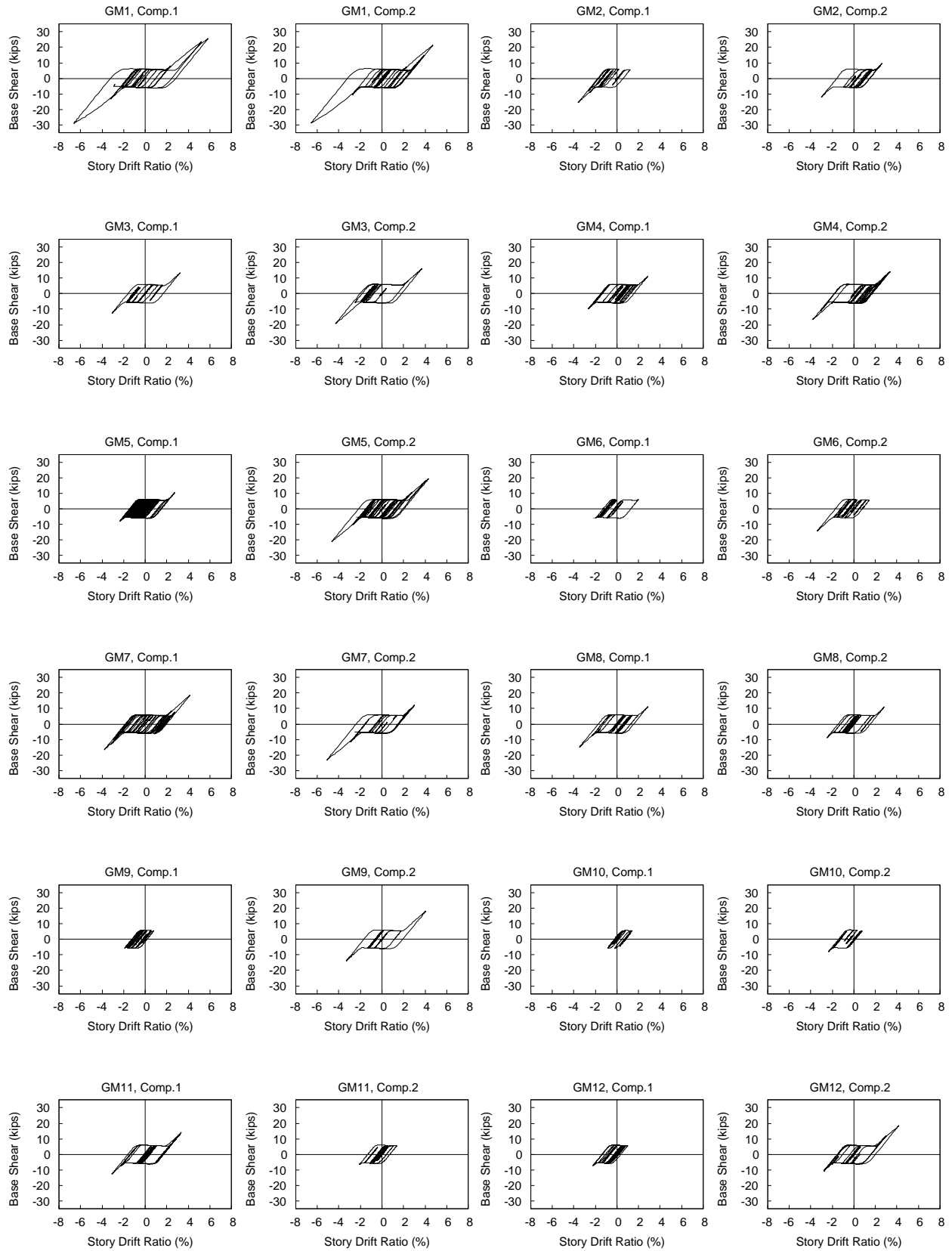


Figure B.1 Archetype 1 (DBE)

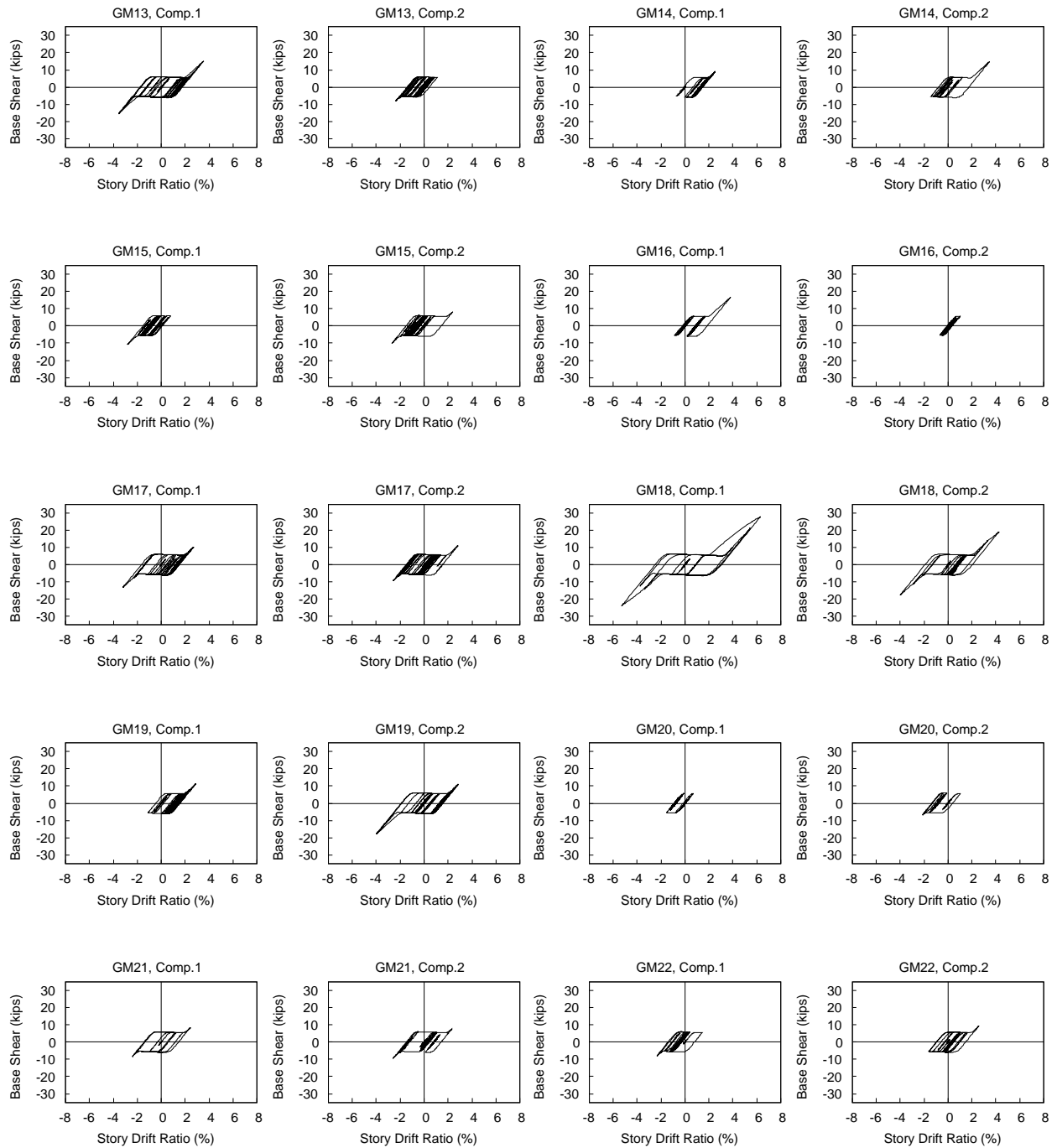


Figure B.1 Archetype 1 (DBE) (cont.)

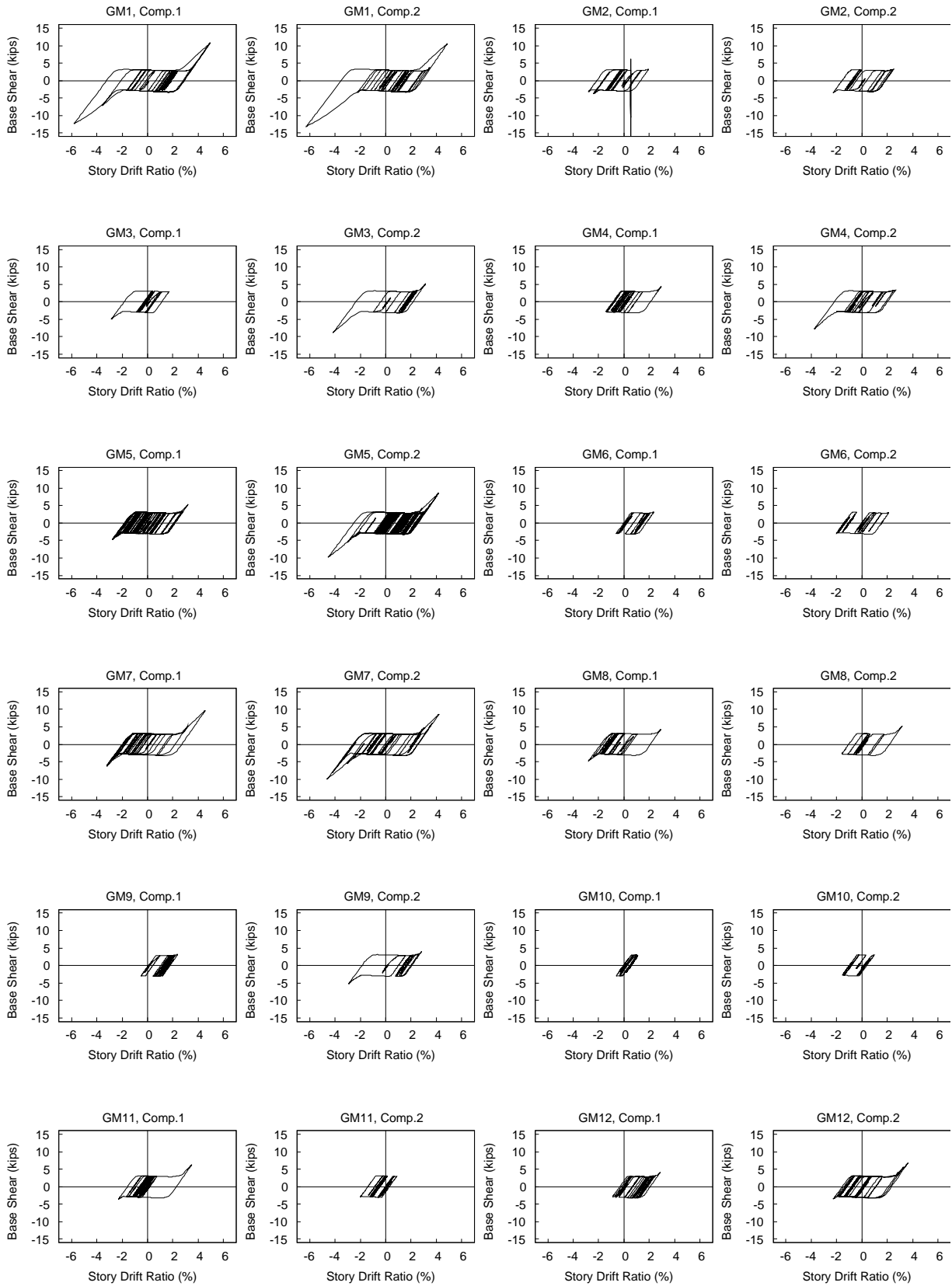


Figure B.2 Archetype 2 (DBE)

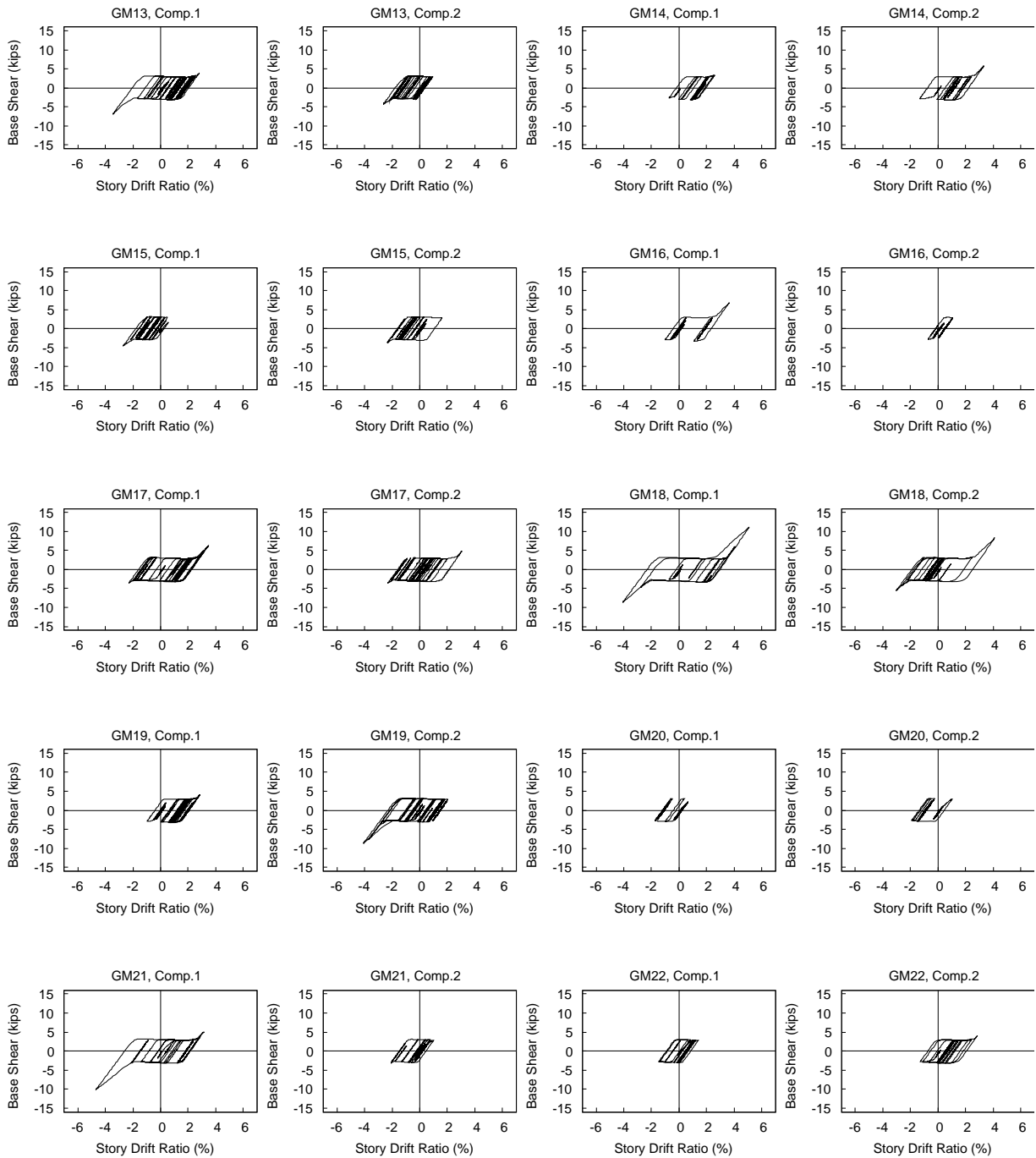


Figure B.2 Archetype 2 (DBE) (cont.)

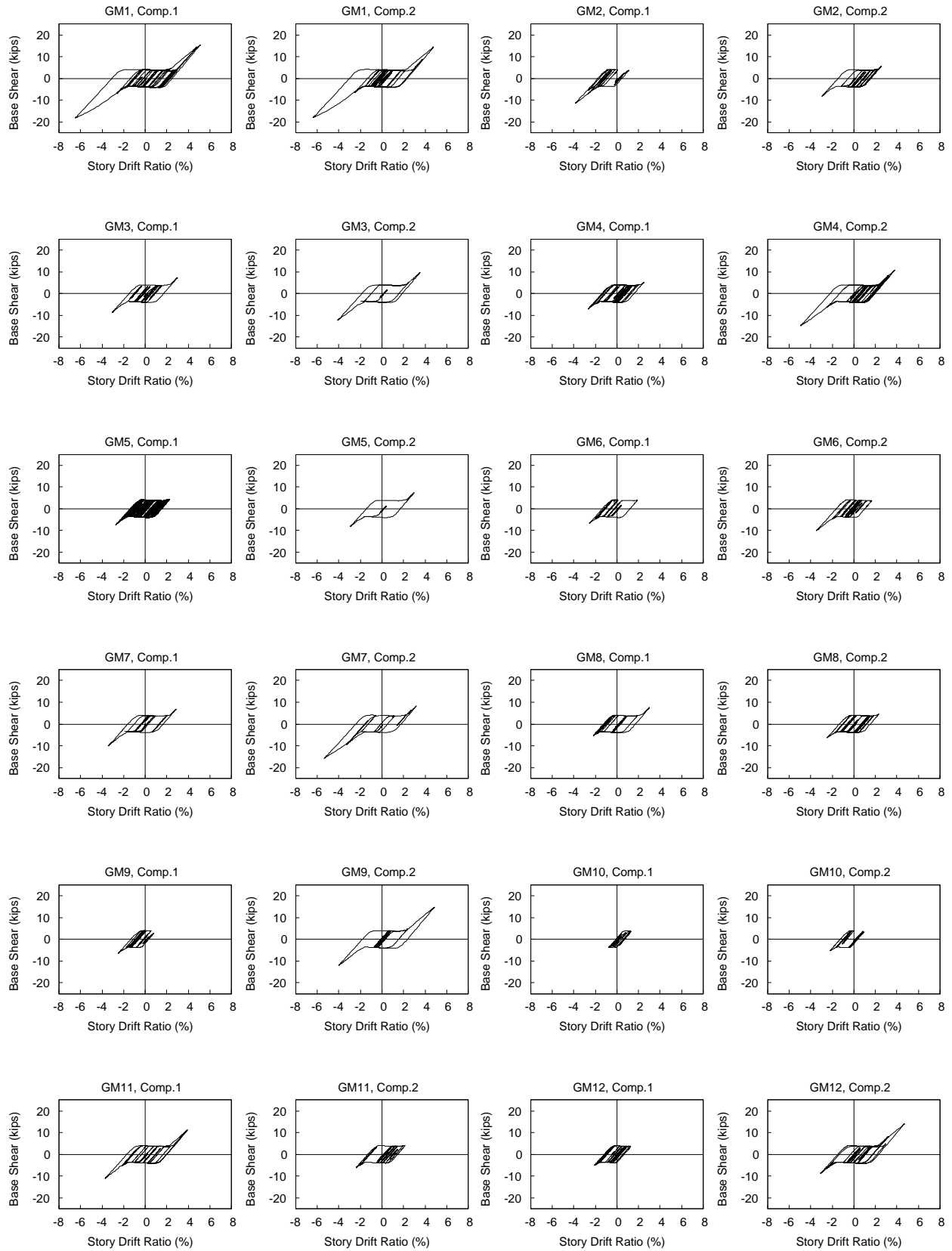


Figure B.3 Archetype 3 (DBE)

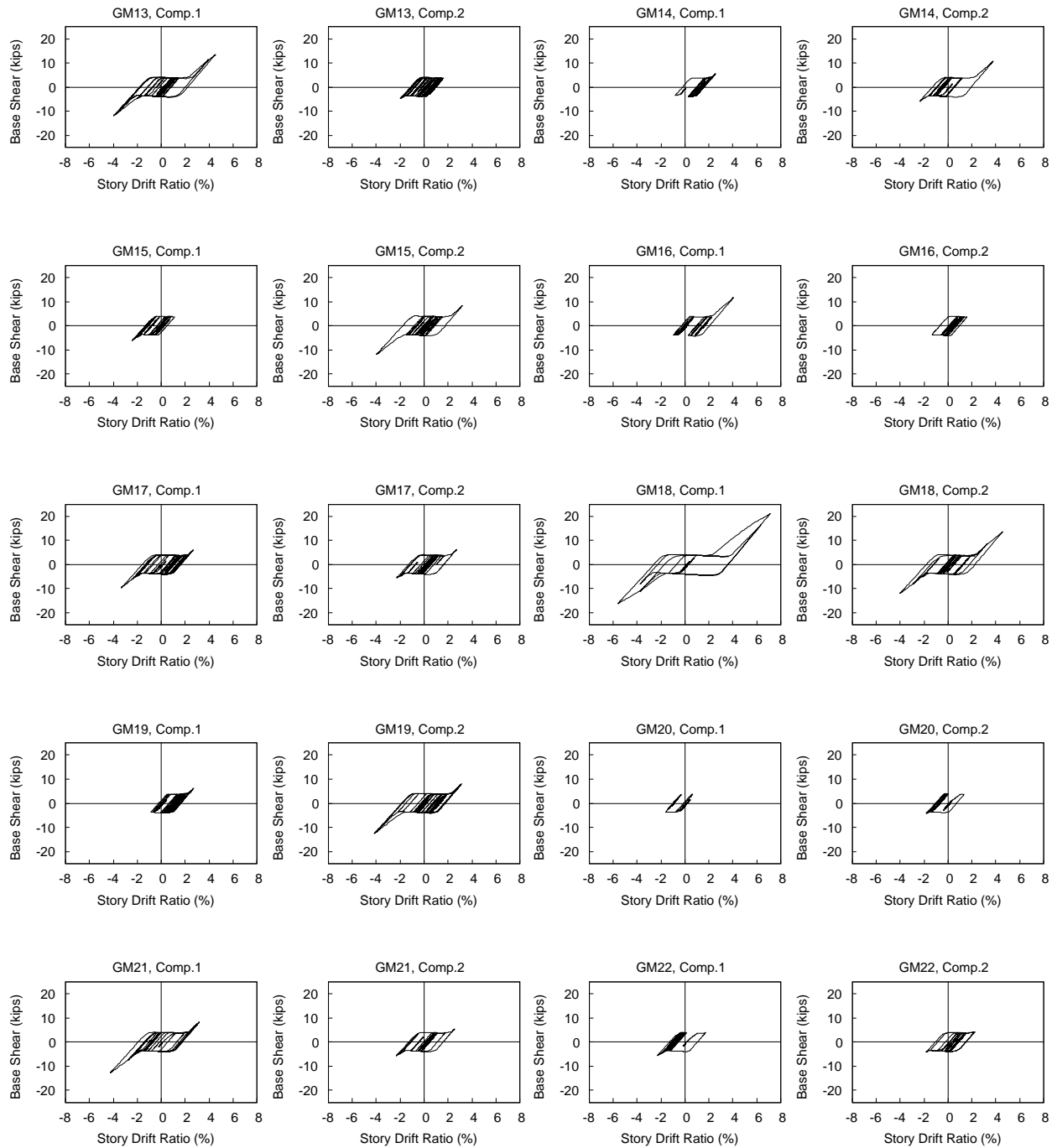


Figure B.3 Archetype 3 (DBE) (cont.)

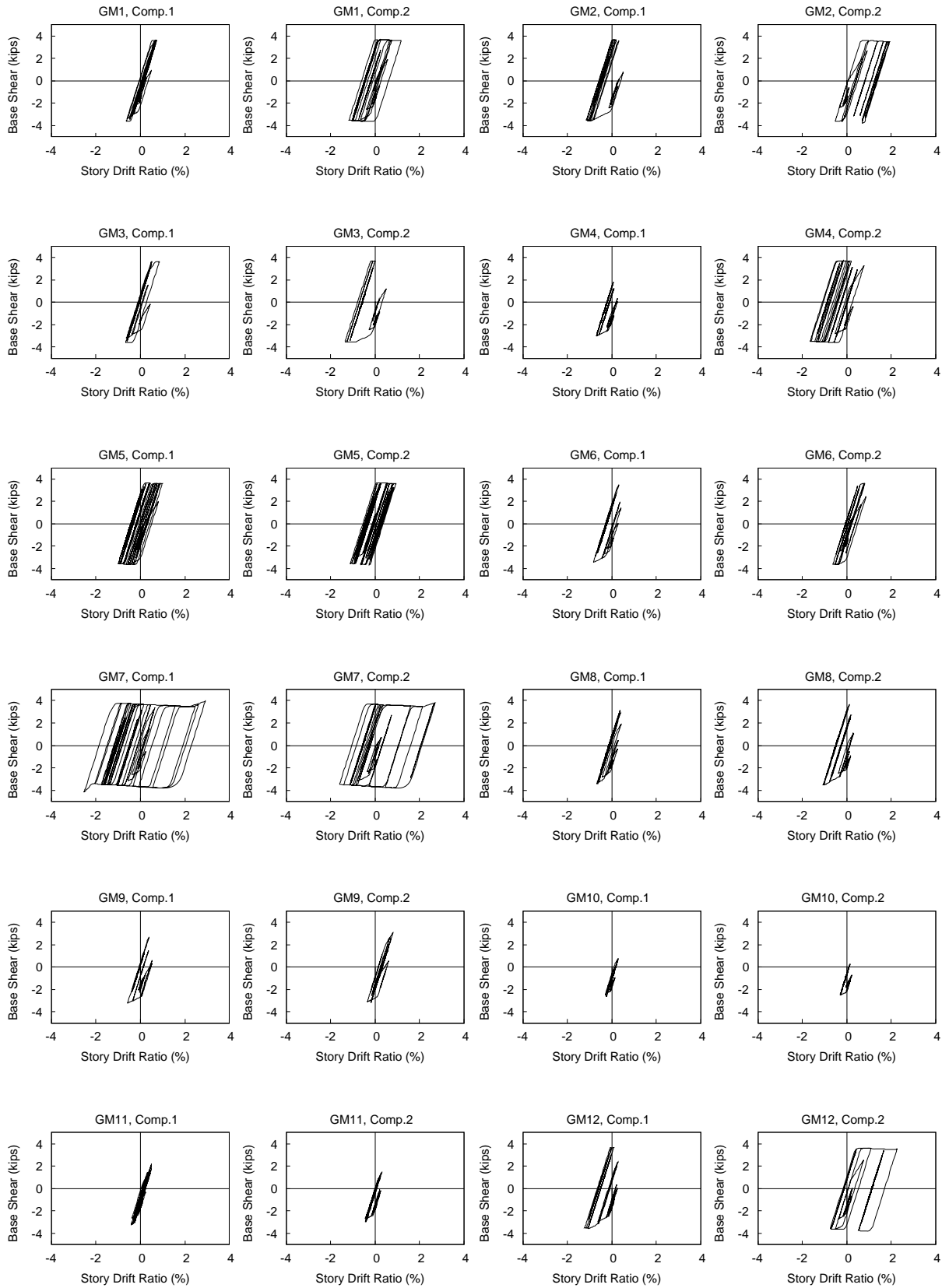


Figure B.4 Archetype 4 (DBE)

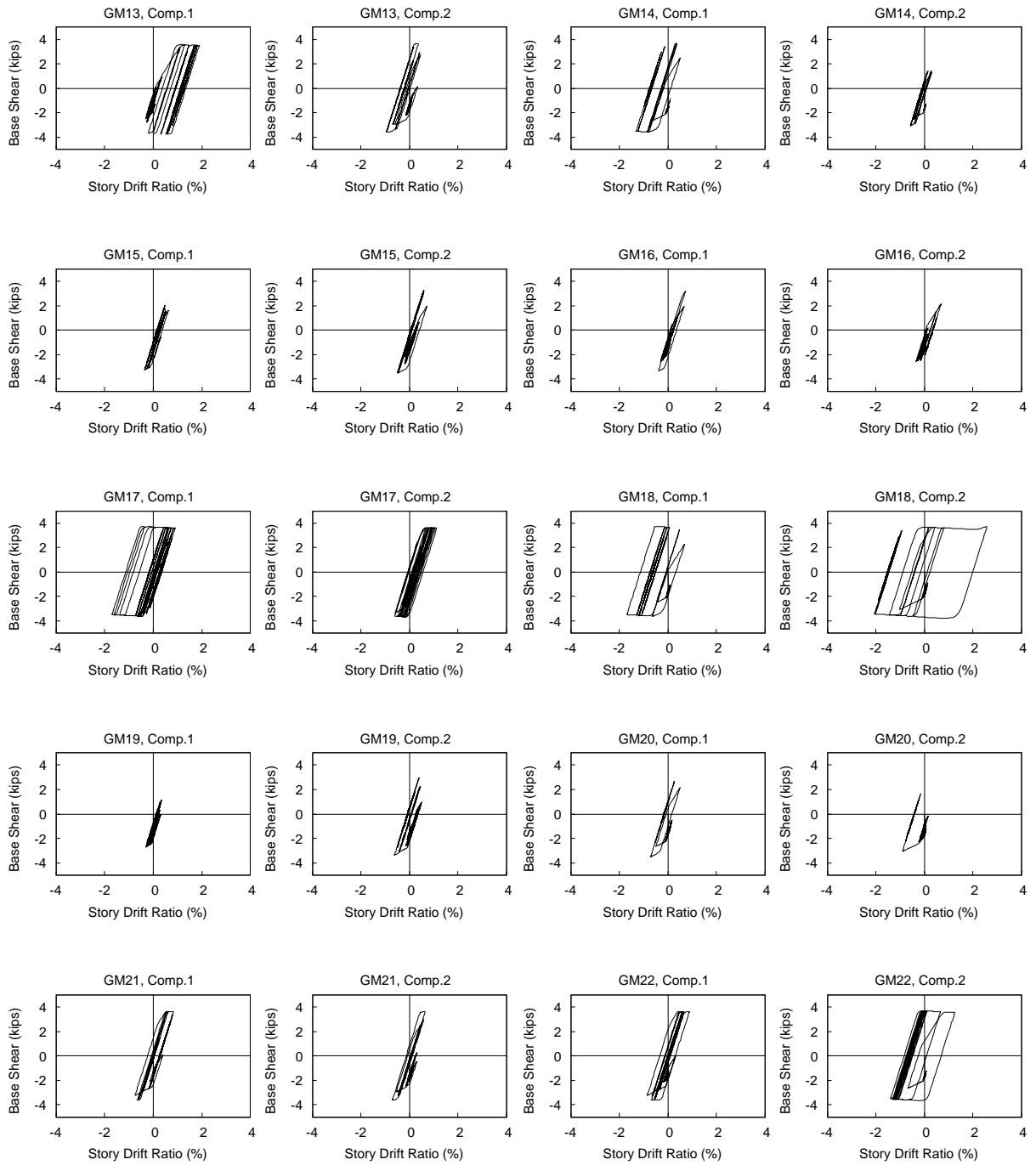


Figure B.4 Archetype 4 (DBE) (cont.)

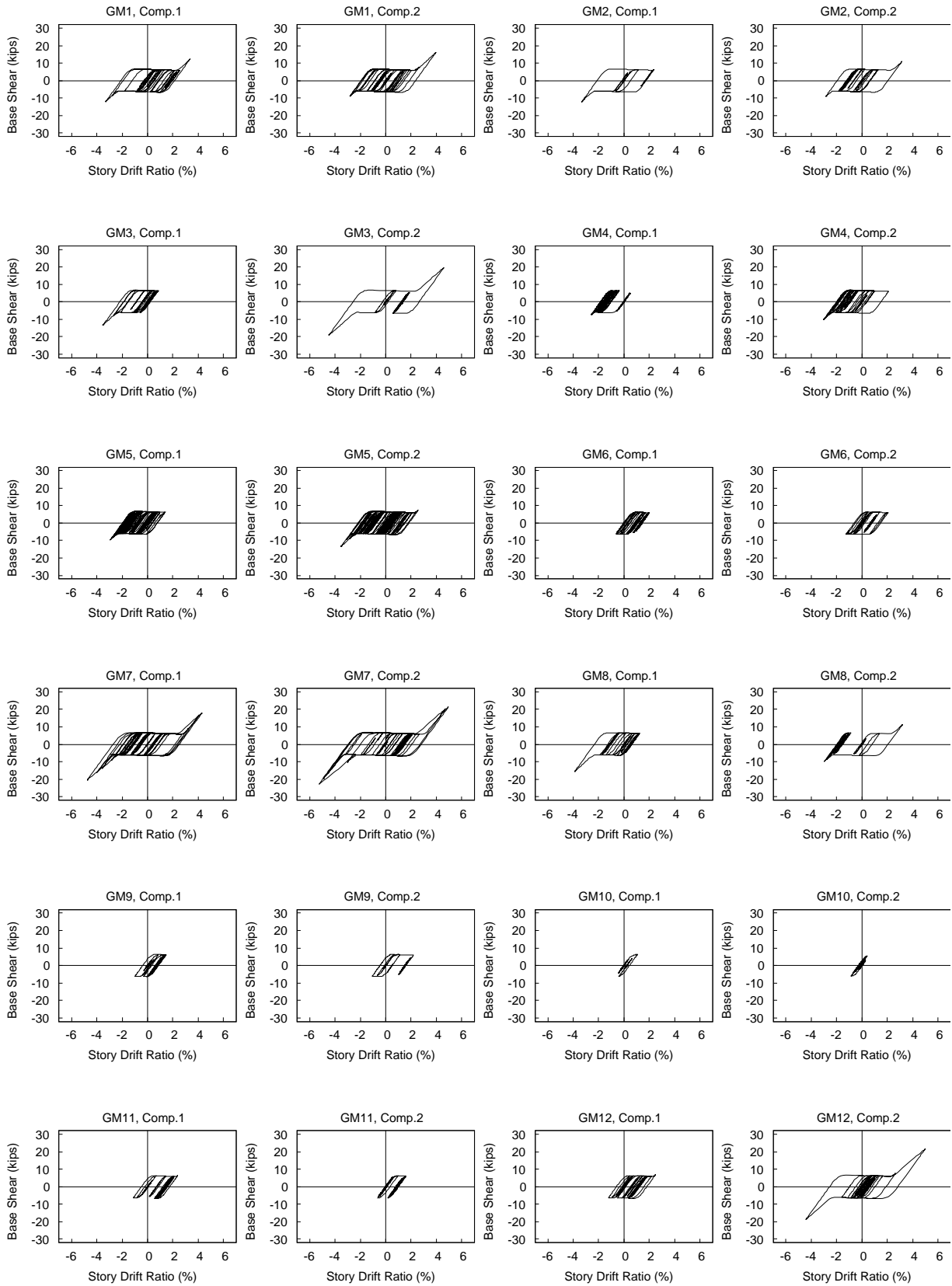


Figure B.5 Archetype 5 (DBE)

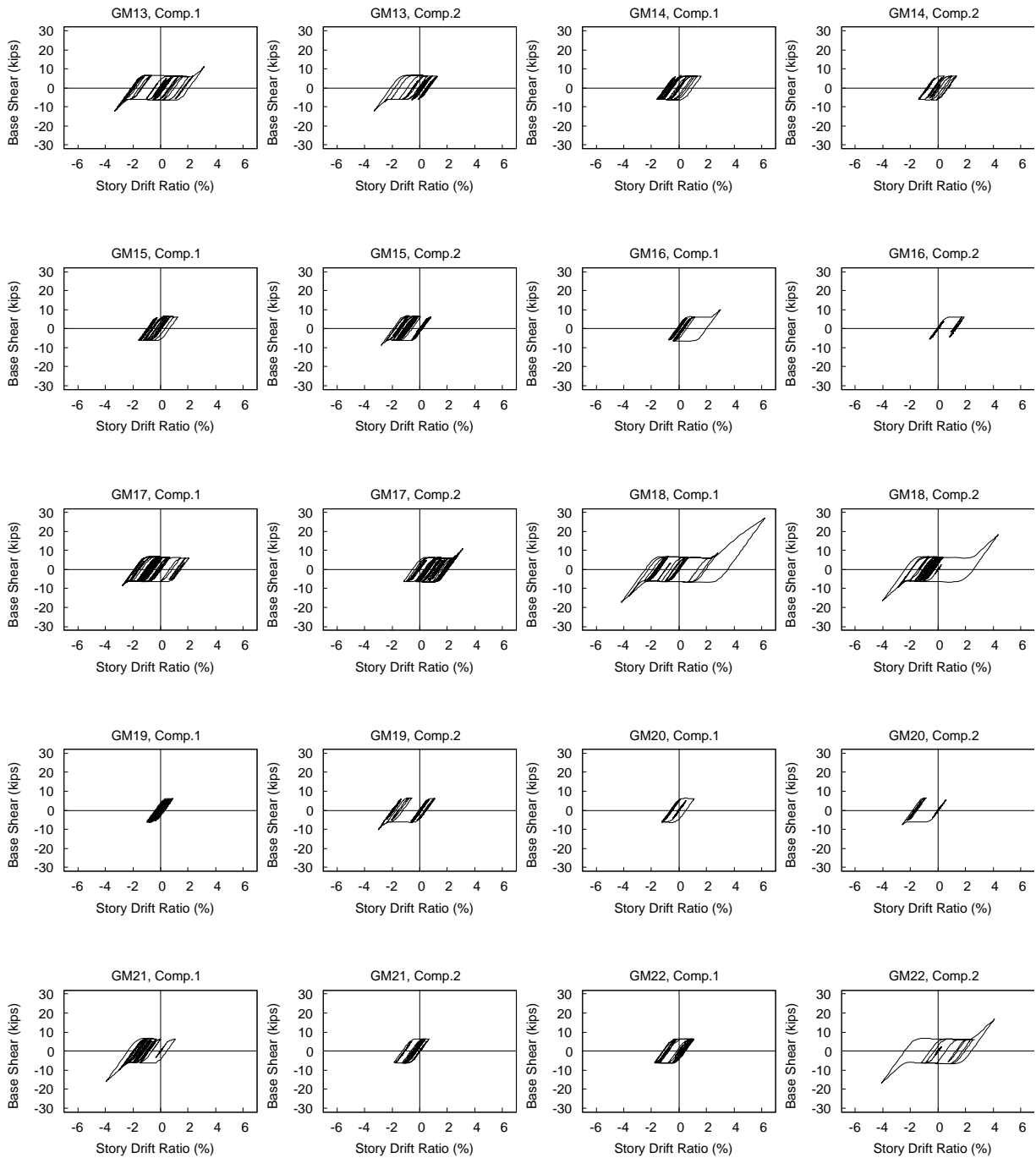


Figure B.5 Archetype 5 (DBE) (cont.)

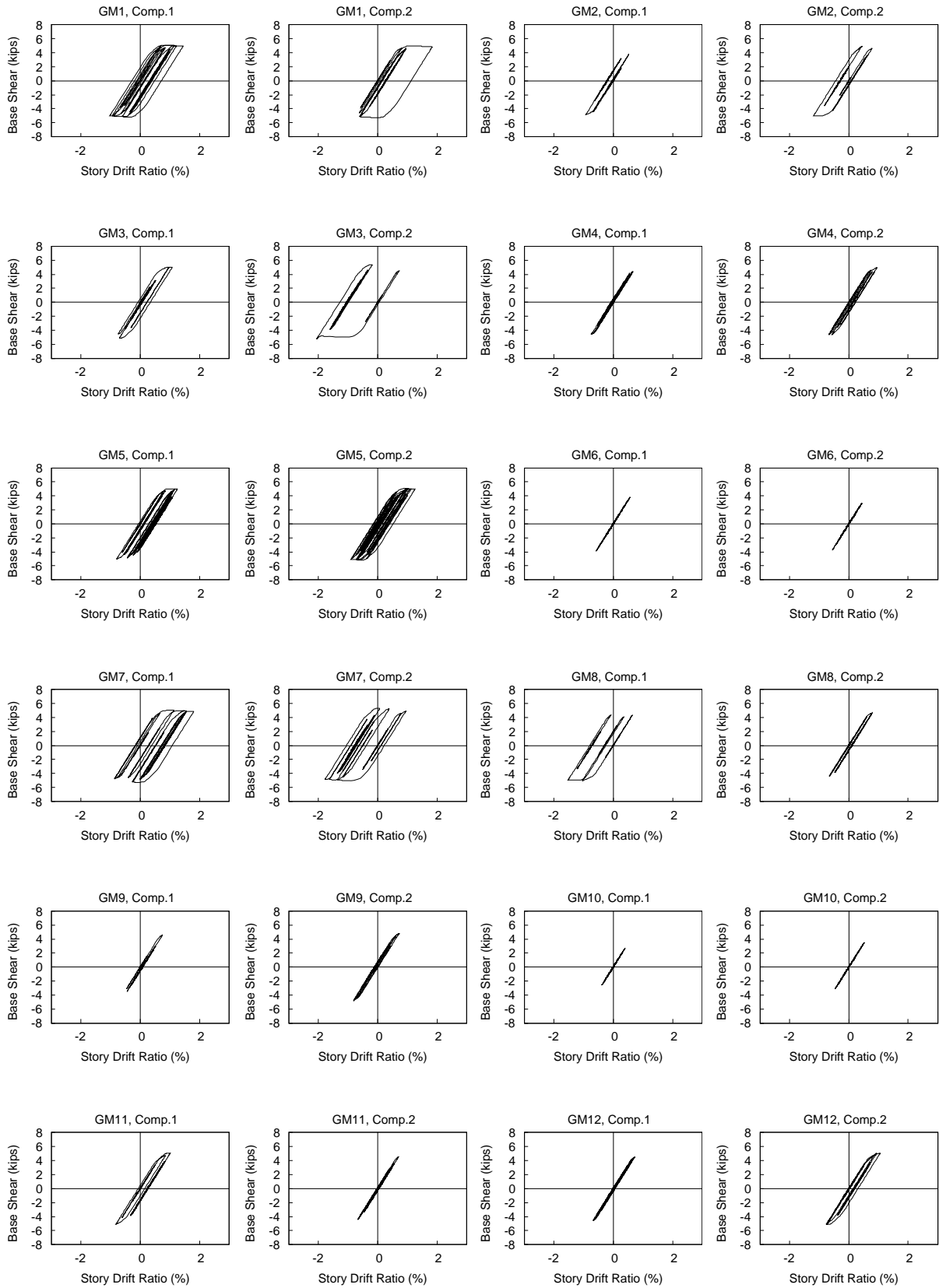


Figure B.6 Archetype 6 (DBE)

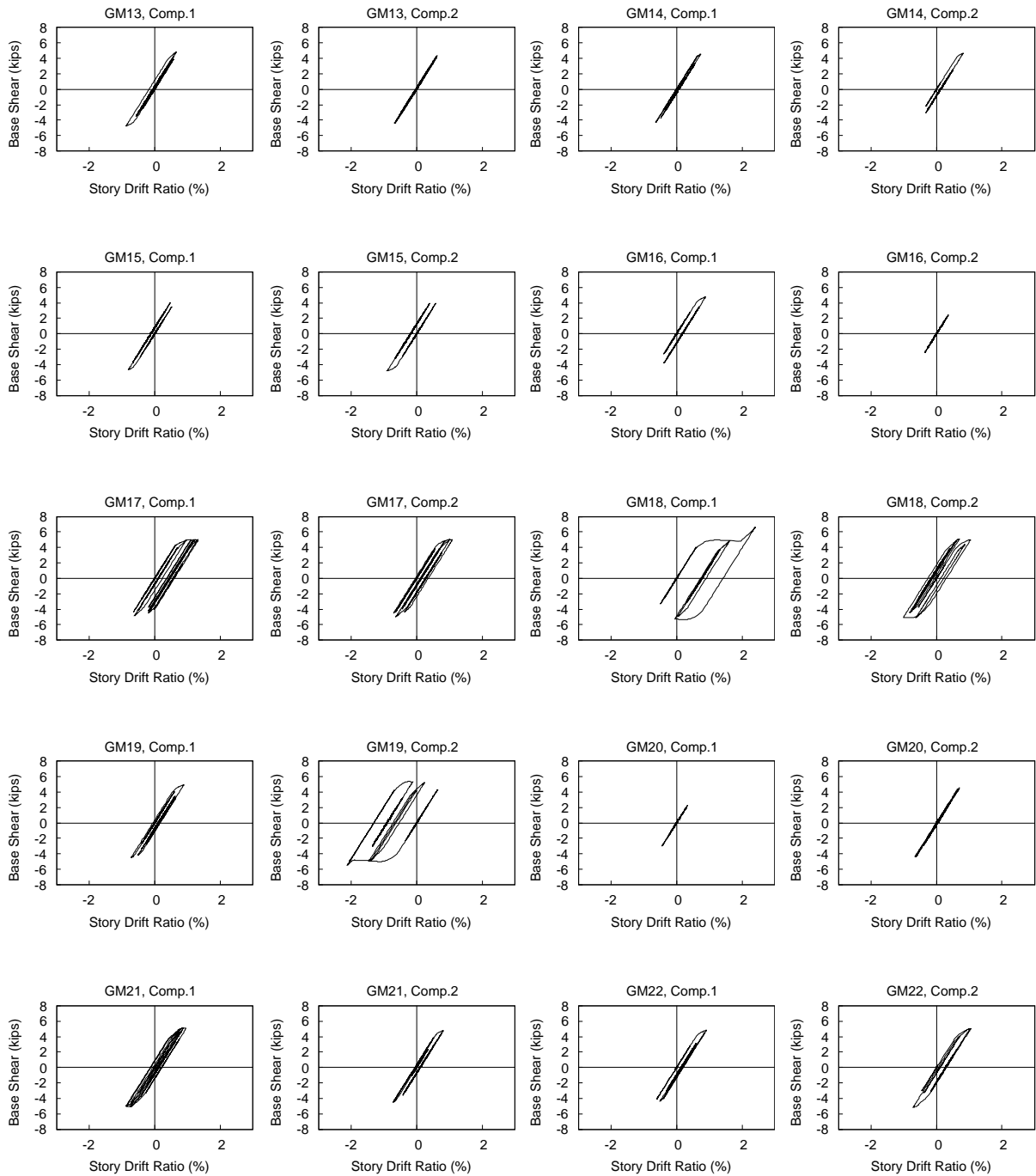


Figure B.6 Archetype 6 (DBE) (cont.)

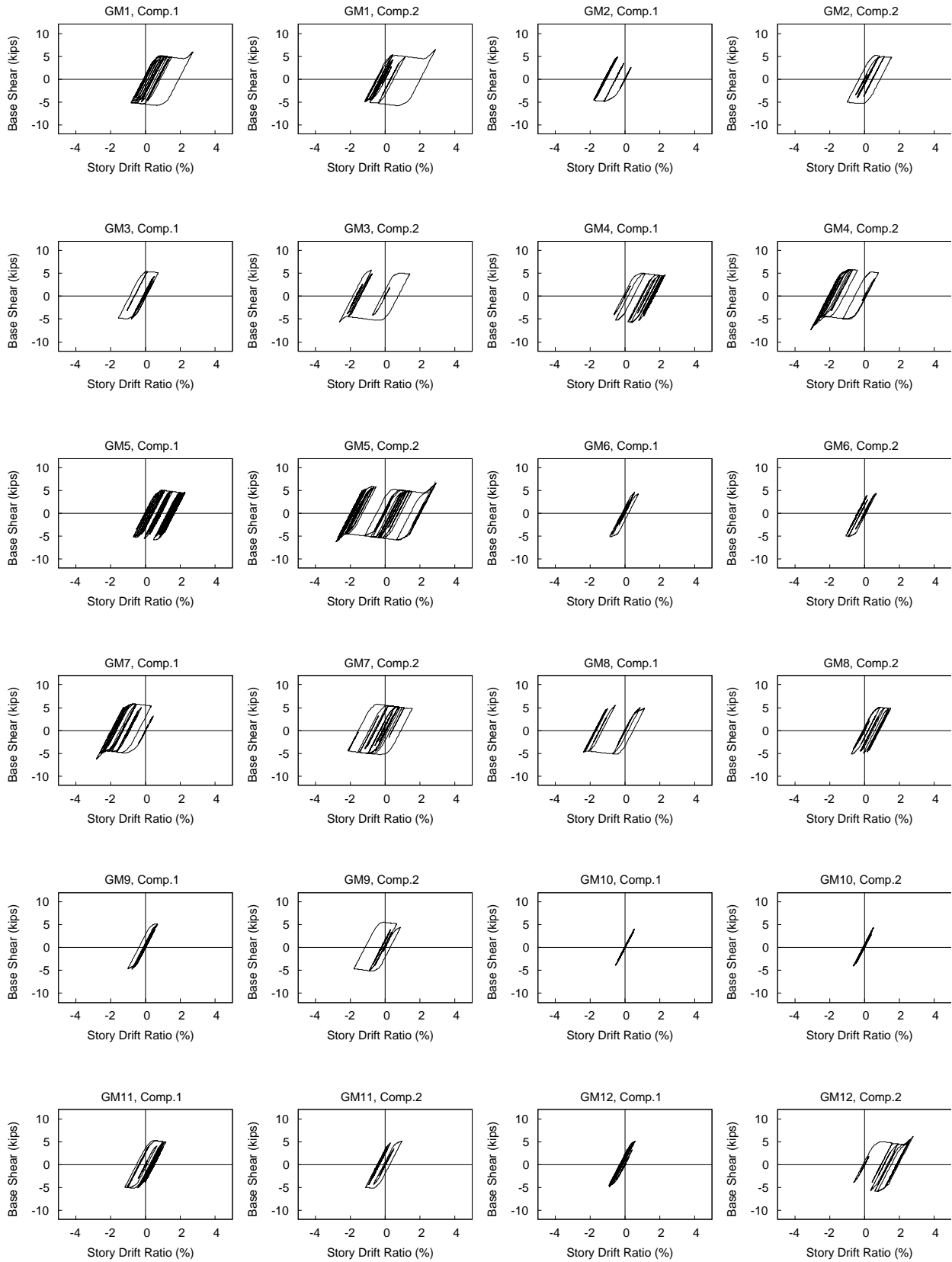


Figure B.7 Archetype 7 (DBE)

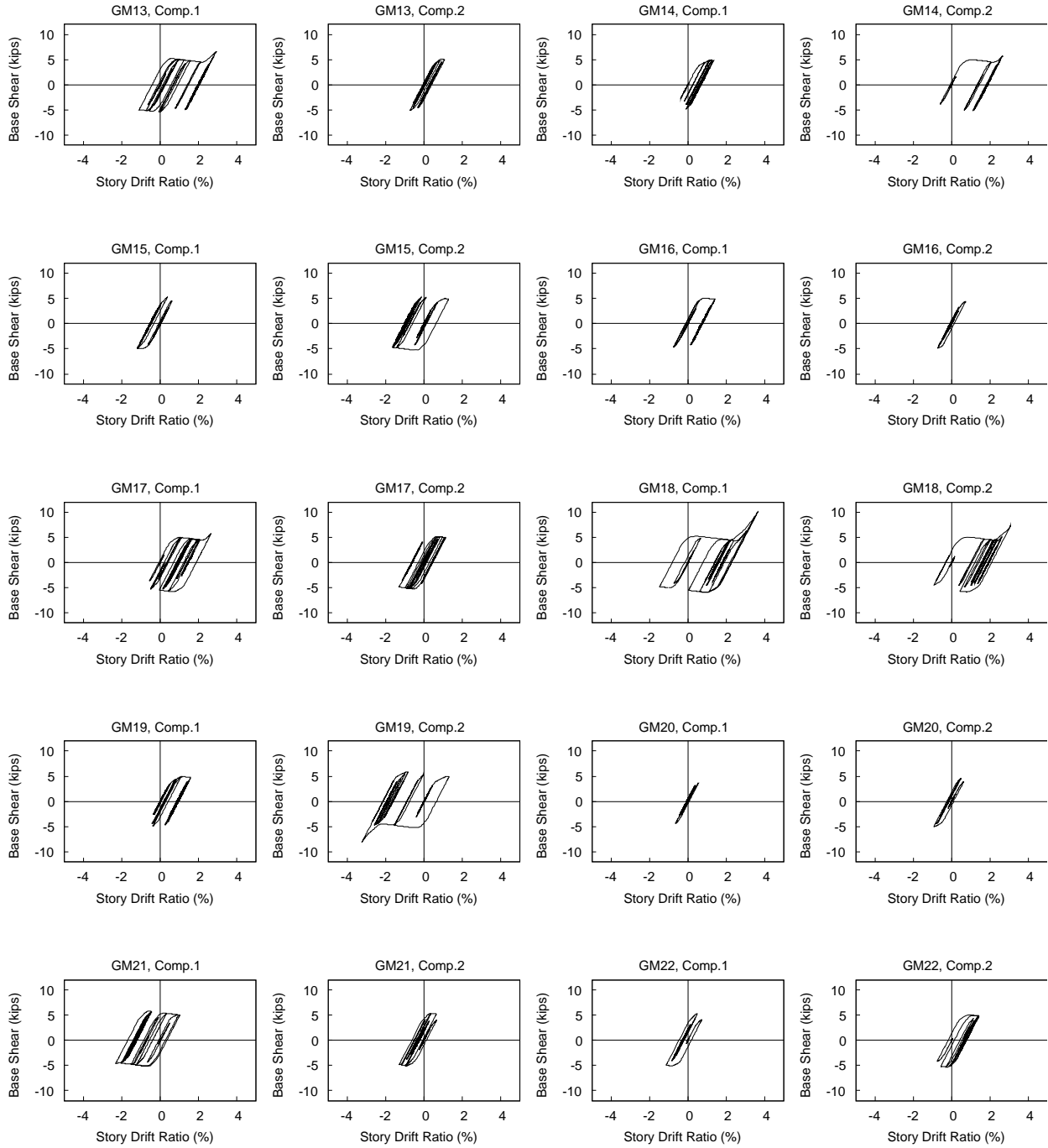


Figure B.7 Archetype 7 (DBE) (cont.)

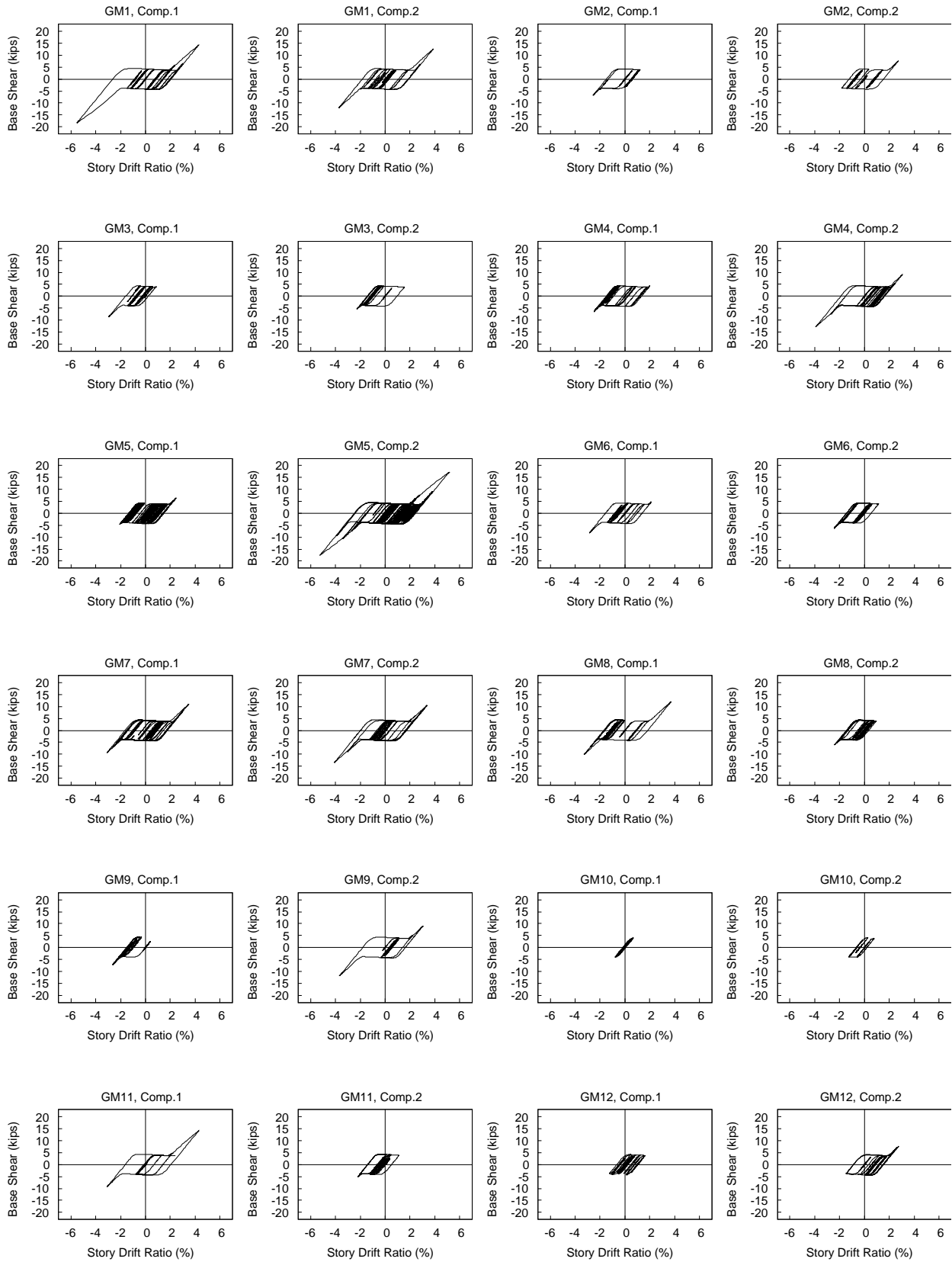


Figure B.8 Archetype 8 (DBE)

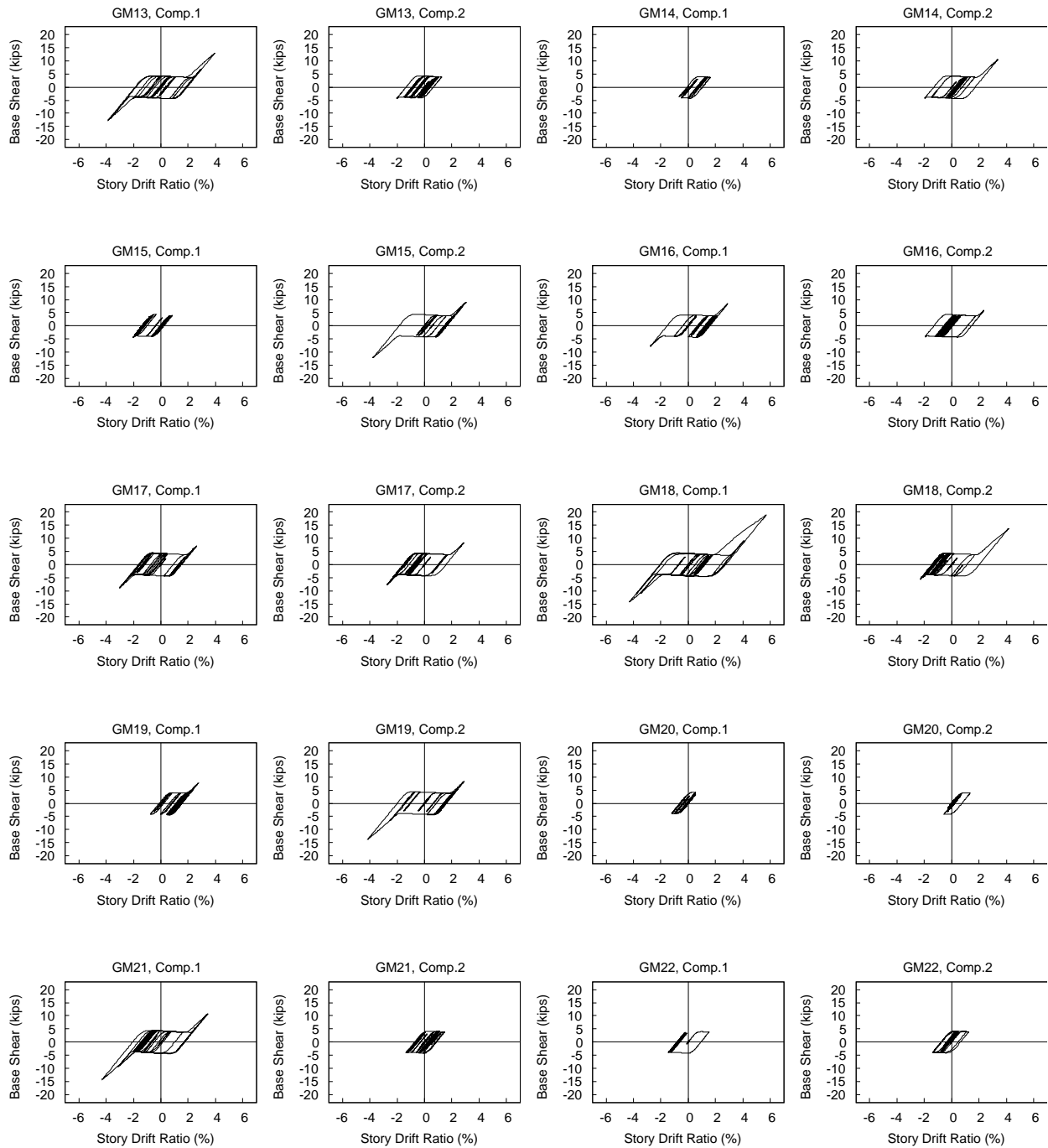


Figure B.8 Archetype 8 (DBE) (cont.)

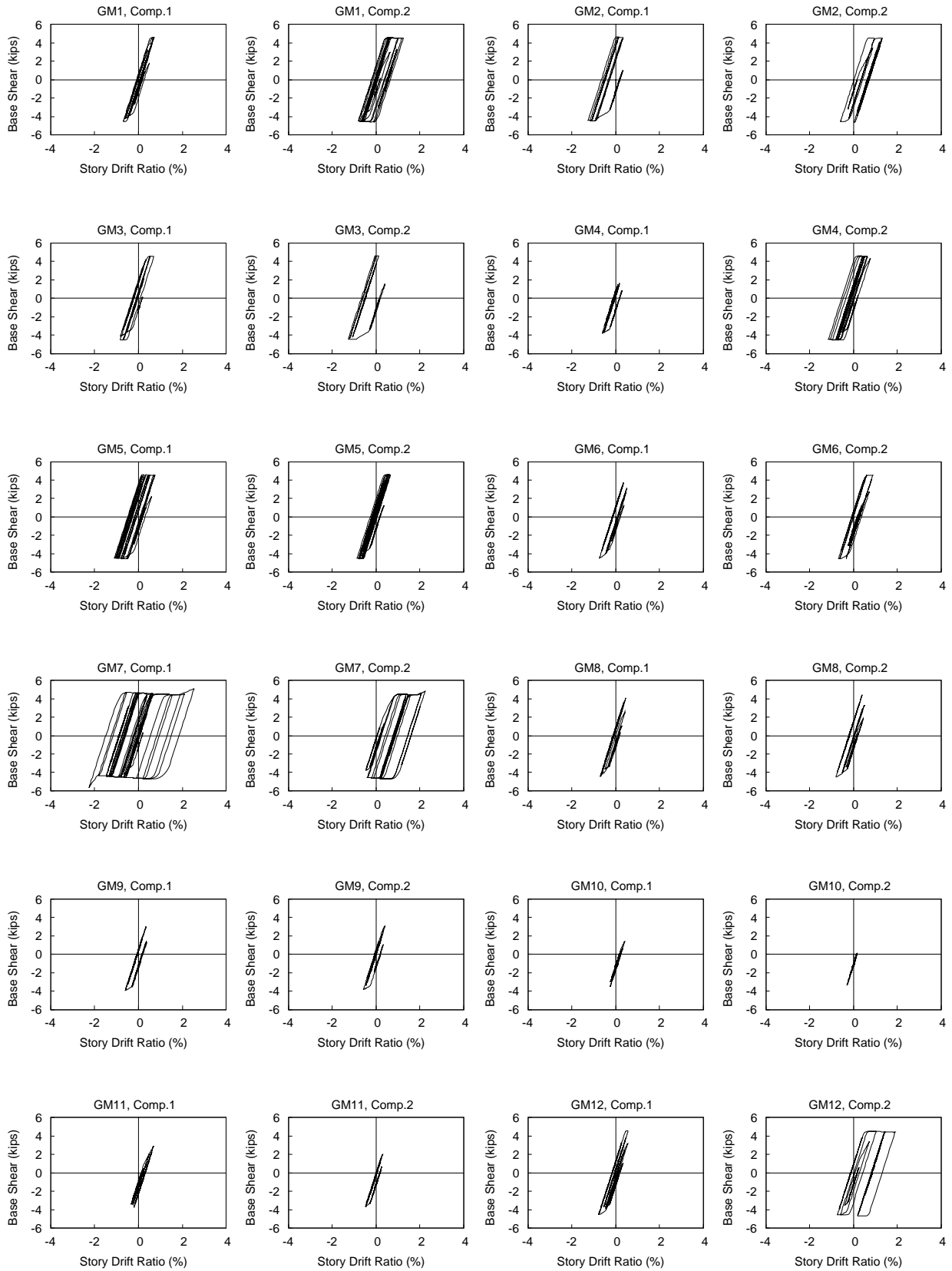


Figure B.9 Archetype 9 (DBE)

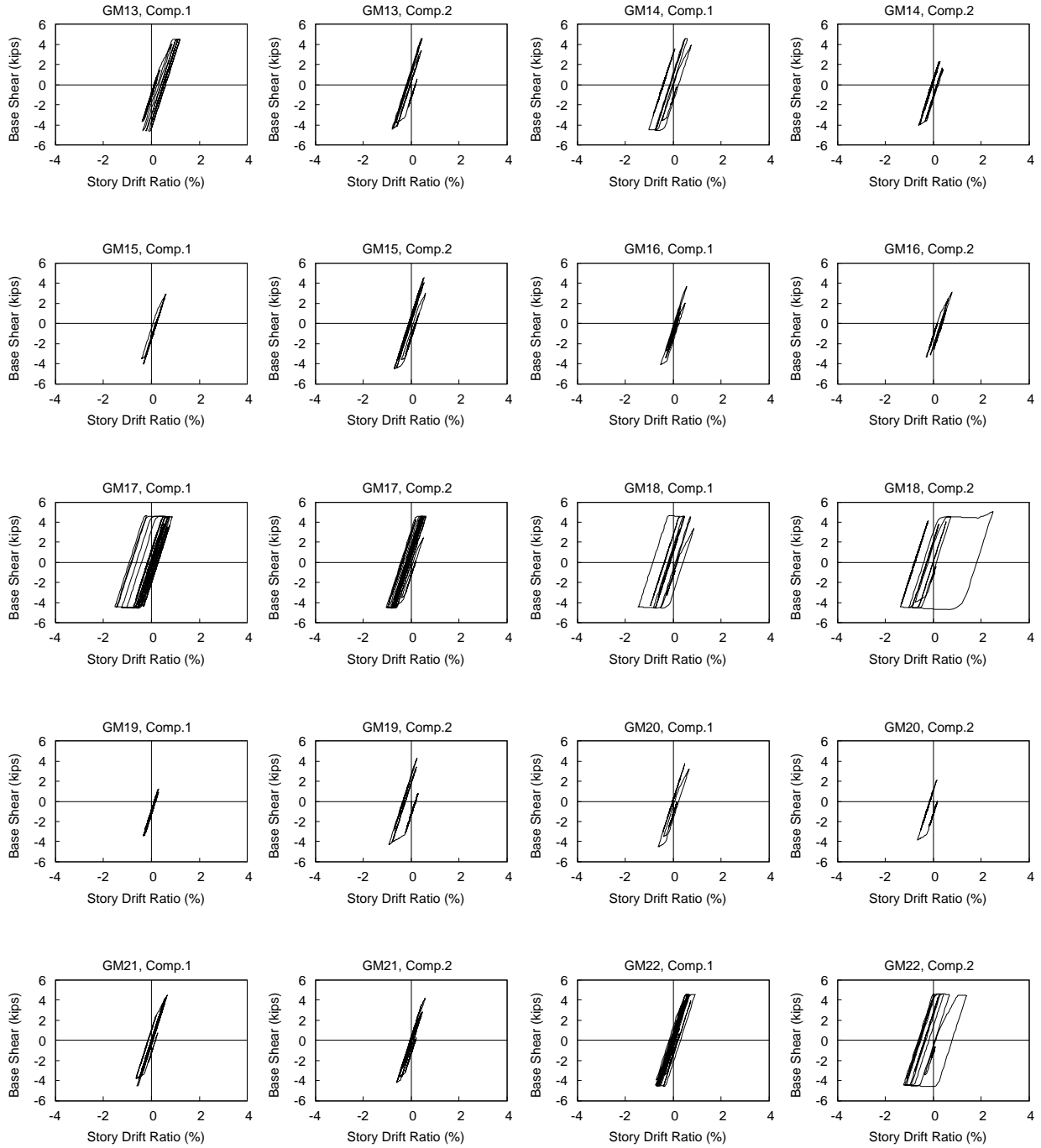


Figure B.9 Archetype 9 (DBE) (cont.)

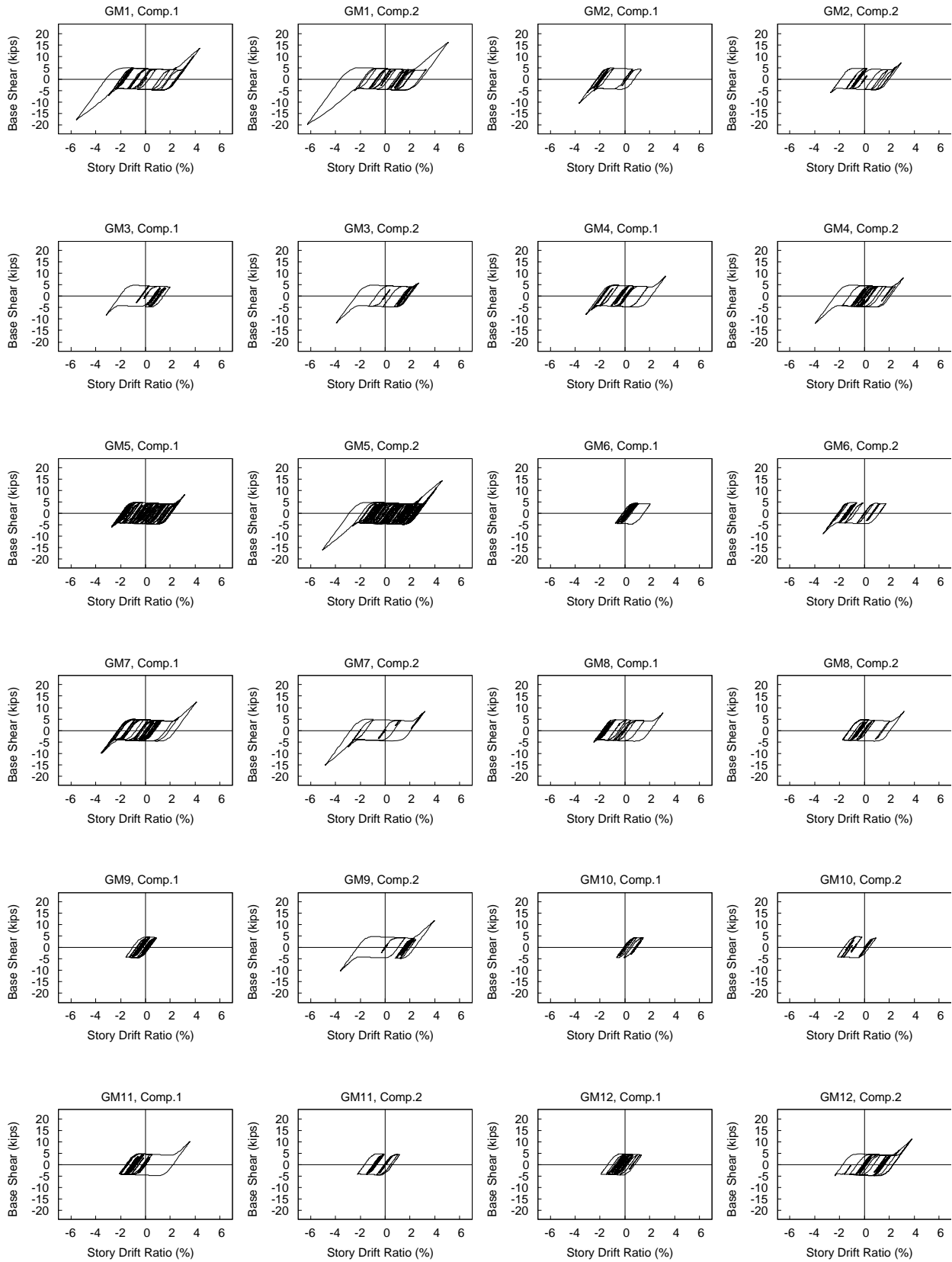


Figure B.10 Archetype 10 (DBE)

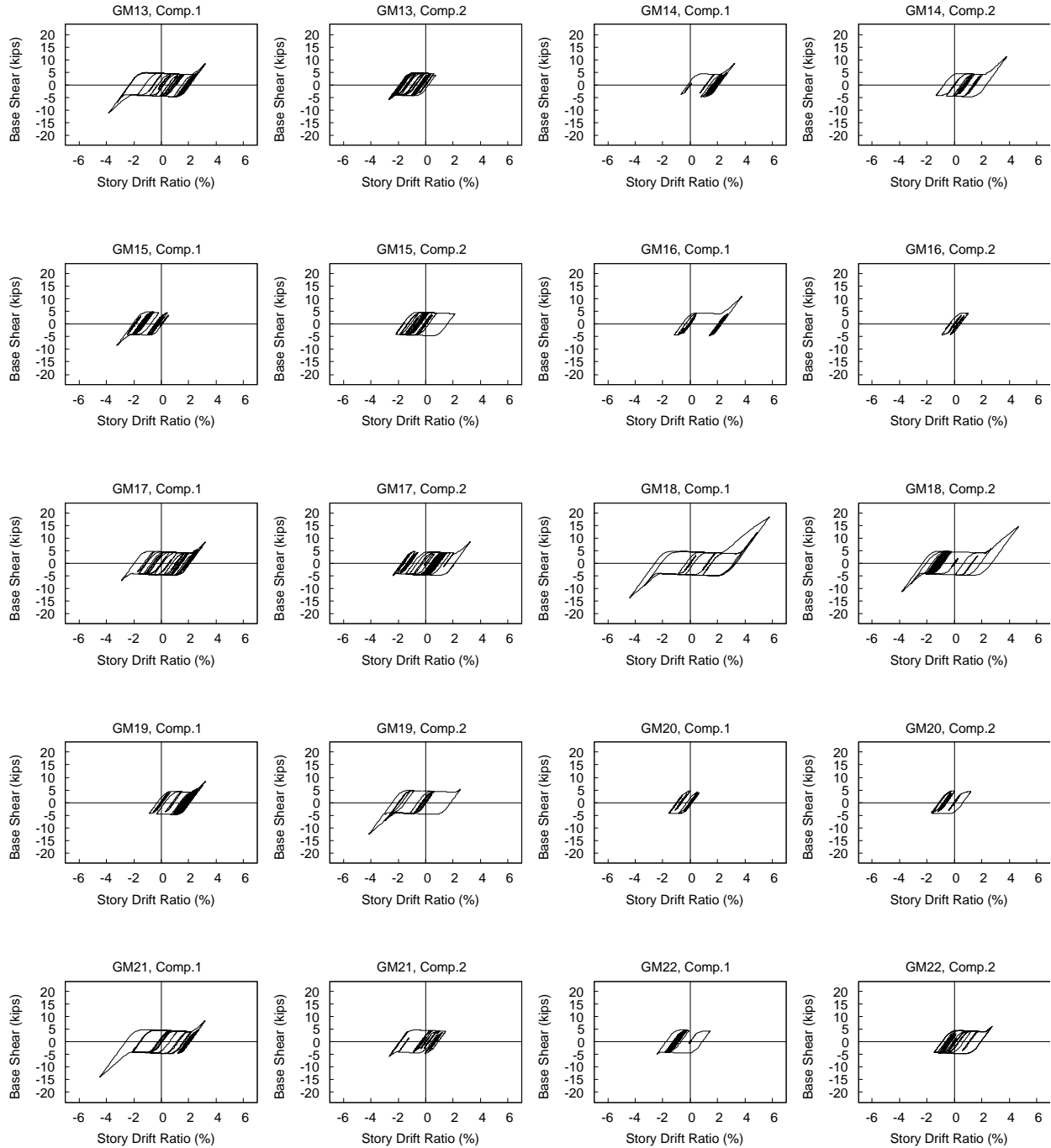


Figure B.10 Archetype 10 (DBE) (cont.)

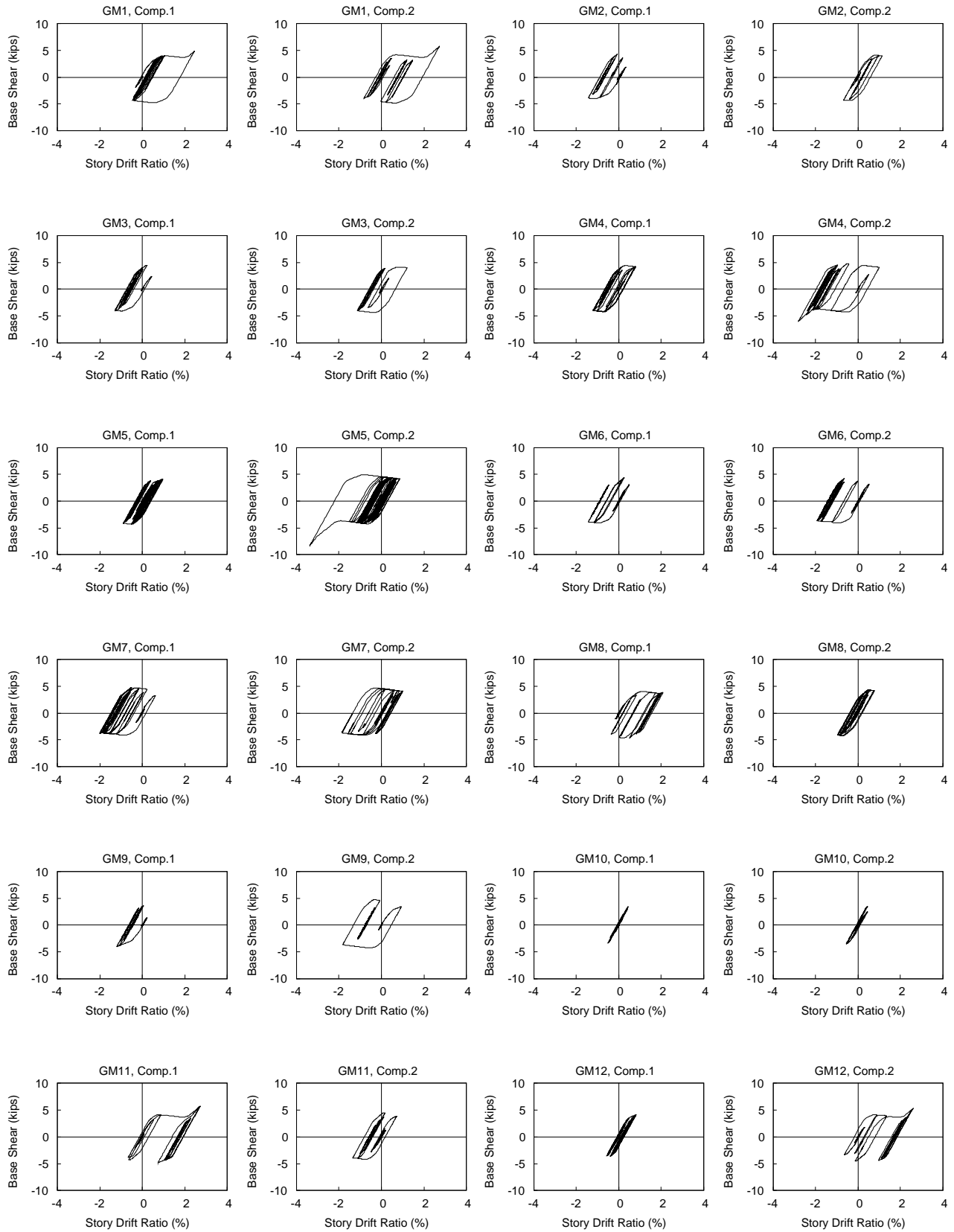


Figure B.11 Archetype 11 (DBE)

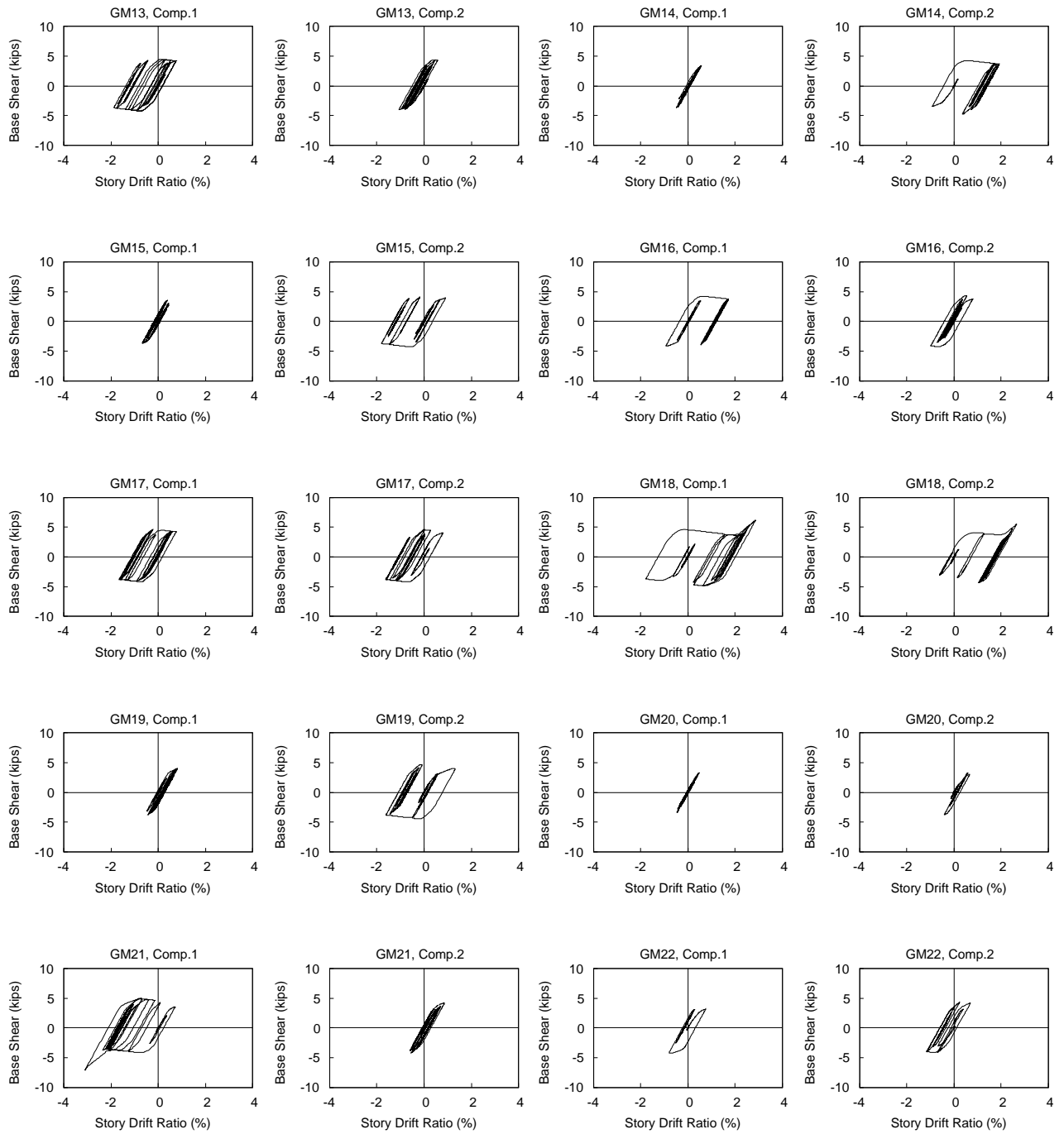


Figure B.11 Archetype 11 (DBE) (cont.)

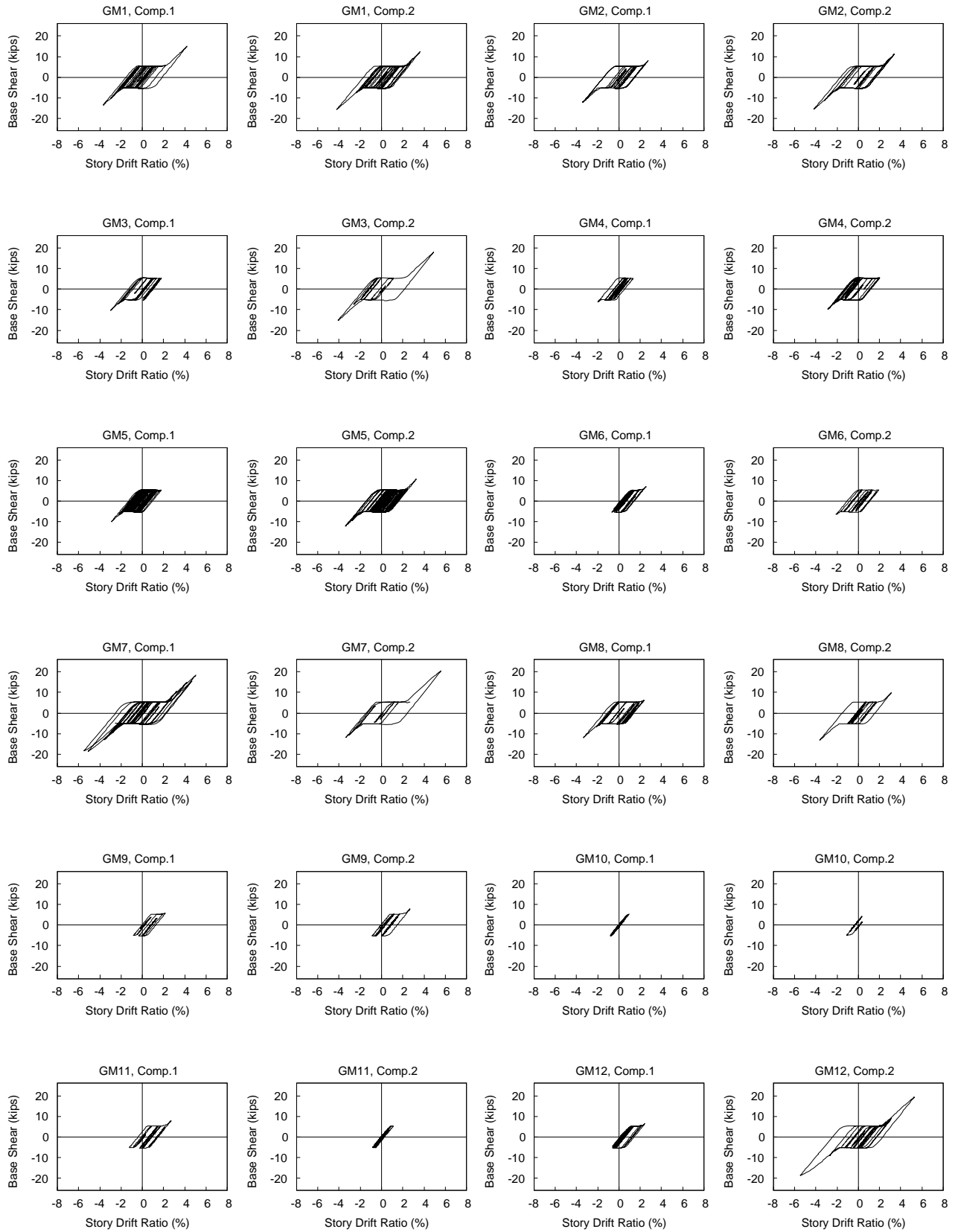


Figure B.12 Archetype 12 (DBE)

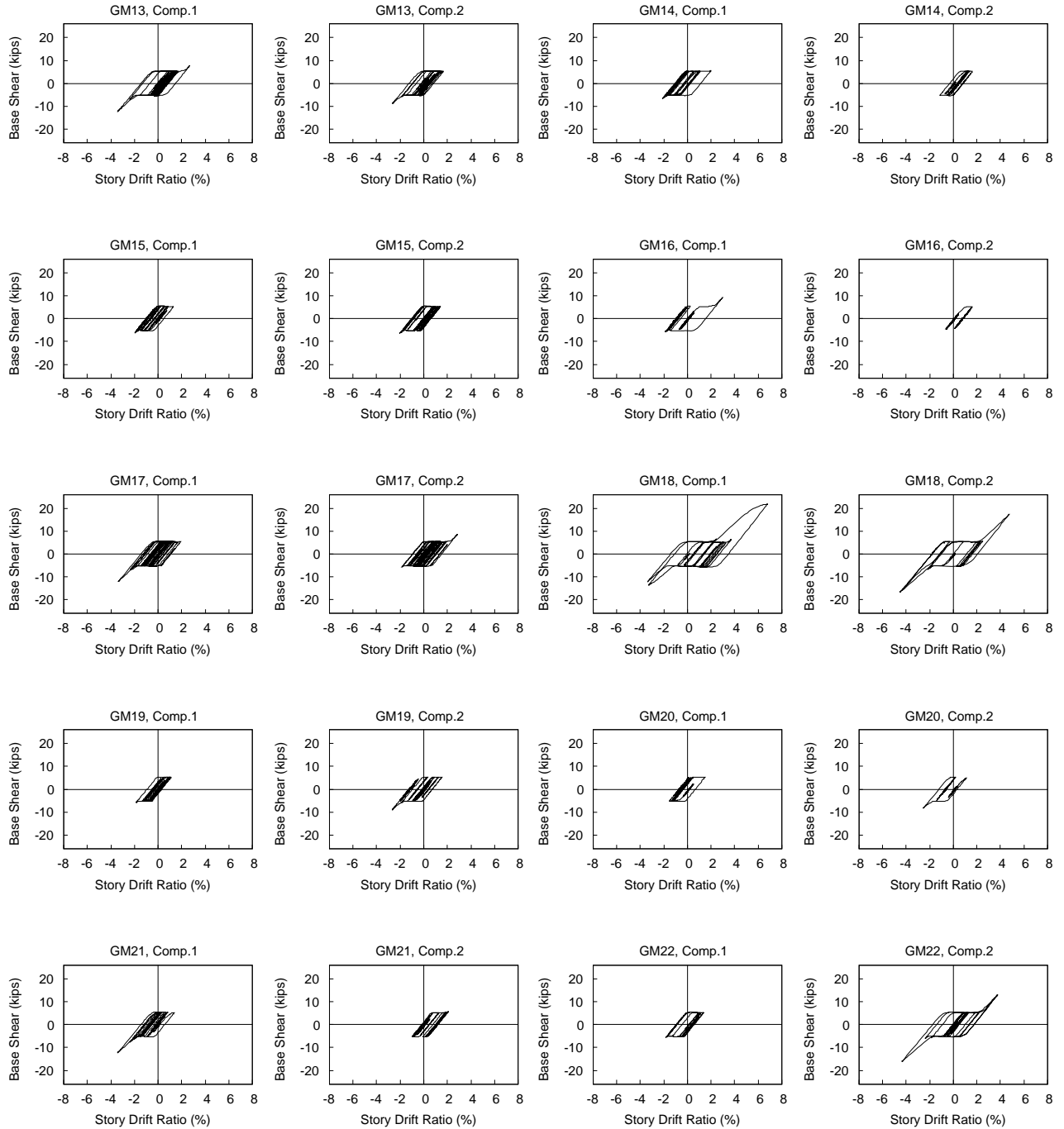


Figure B.12 Archetype 12 (DBE) (cont.)

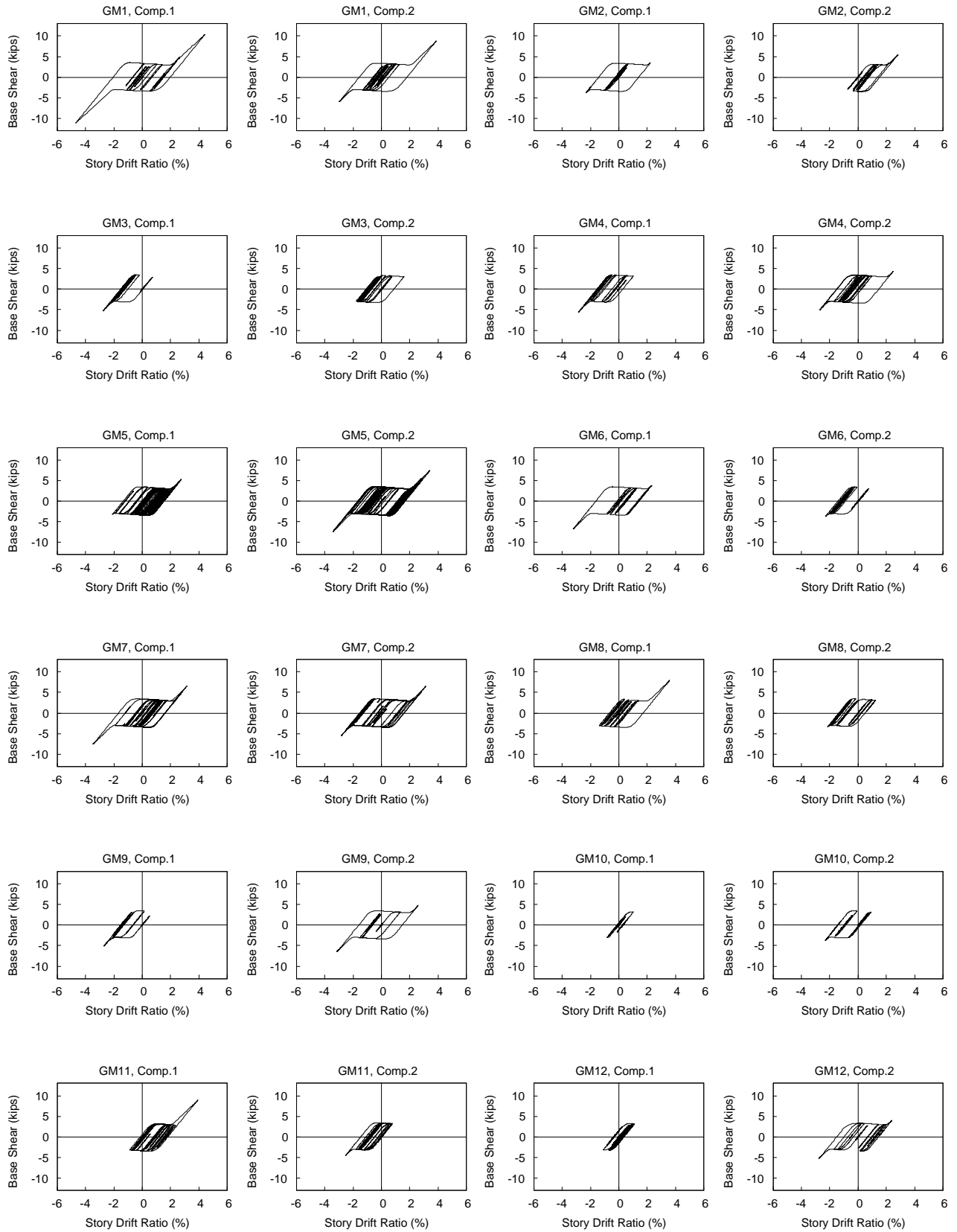


Figure B.13 Archetype 13 (DBE)

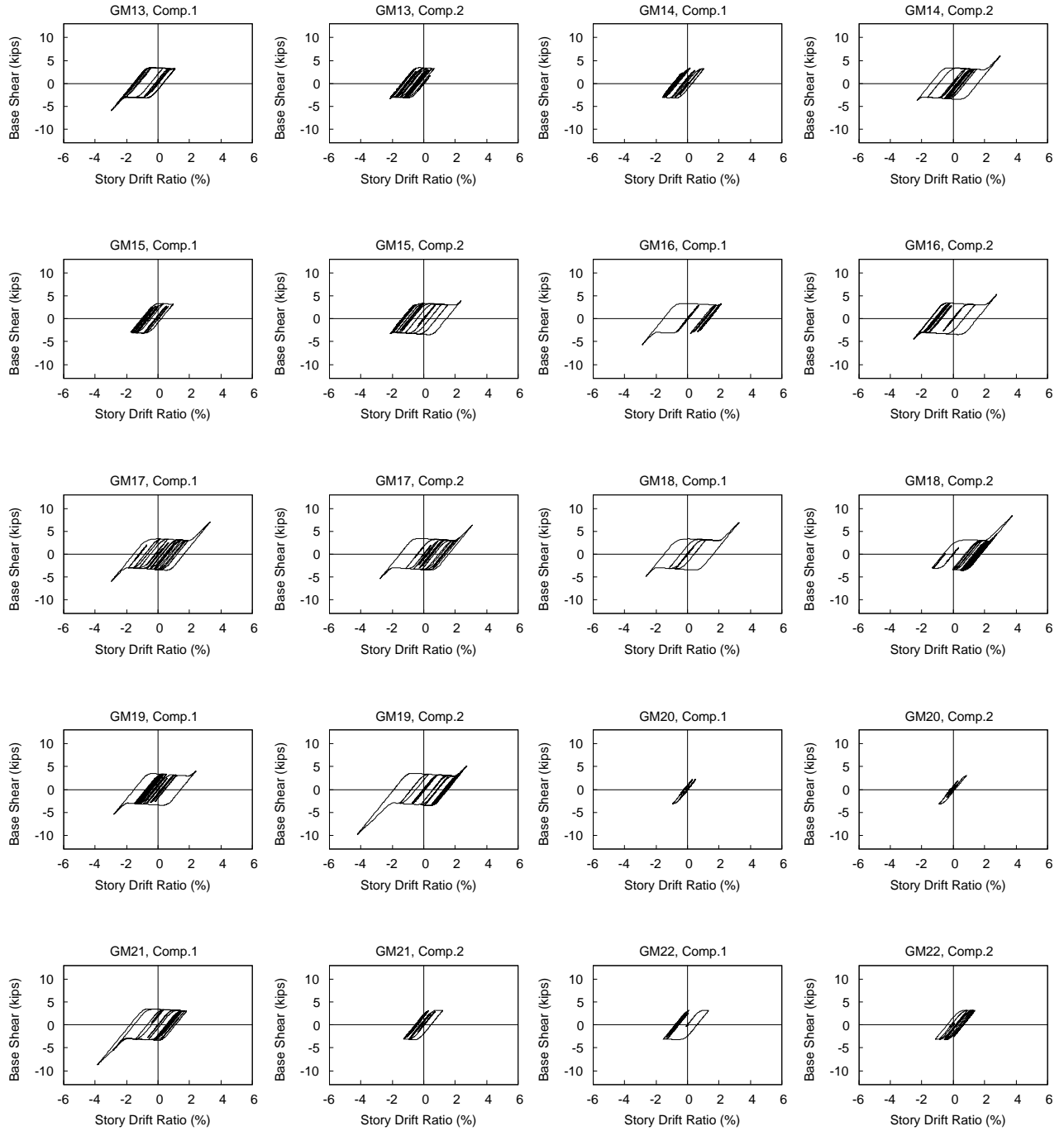
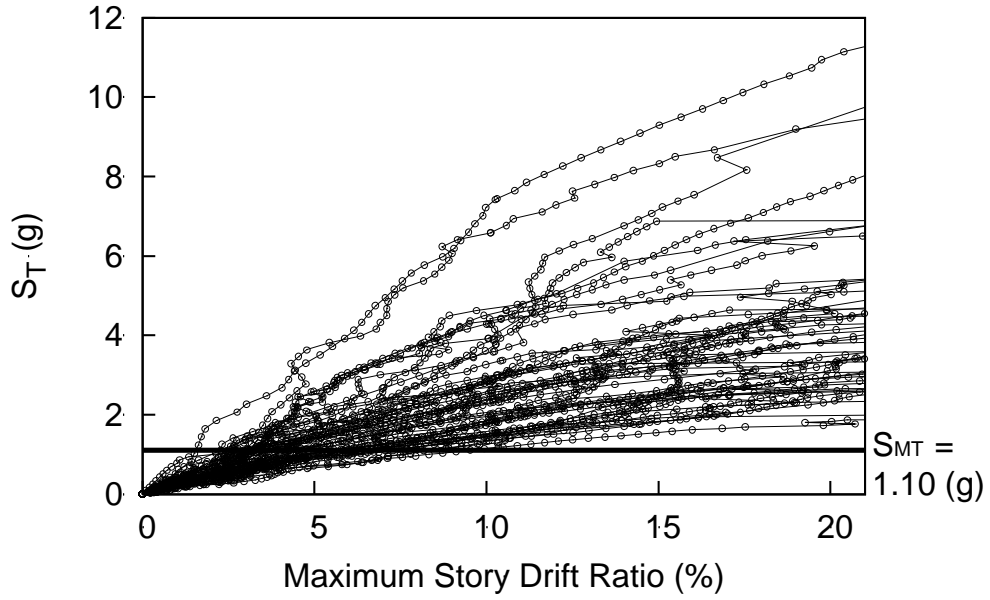
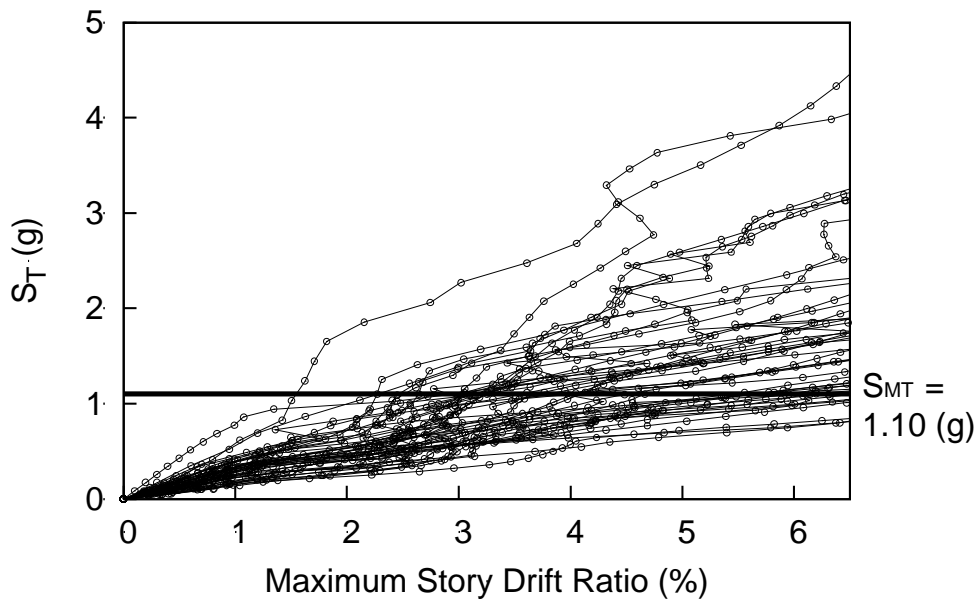


Figure B.13 Archetype 13 (DBE) (cont.)

APPENDIX C: Incremental Dynamic Analysis Results



(a) Story Drift Ratio up to 20%



(a) Close-up Story Drift Ratio 6%

Figure C.1 Archetype 1

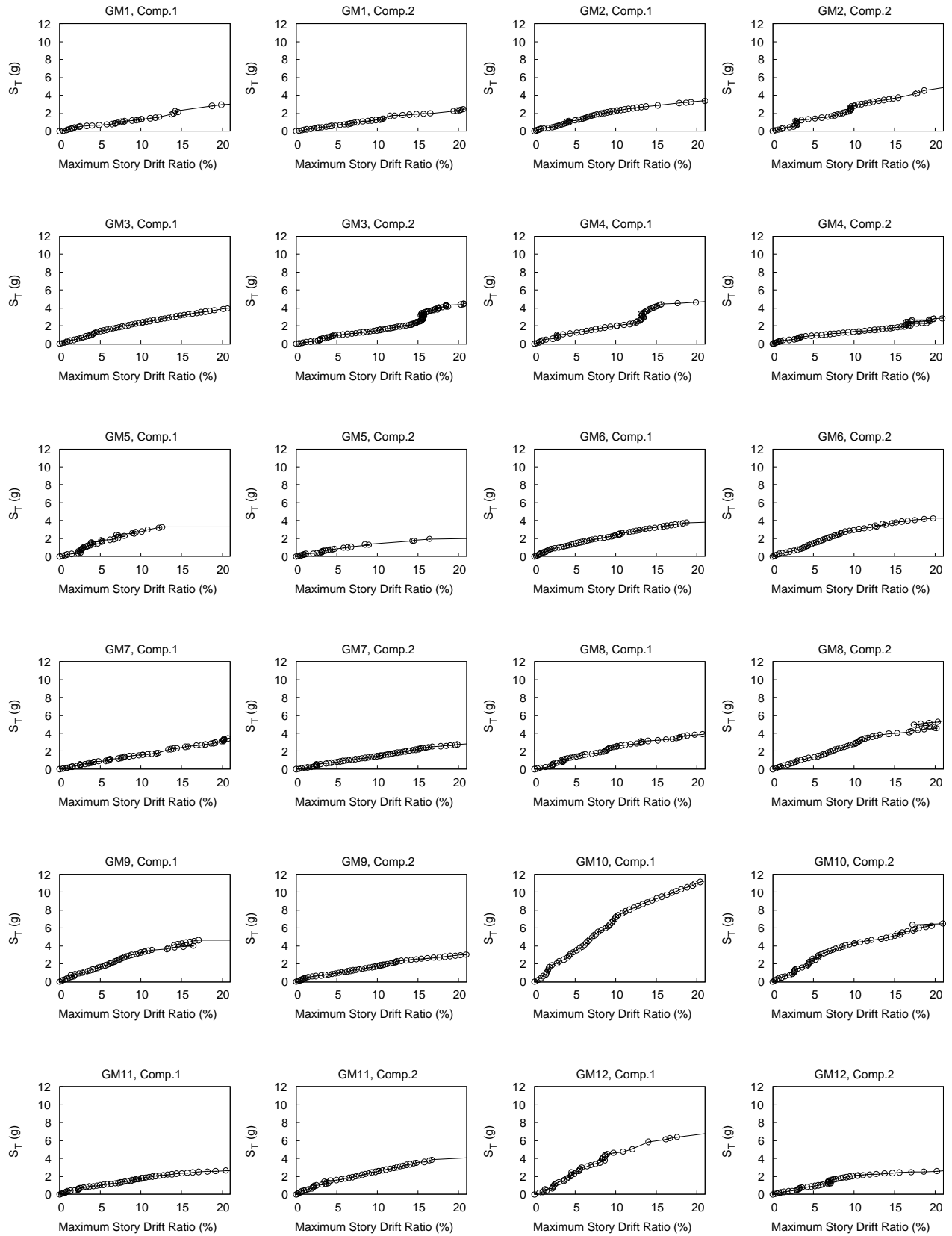


Figure C.2 Archetype 1

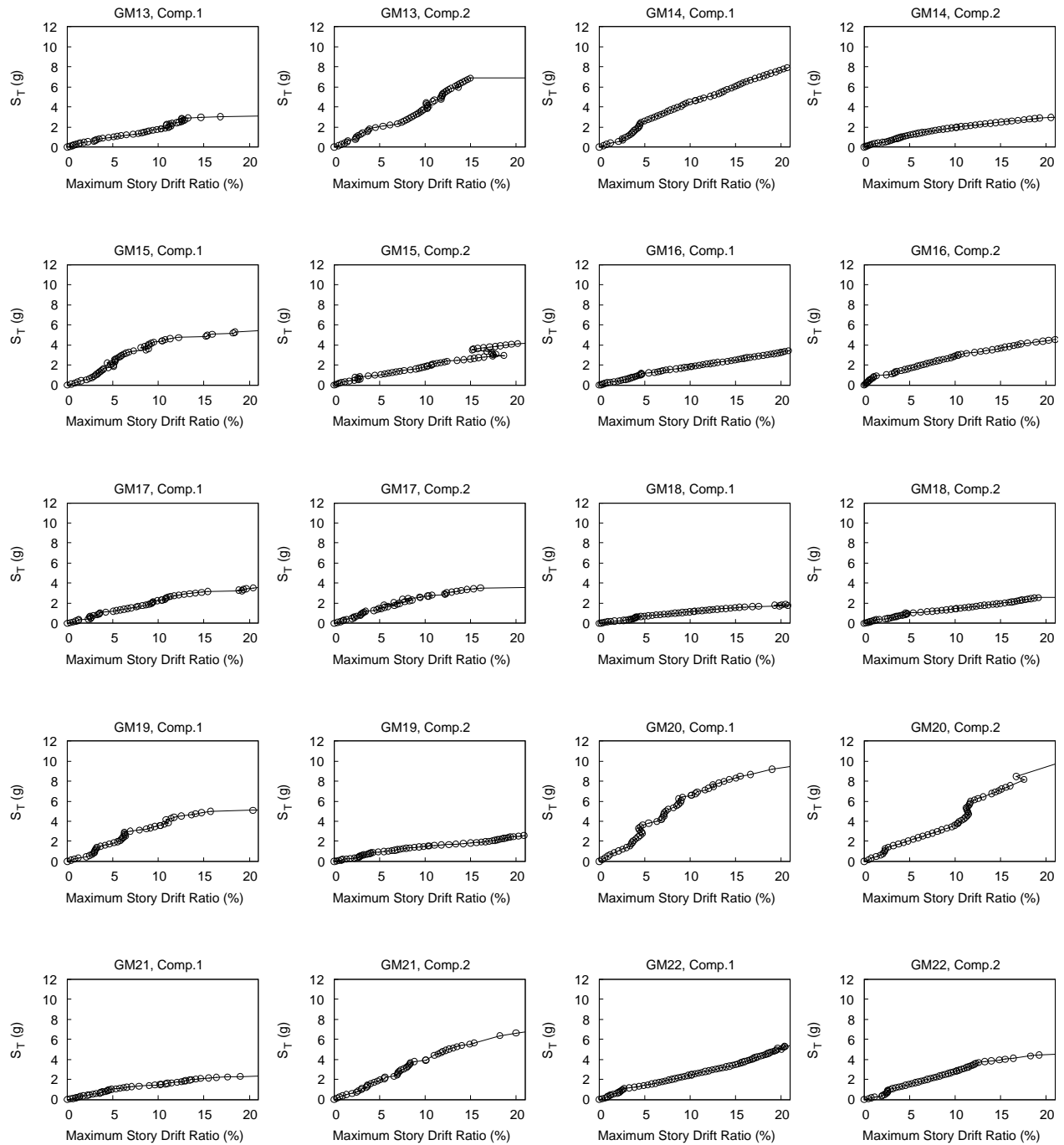
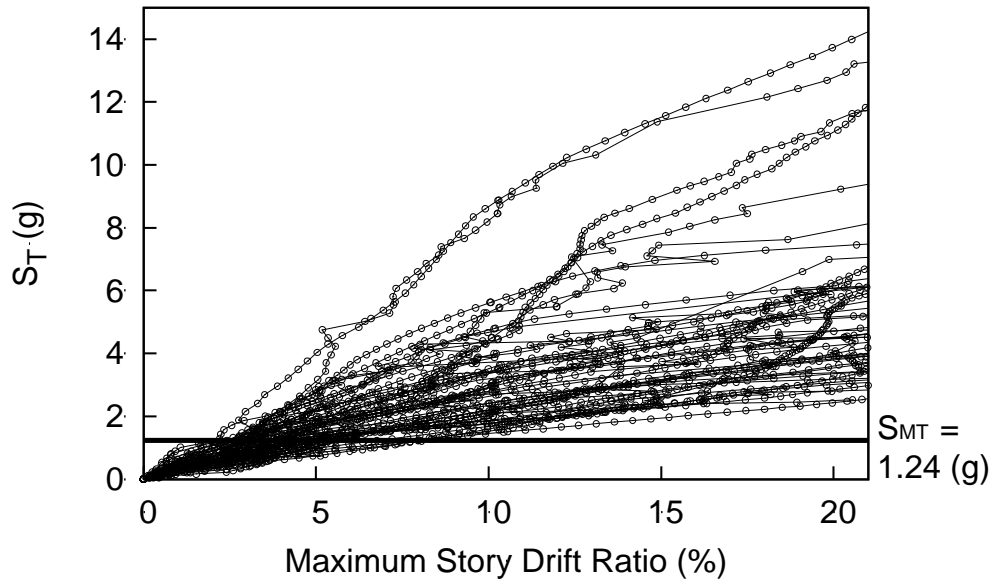
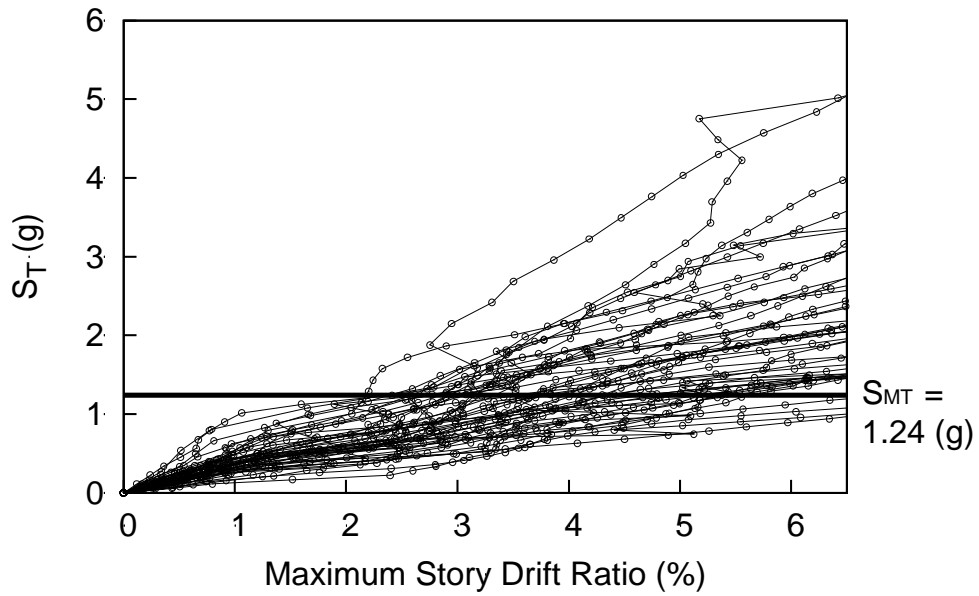


Figure C.2 Archetype 1 (cont.)



(a) Story Drift Ratio up to 20%



(a) Close-up Story Drift Ratio 6%

Figure C.3 Archetype 2

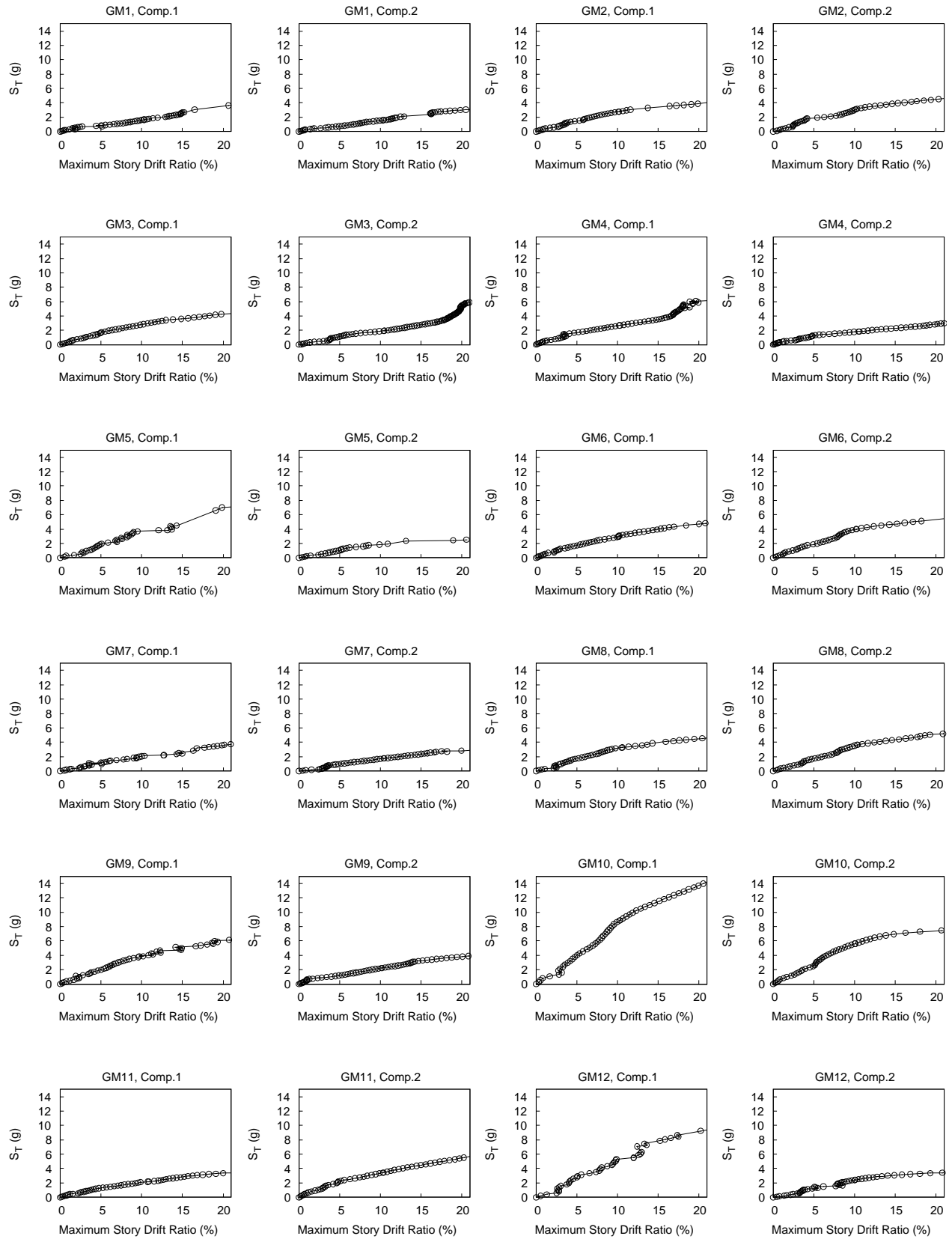


Figure C.4 Archetype 2

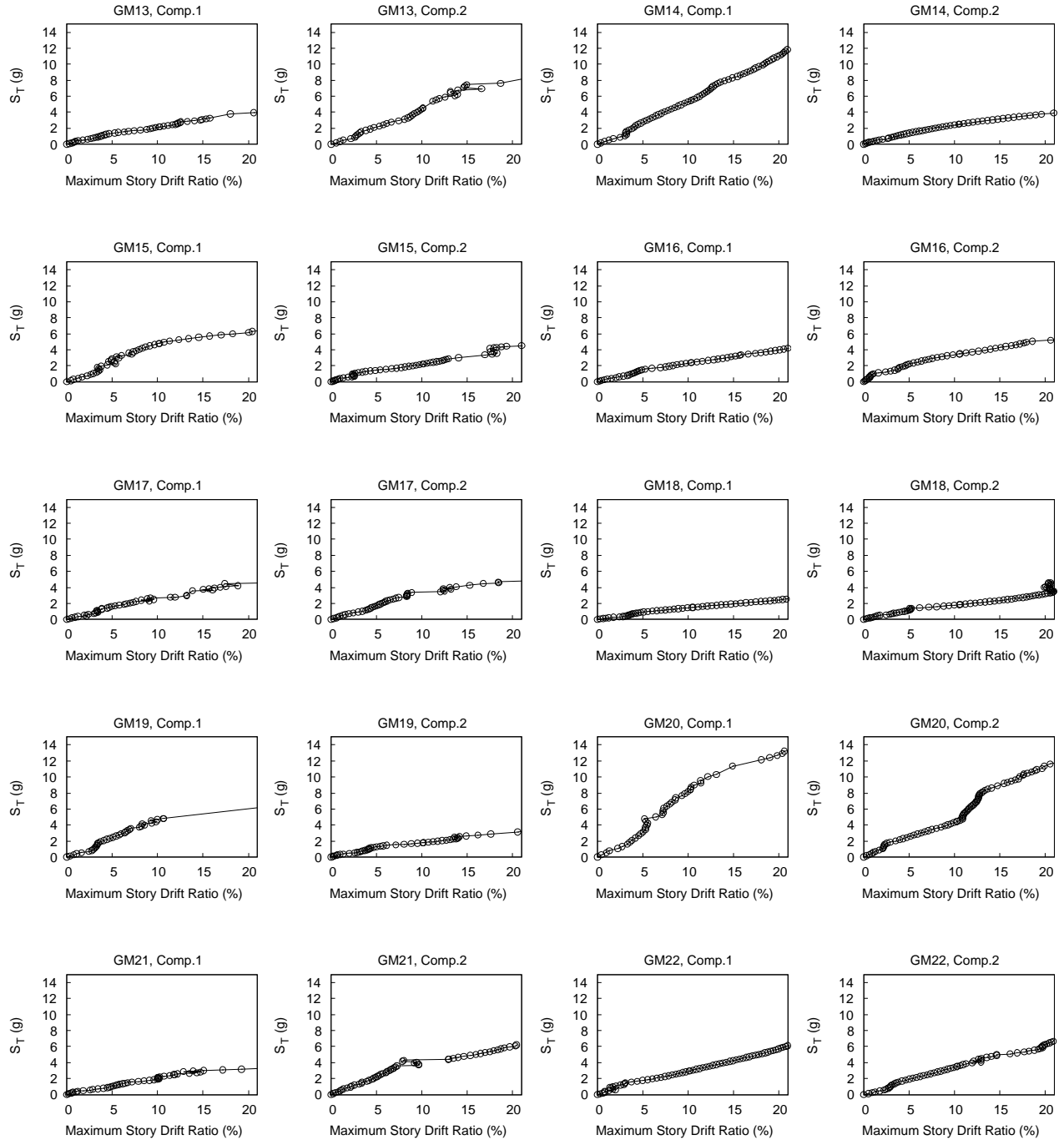
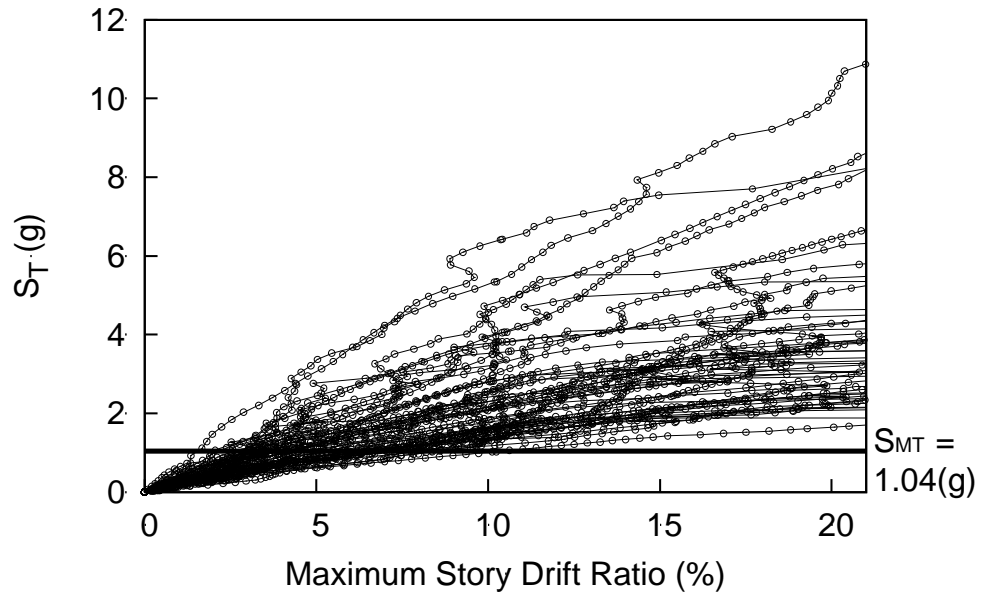
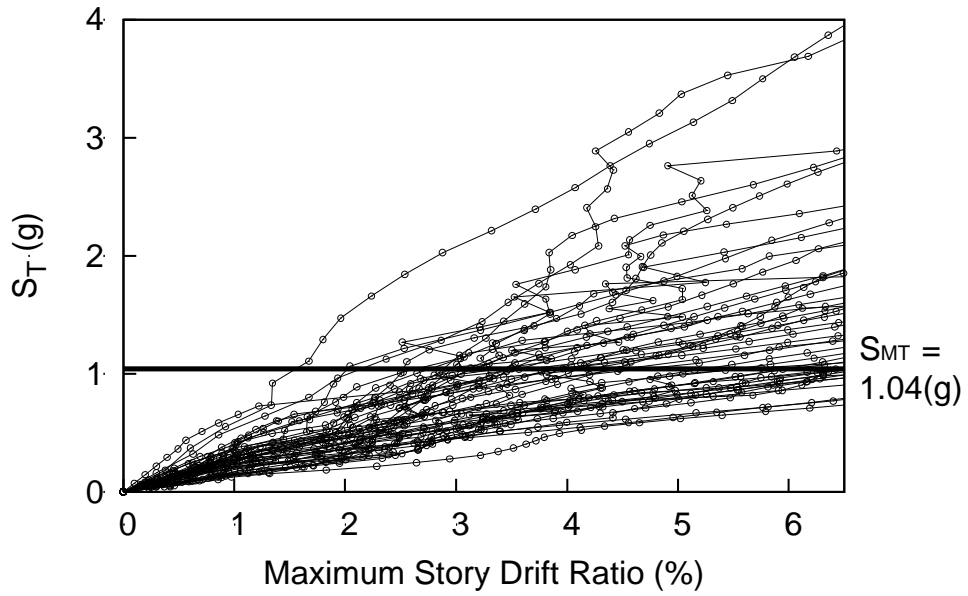


Figure C.4 Archetype 2 (cont.)



(a) Story Drift Ratio up to 20%



(a) Close-up Story Drift Ratio 6%

Figure C.5 Archetype 3

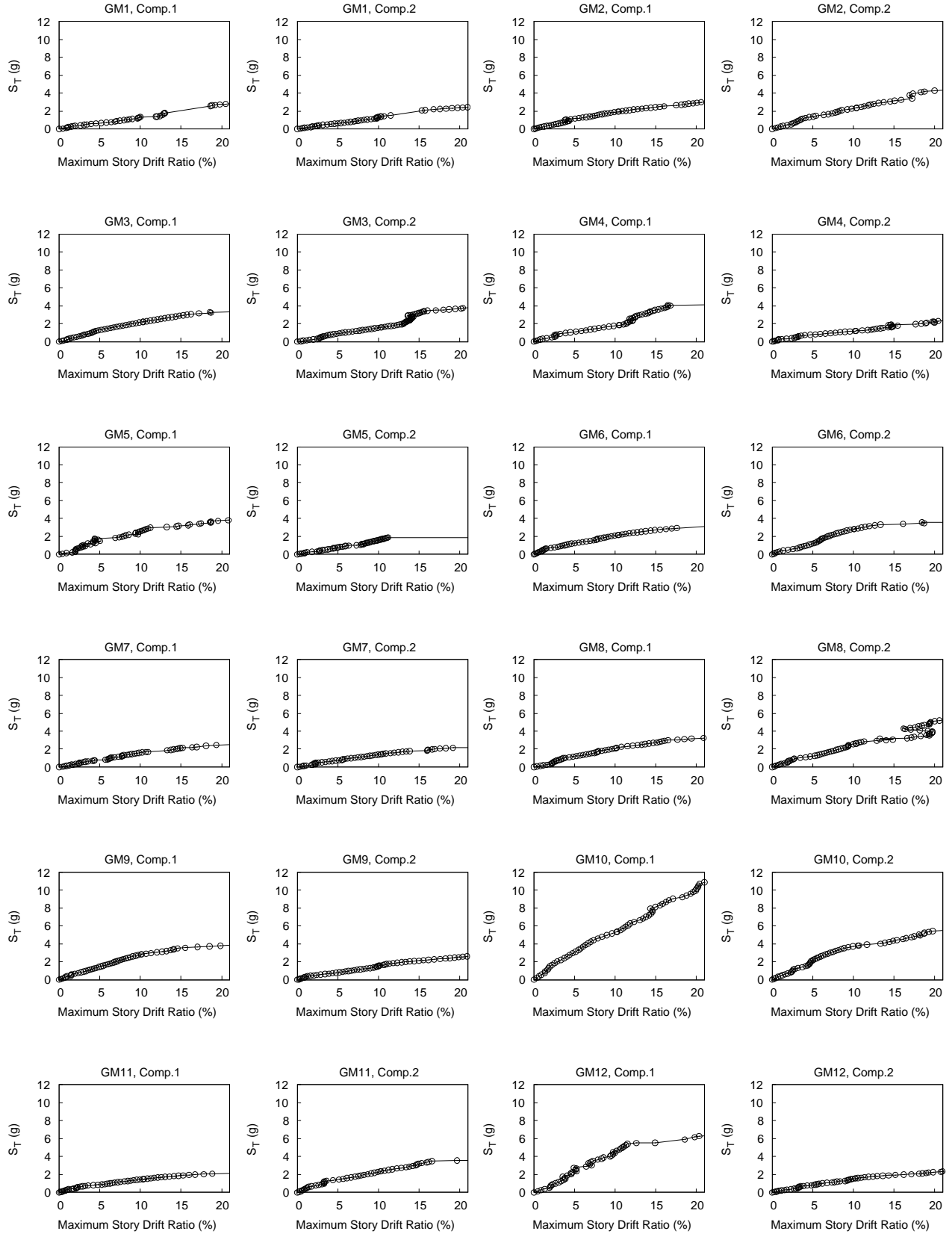


Figure C.6 Archetype 3

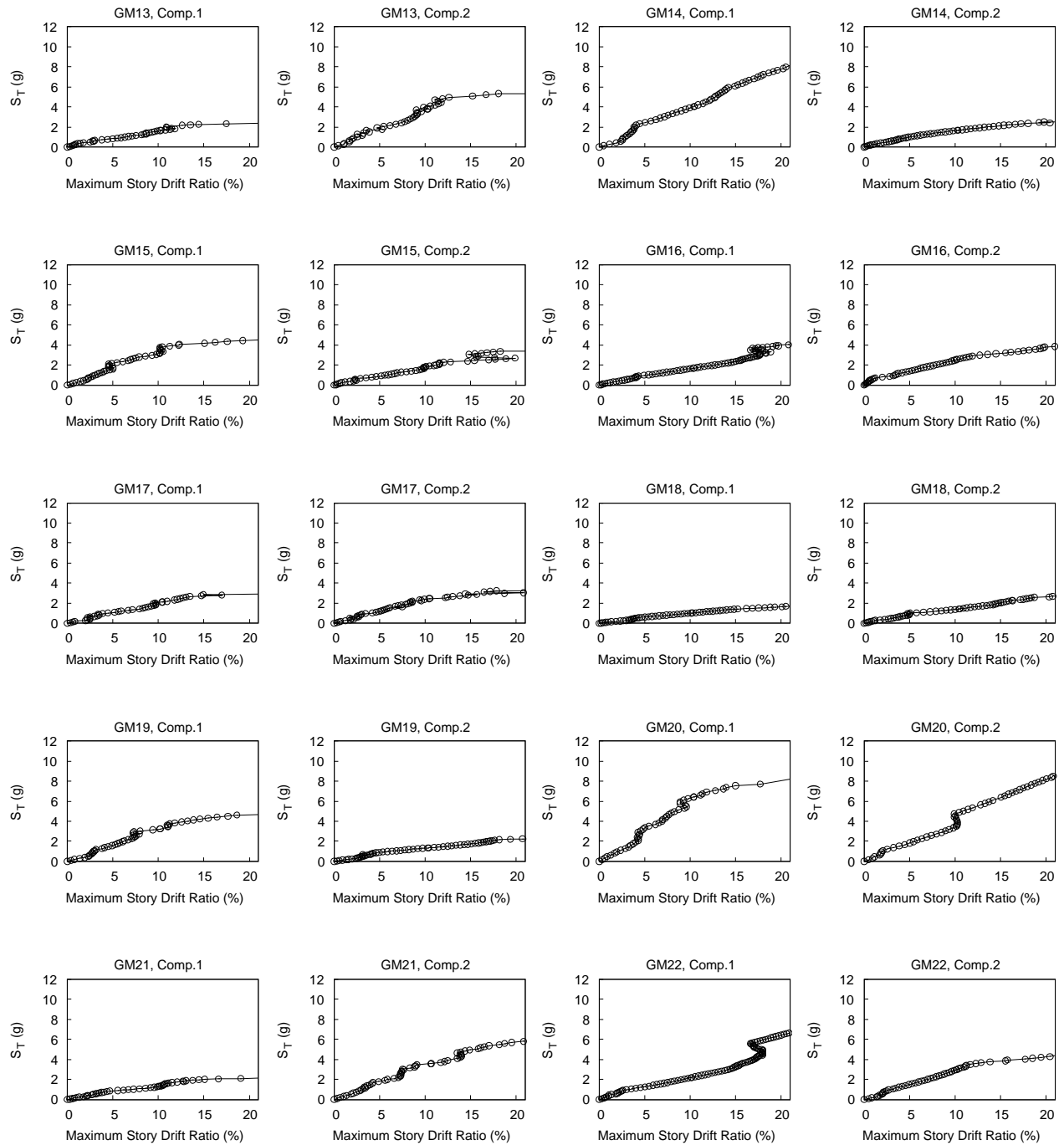
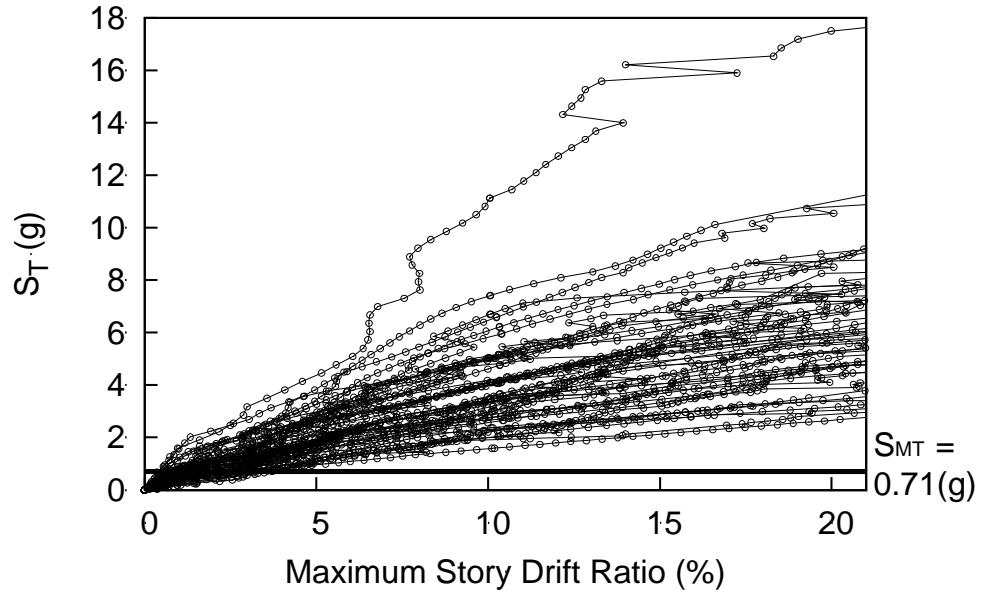
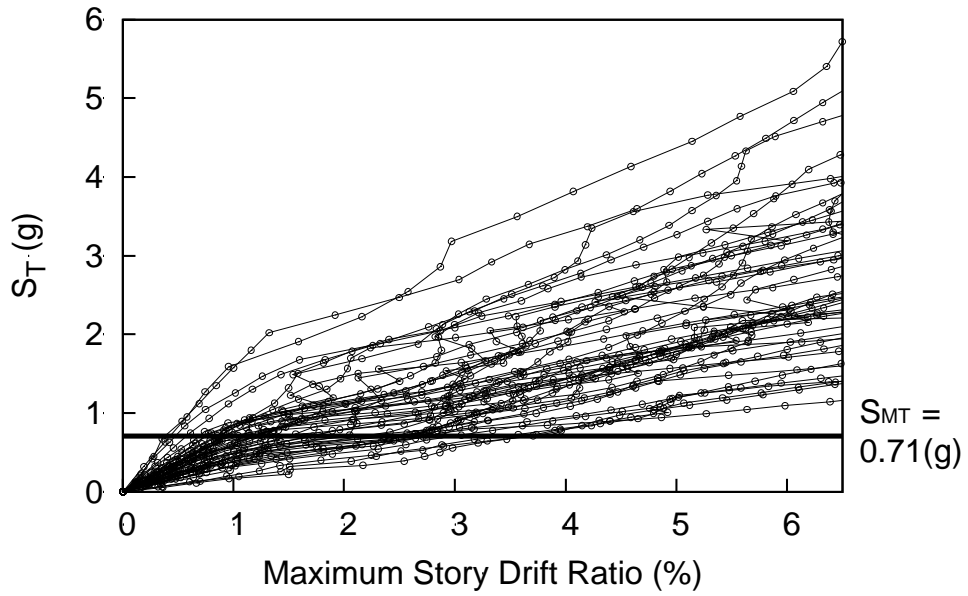


Figure C.6 Archetype 3 (cont.)



(a) Story Drift Ratio up to 20%



(b) Close-up Story Drift Ratio 6%

Figure C.7 Archetype 4

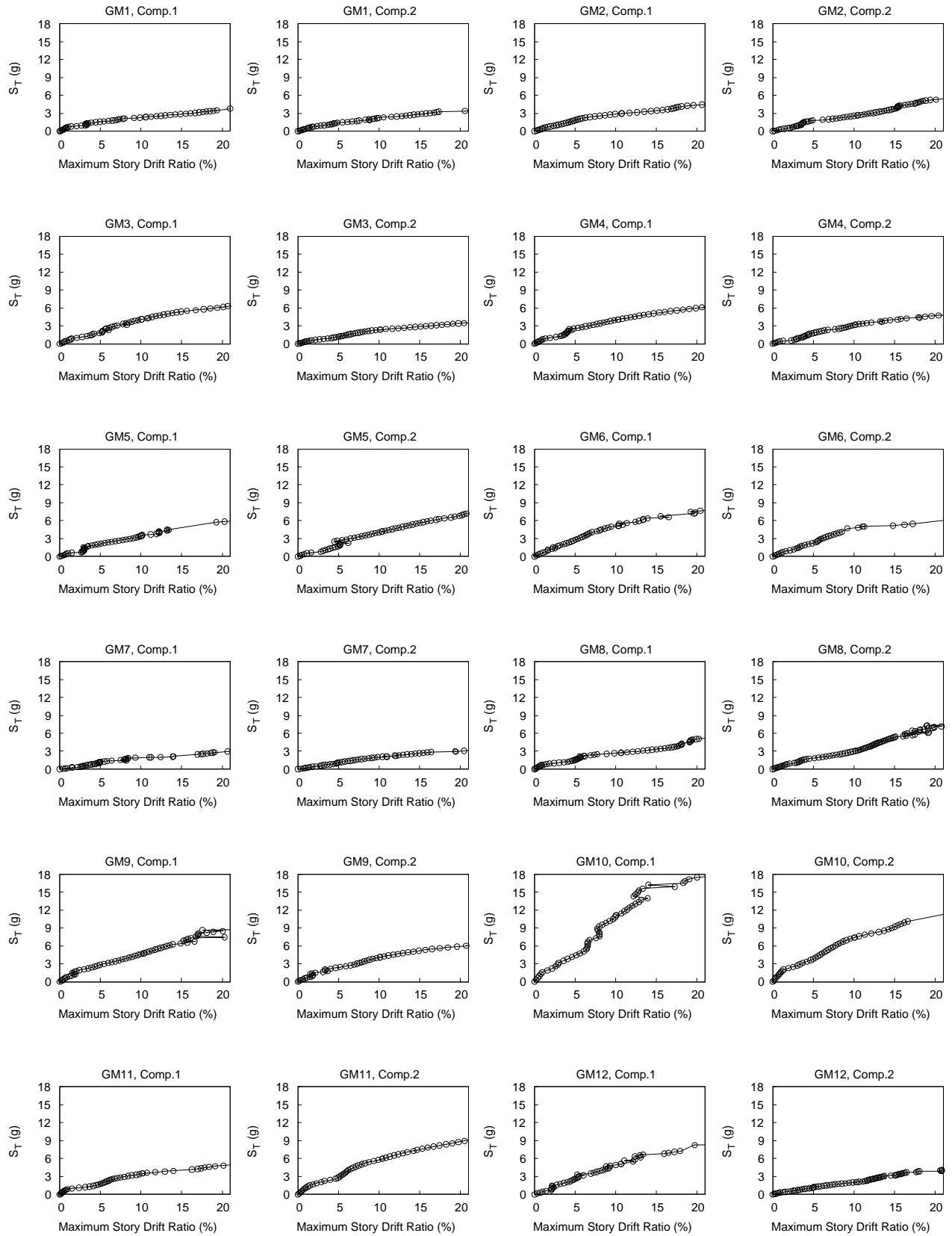


Figure C.8 Archetype 4

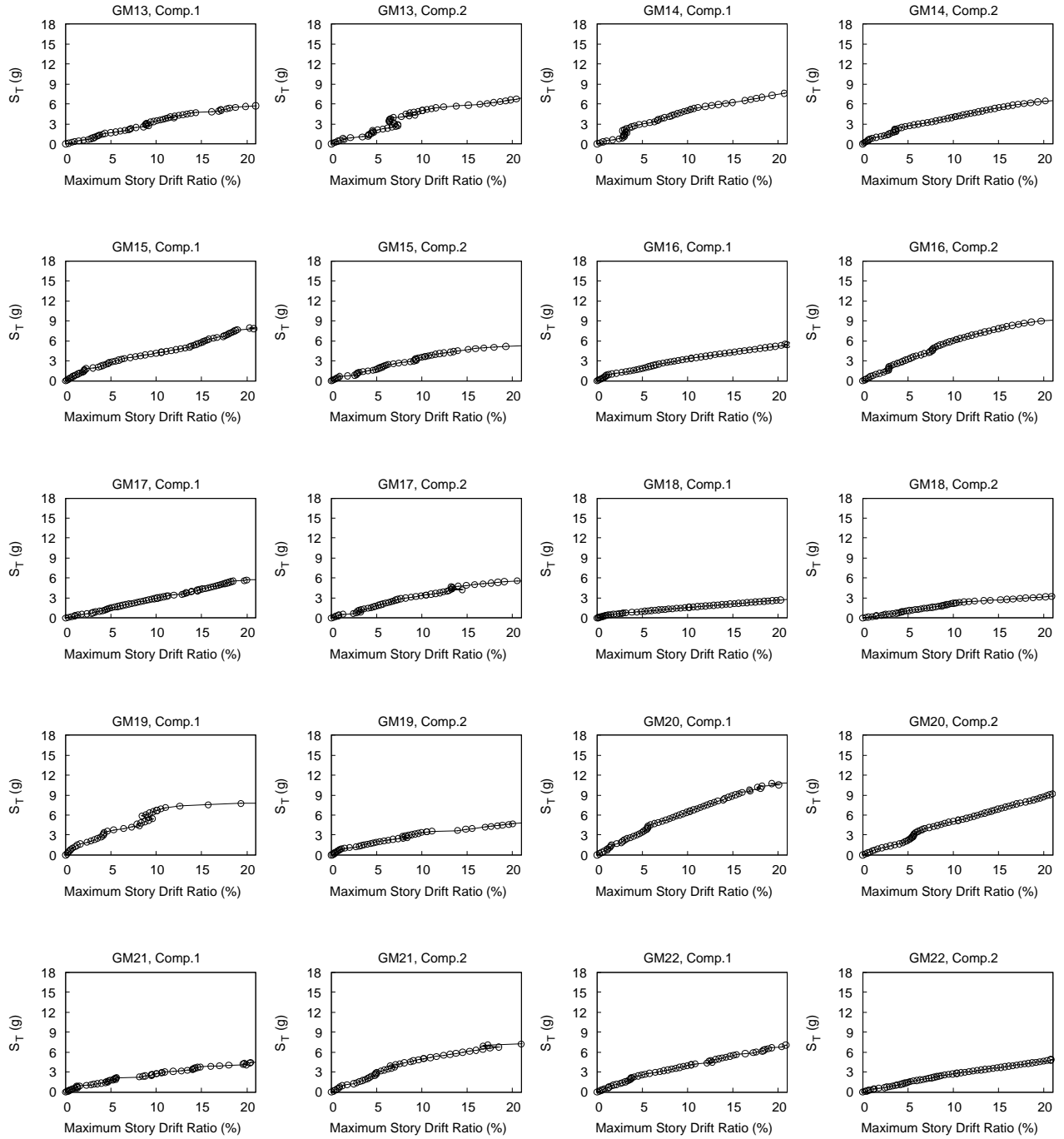
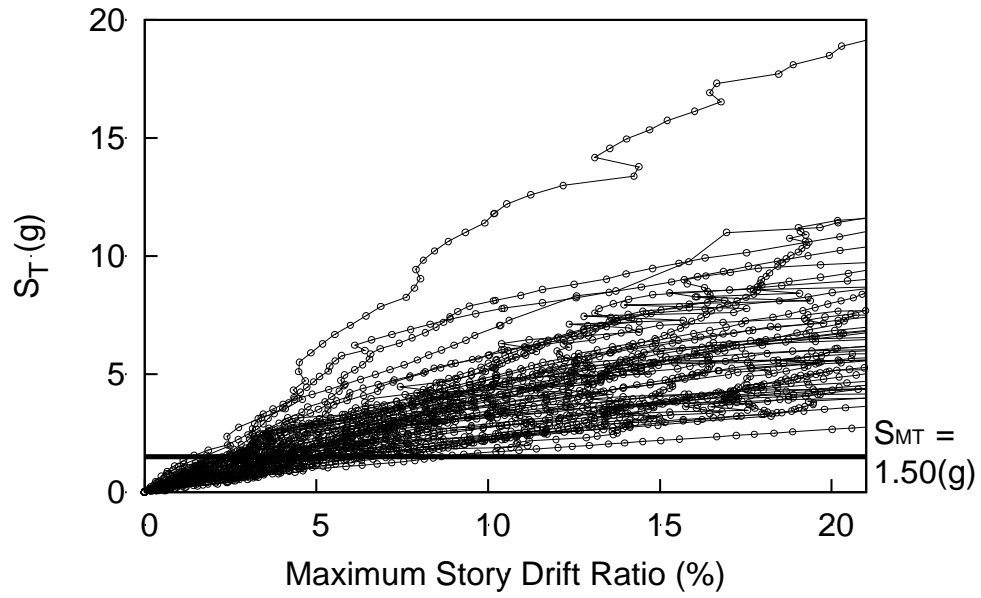
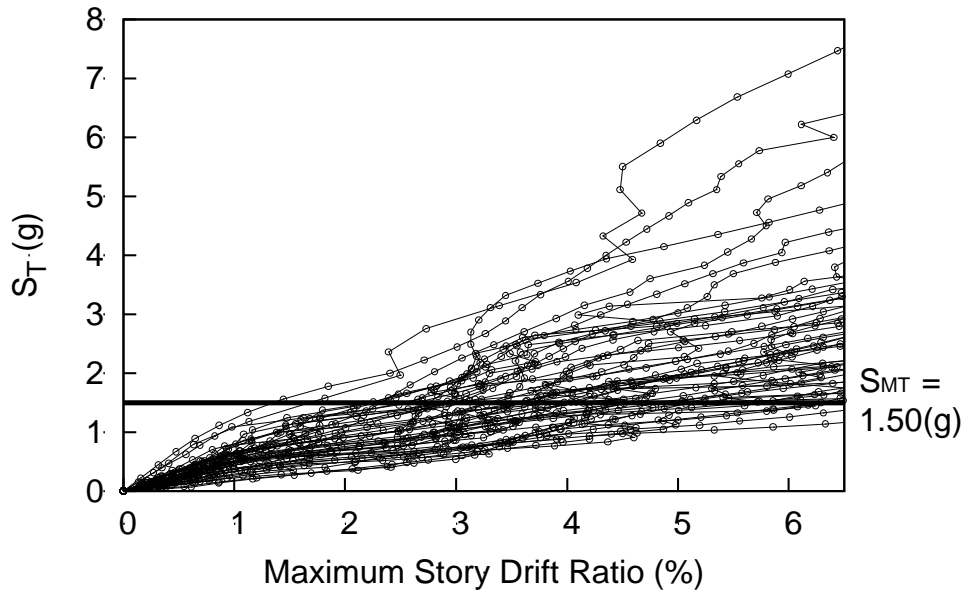


Figure C.8 Archetype 4 (cont.)



(a) Story Drift Ratio up to 20%



(b) Close-up Story Drift Ratio 6%

Figure C.9 Archetype 5

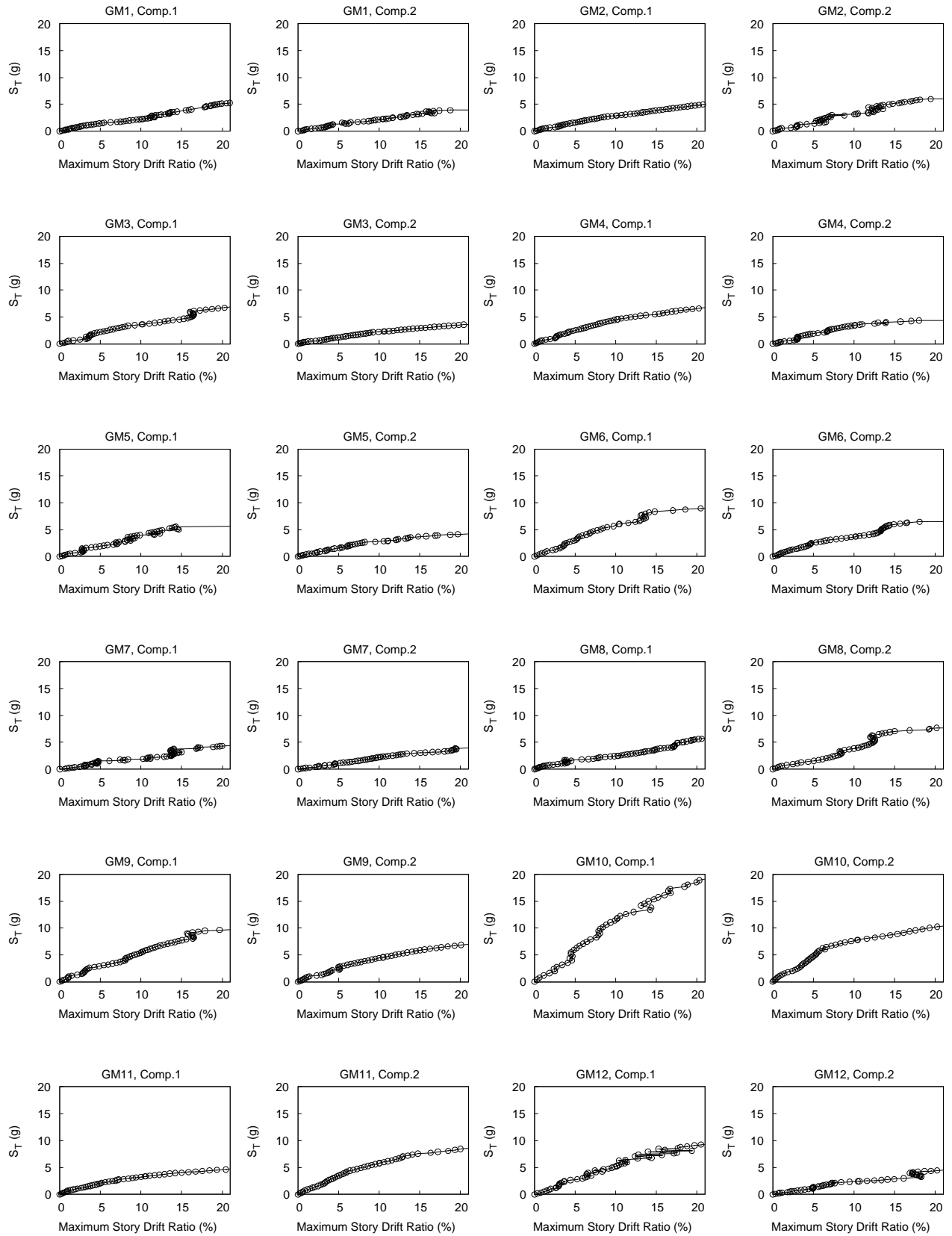


Figure C.10 Archetype 5

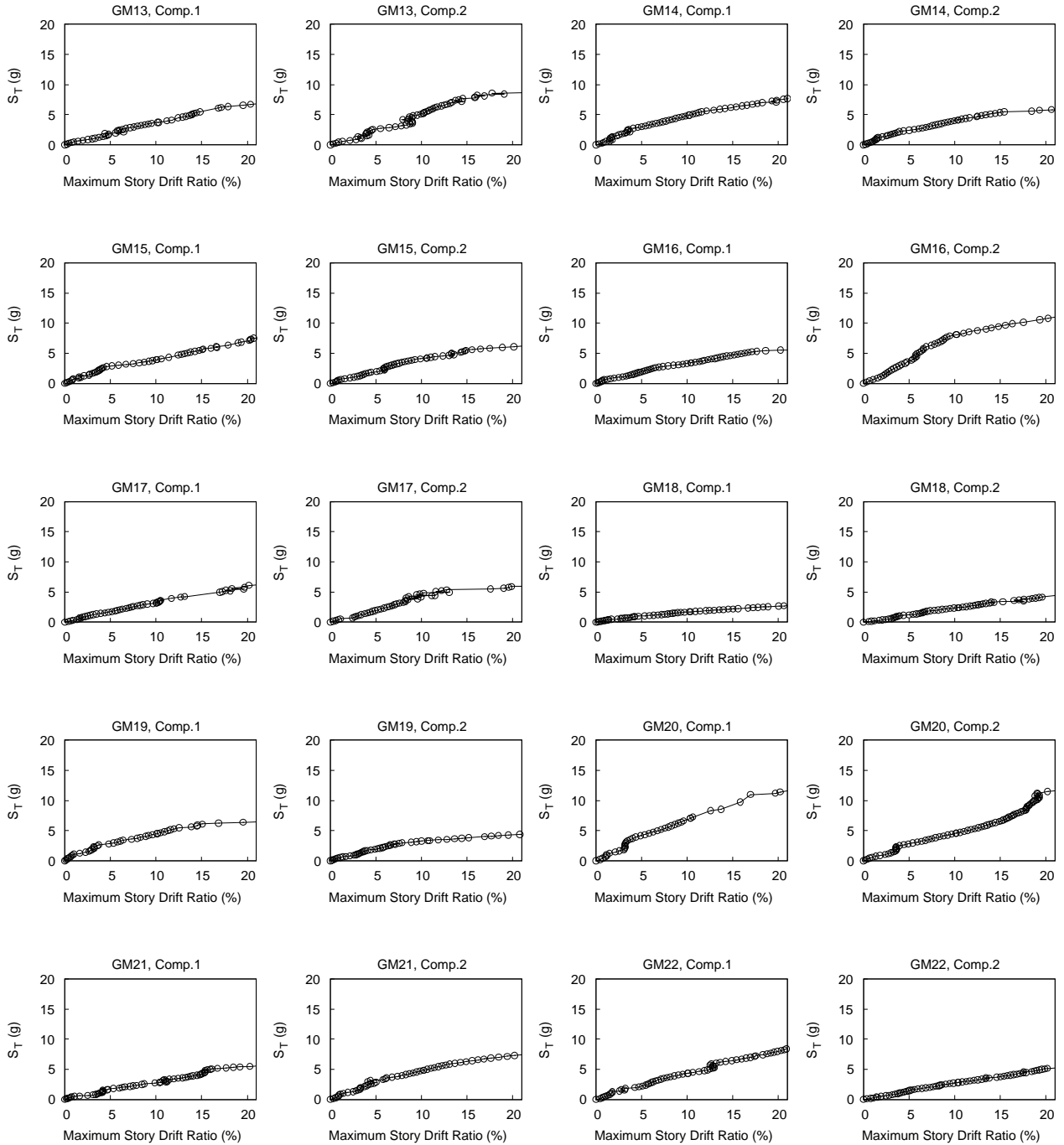
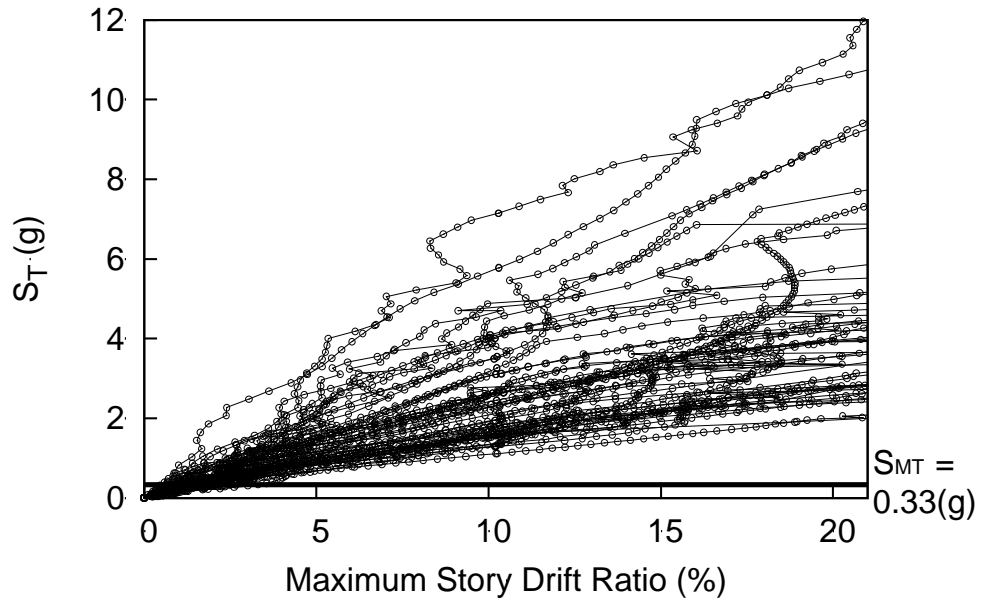
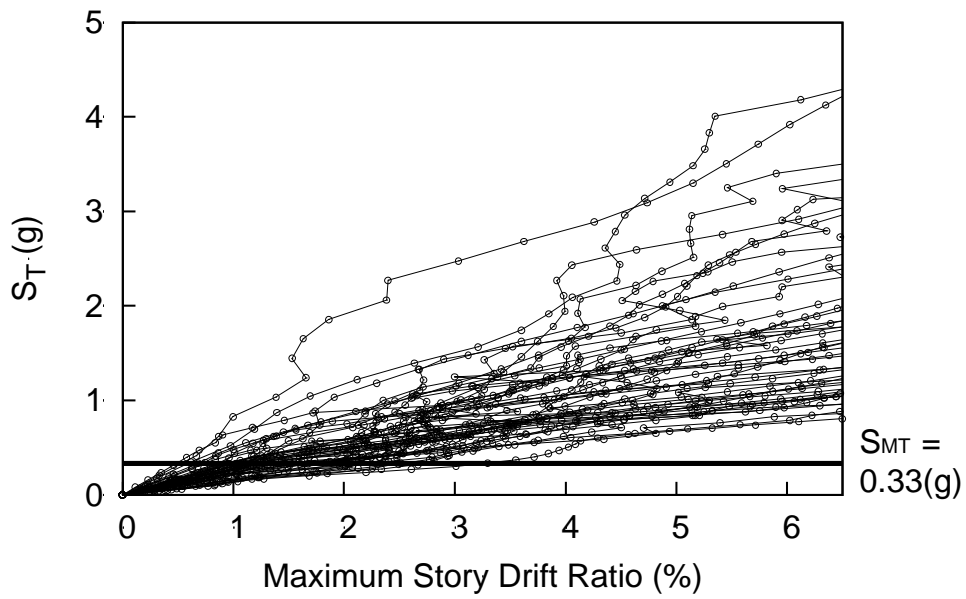


Figure C.10 Archetype 5 (cont.)



(a) Story Drift Ratio up to 20%



(b) Close-up Story Drift Ratio 6%

Figure C.11 Archetype 6

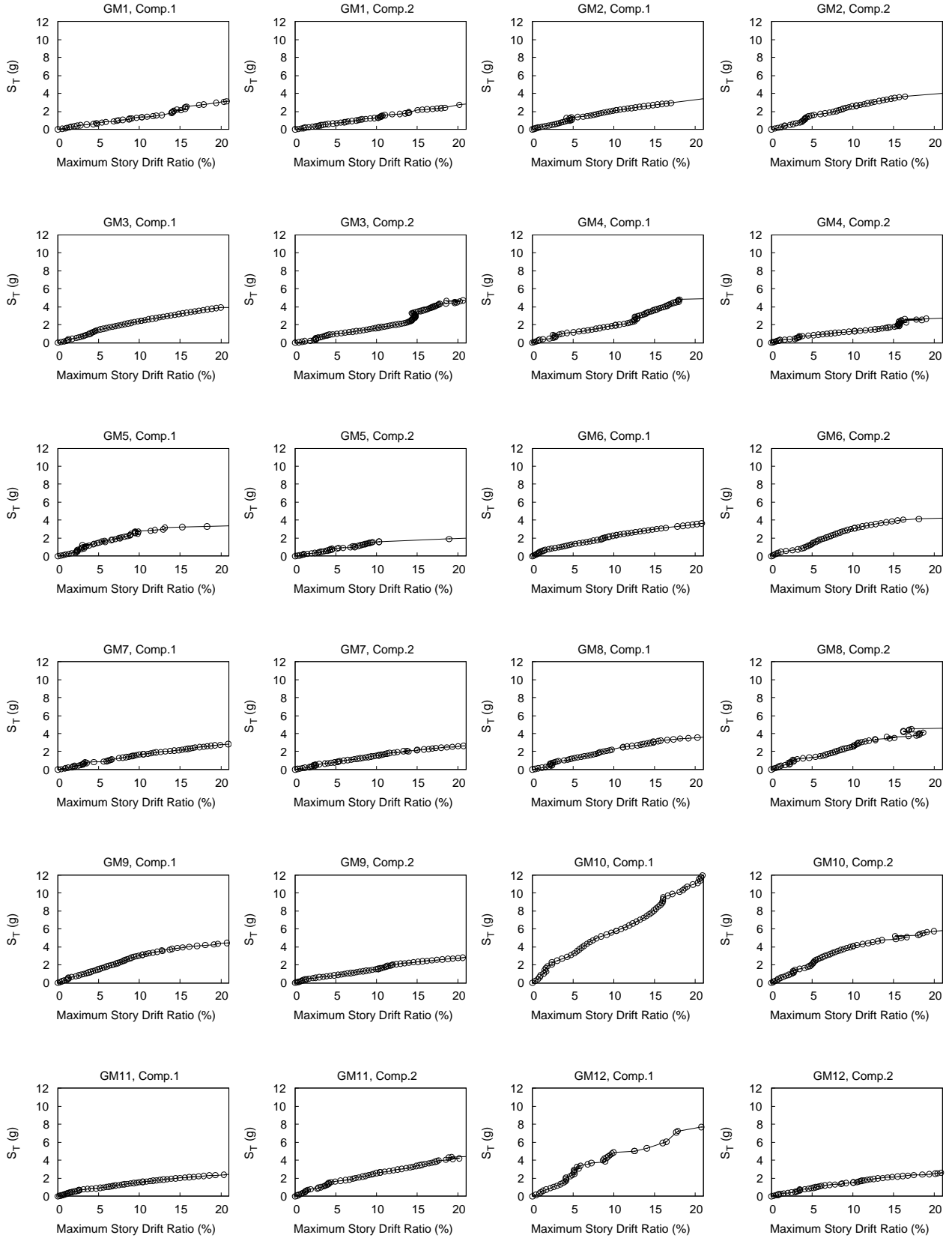


Figure C.12 Archetype 6

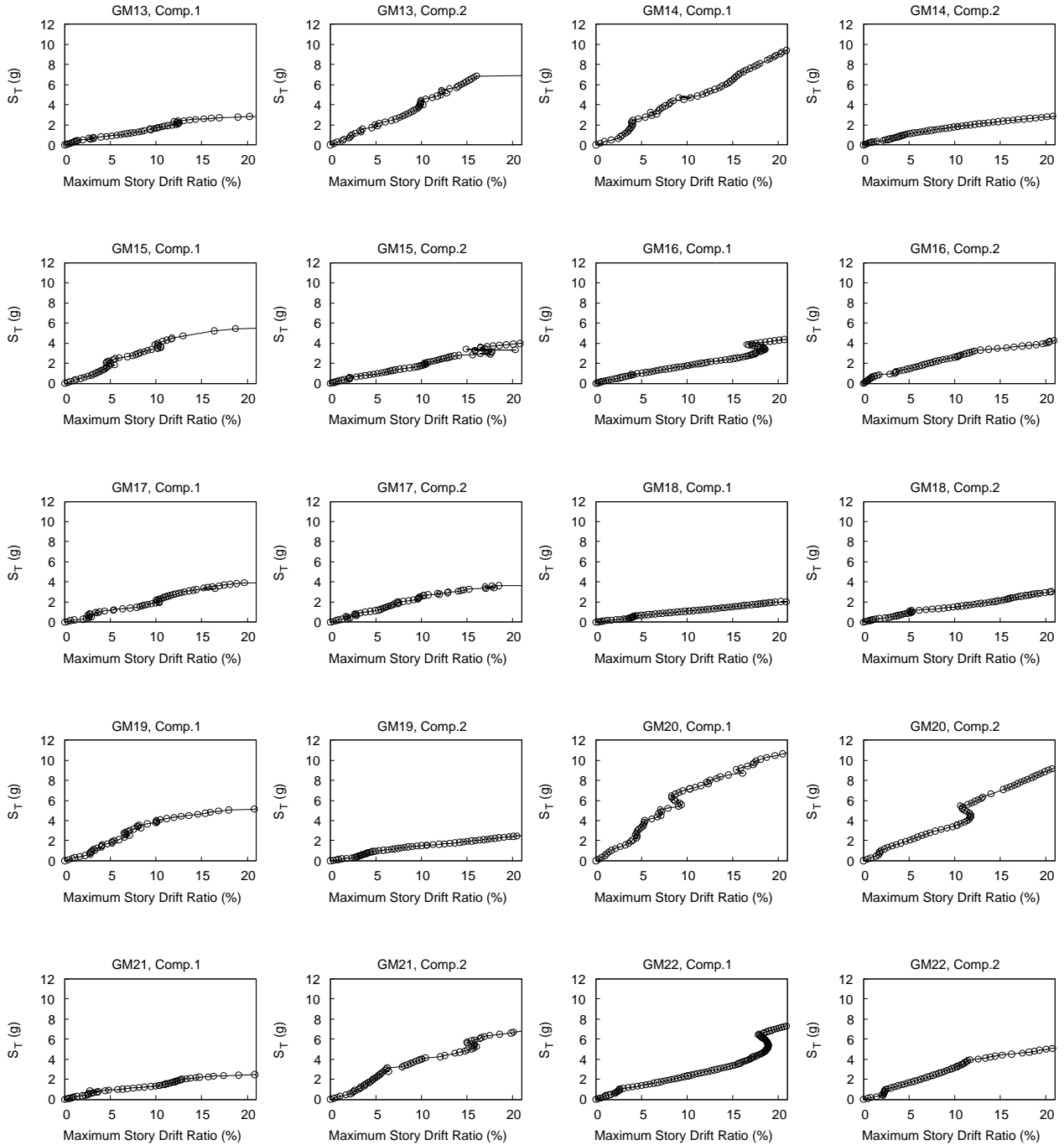
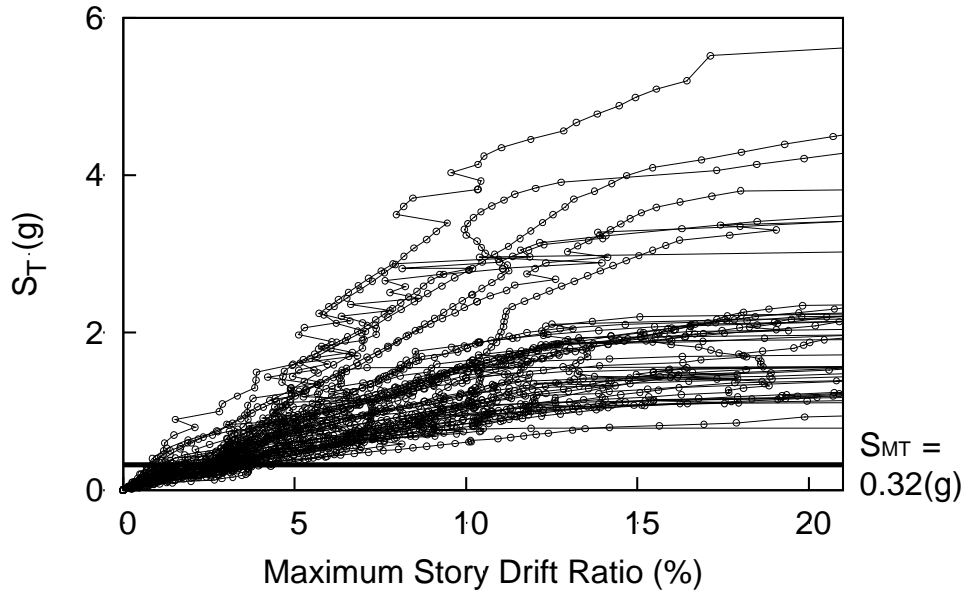
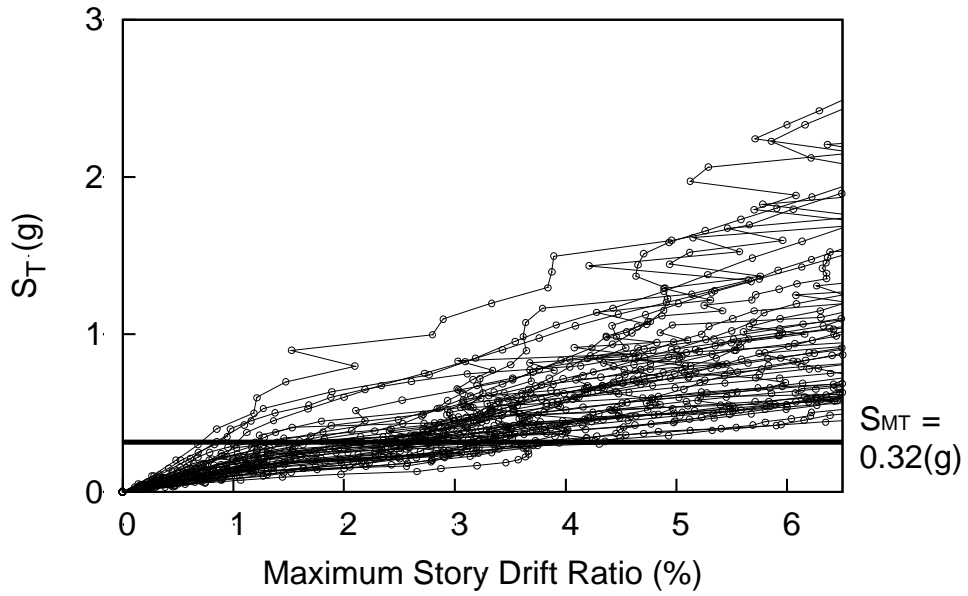


Figure C.12 Archetype 6 (cont.)



(a) Story Drift Ratio up to 20%



(b) Close-up Story Drift Ratio 6%

Figure C.13 Archetype 7

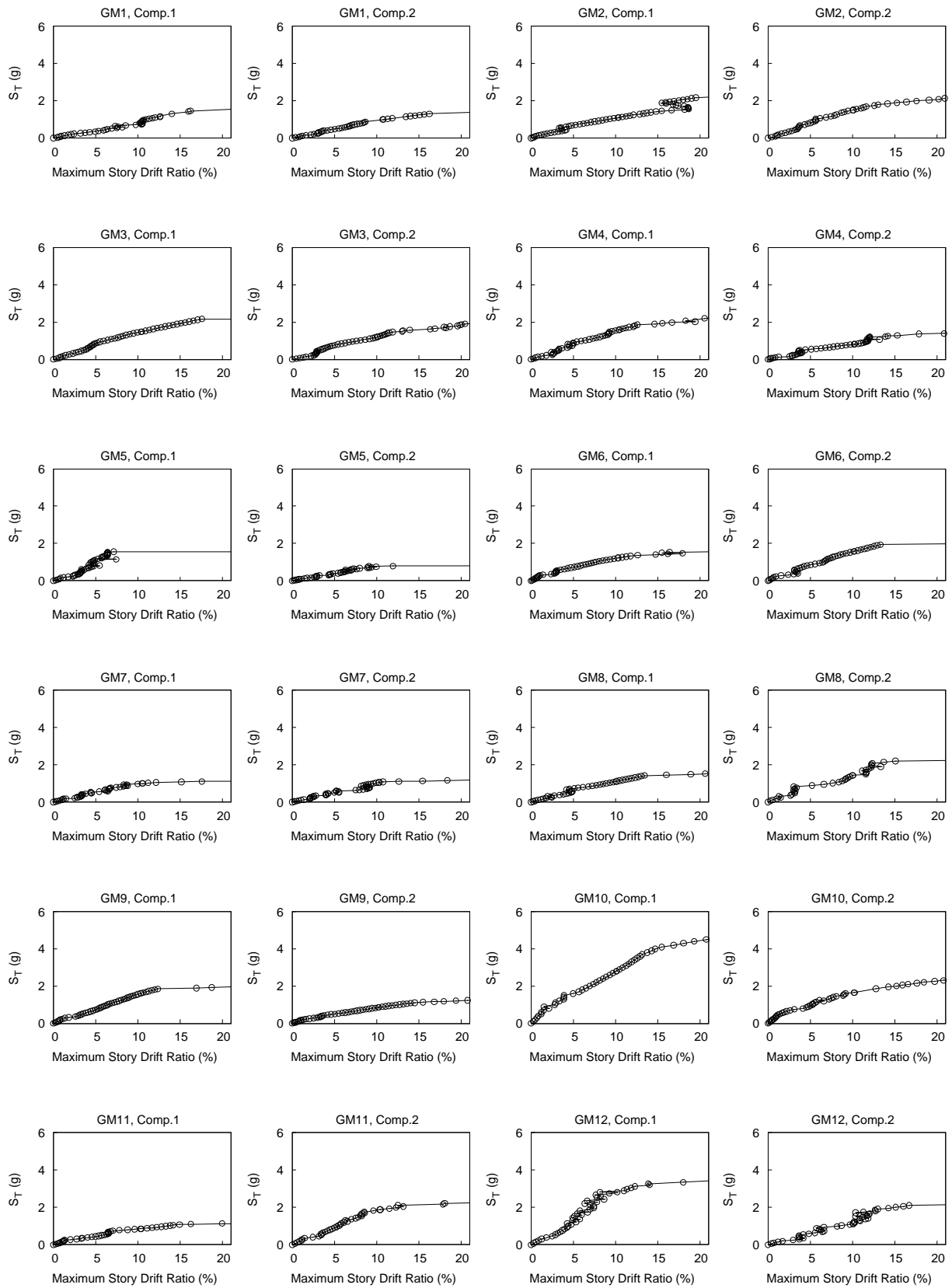


Figure C.14 Archetype 7

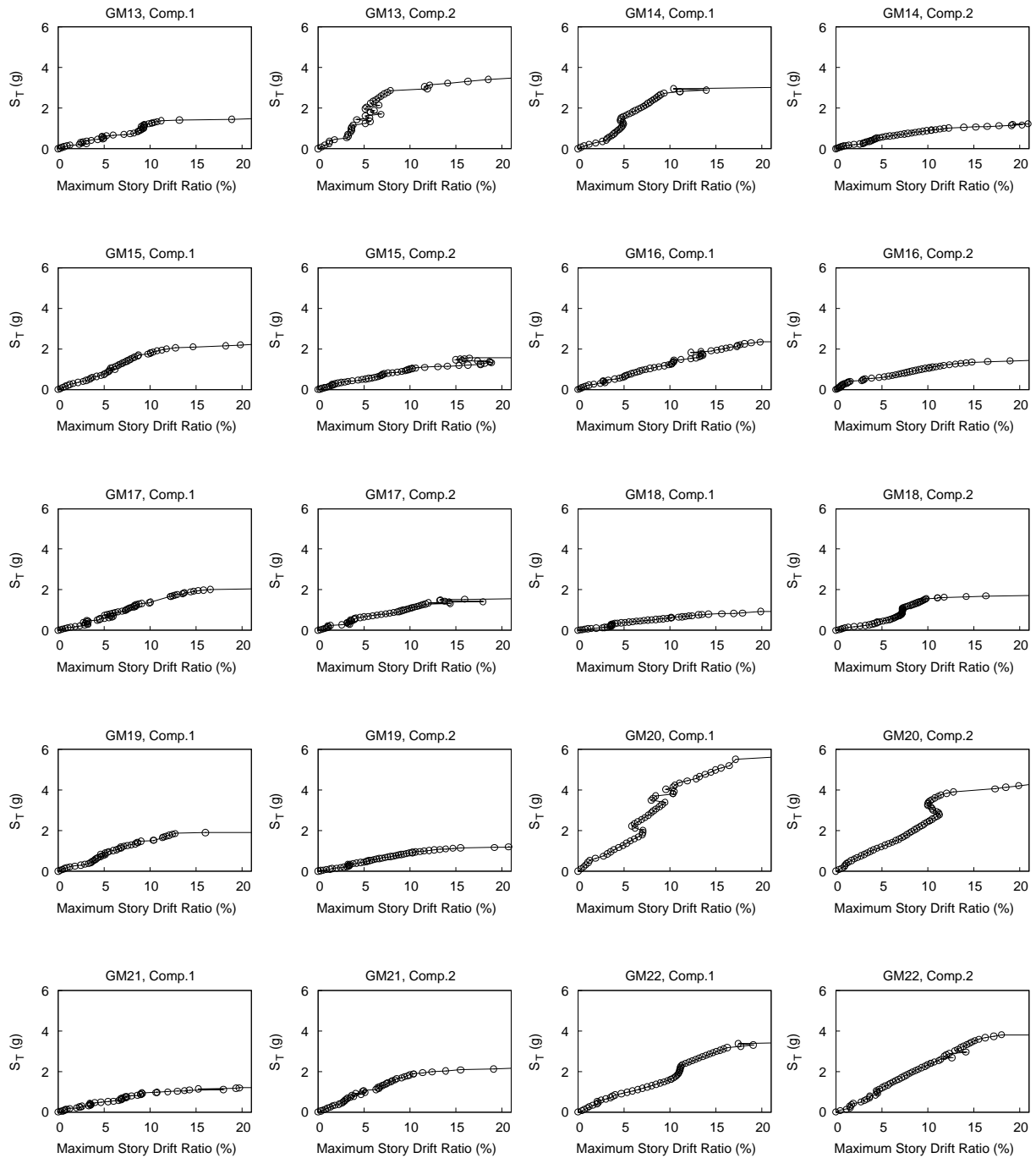
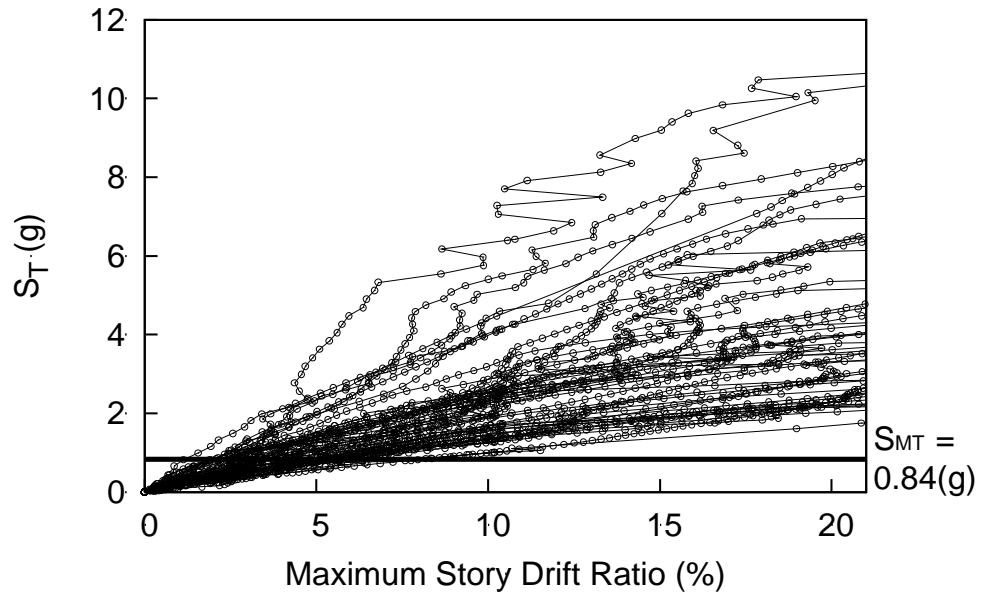
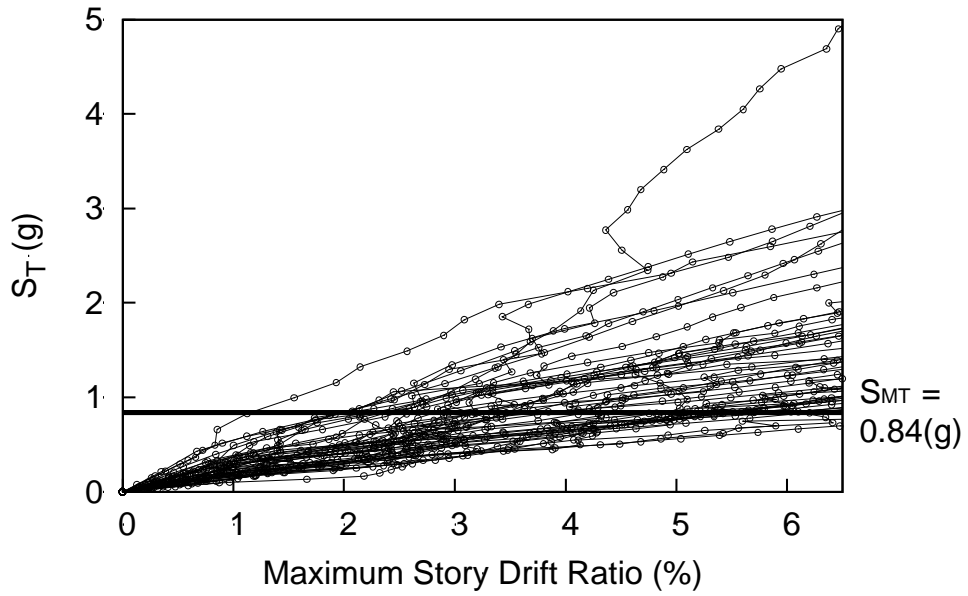


Figure C.14 Archetype 7 (cont.)



(a) Story Drift Ratio up to 20%



(b) Close-up Story Drift Ratio 6%

Figure C.15 Archetype 8

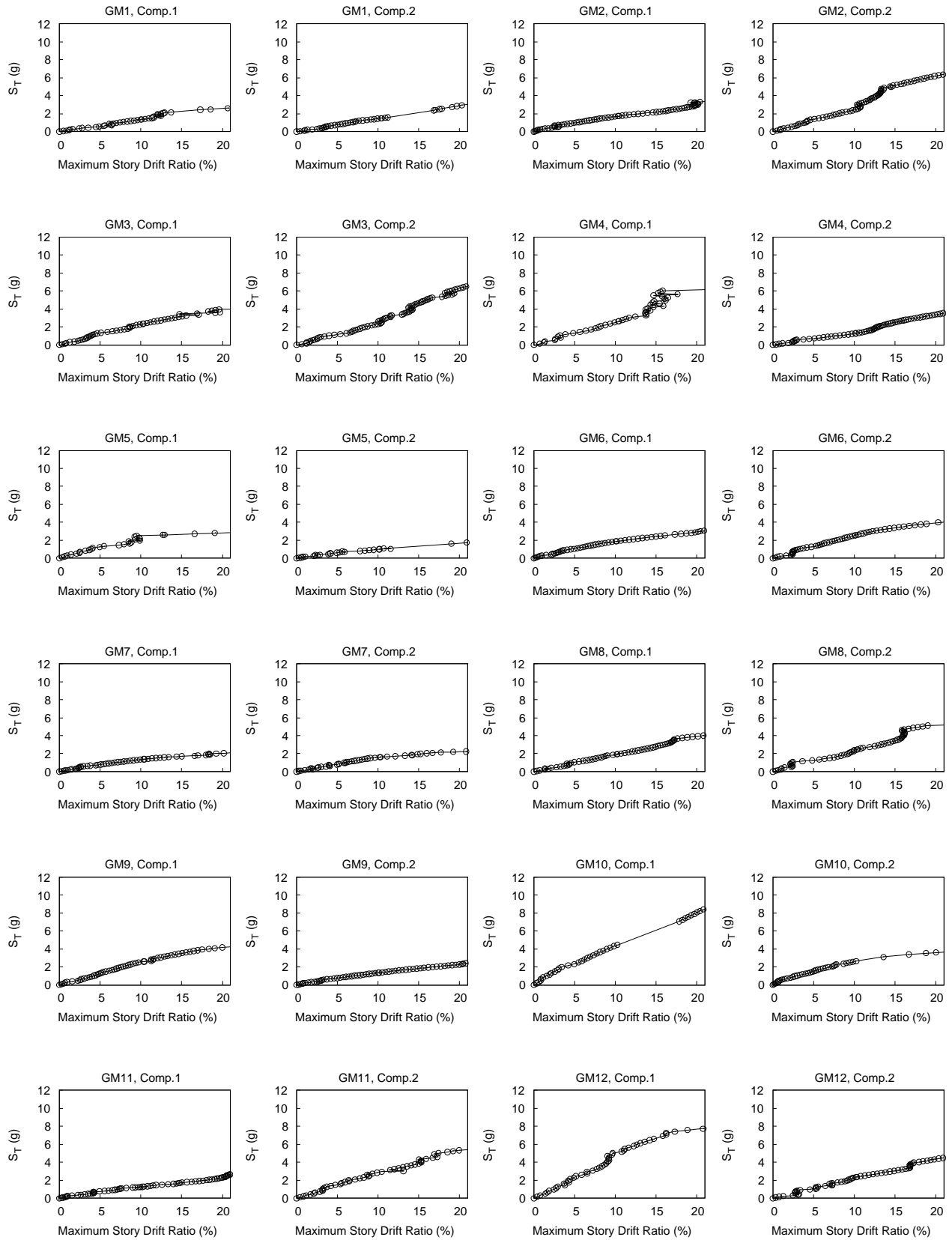


Figure C.16 Archetype 8

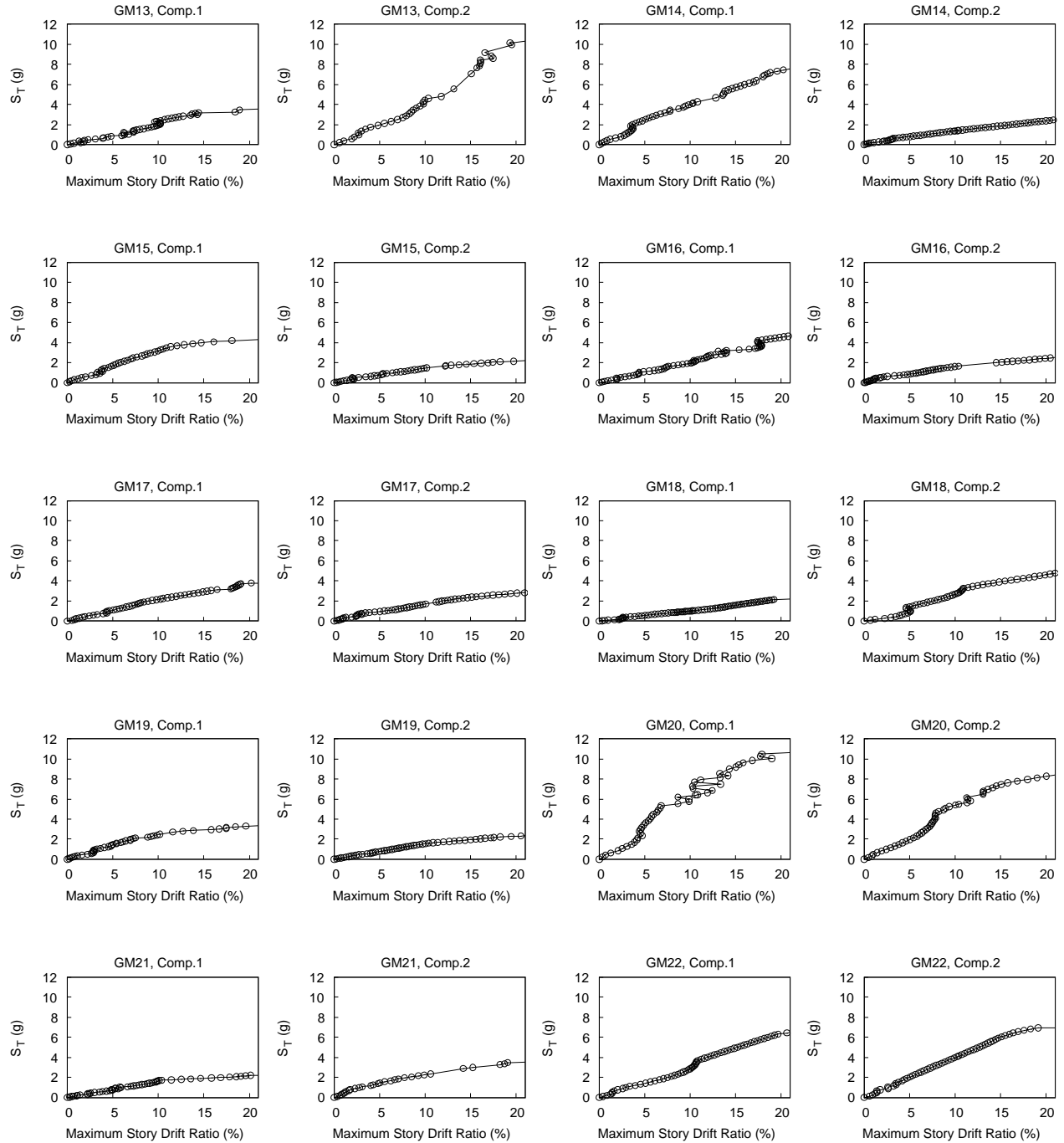
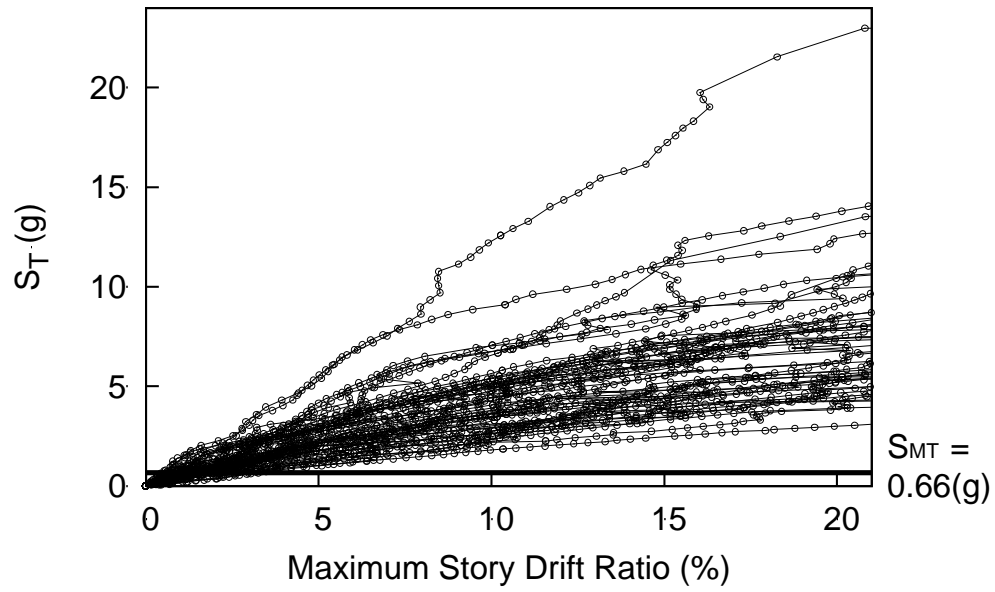
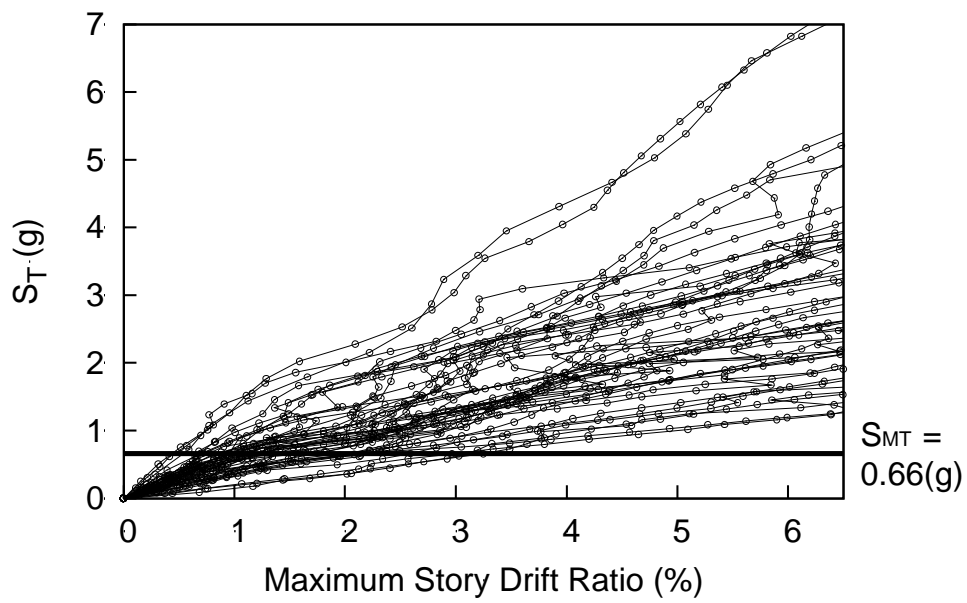


Figure C.16 Archetype 8 (cont.)



(a) Story Drift Ratio up to 20%



(b) Close-up Story Drift Ratio 6%

Figure C.17 Archetype 9

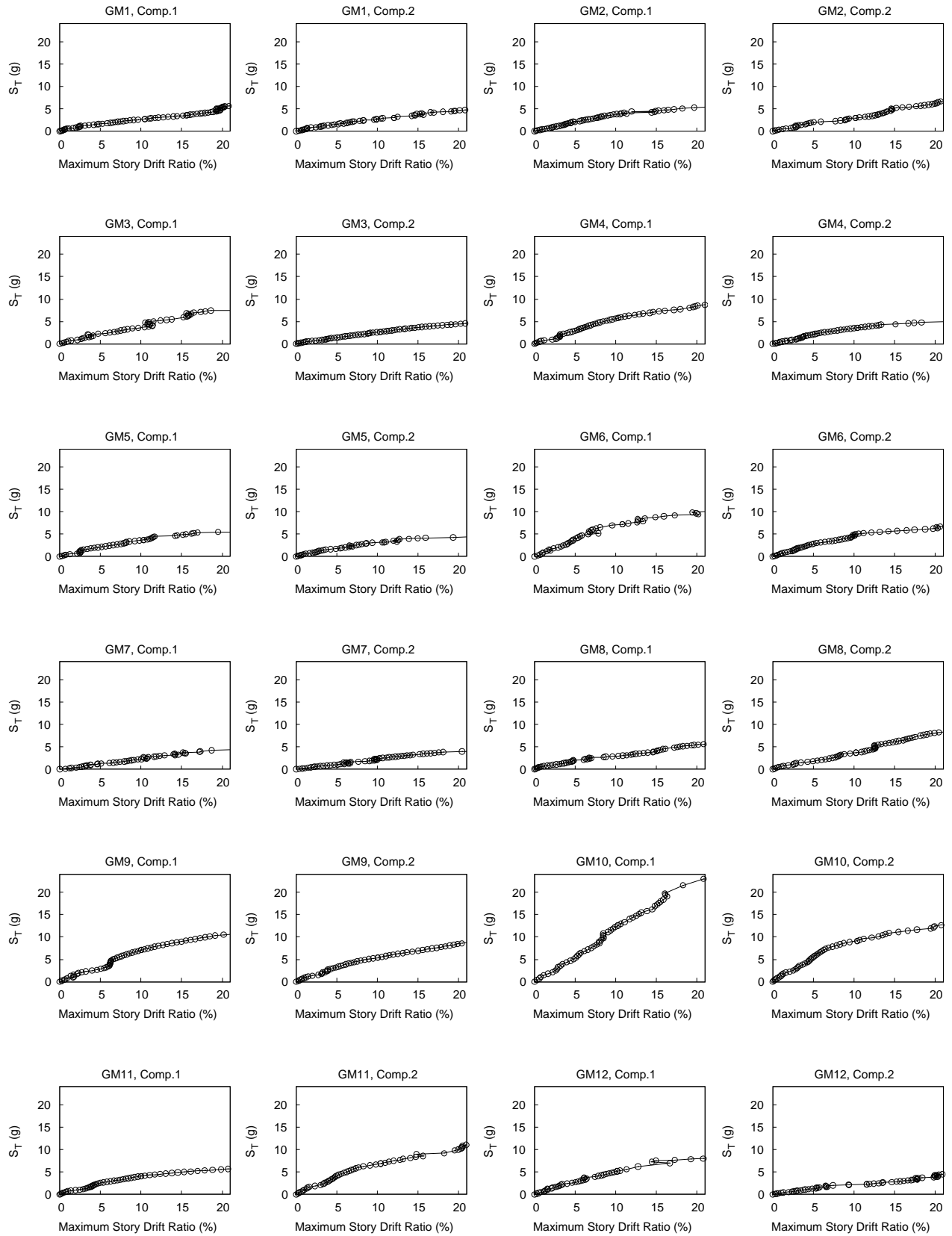


Figure C.18 Archetype 9

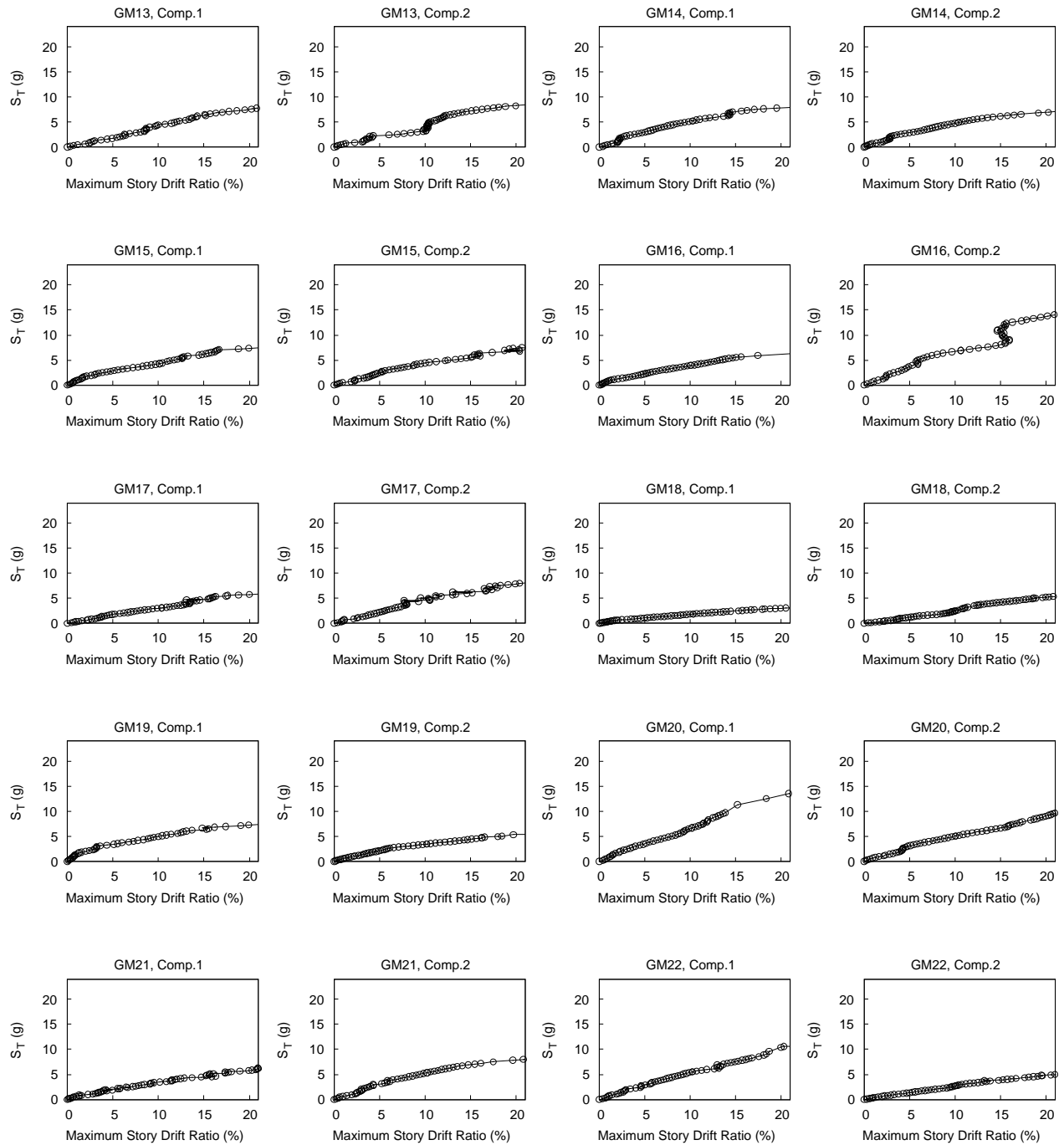


Figure C.18 Archetype 9 (cont.)

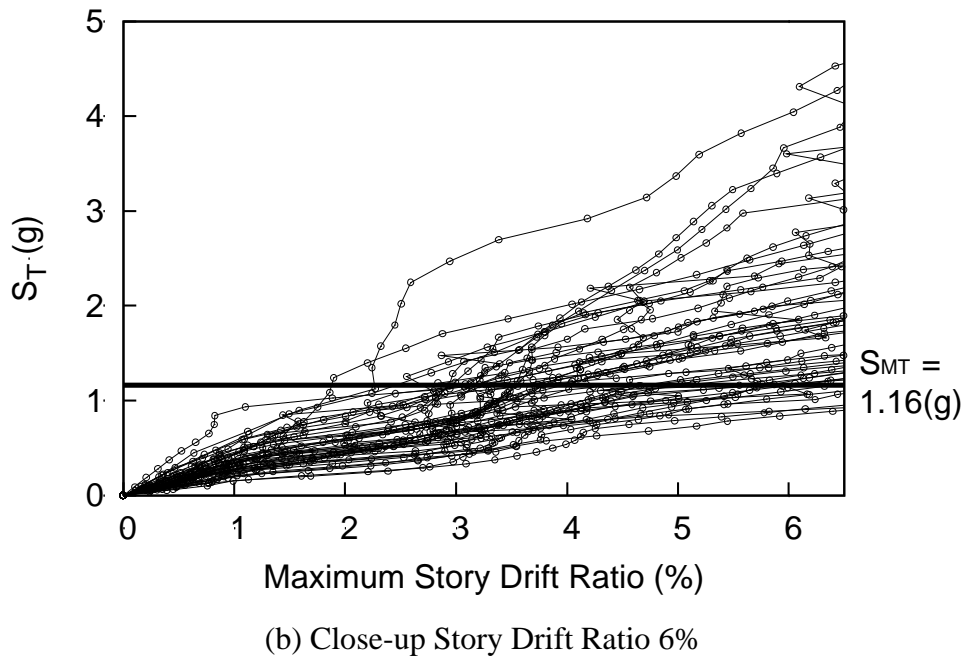
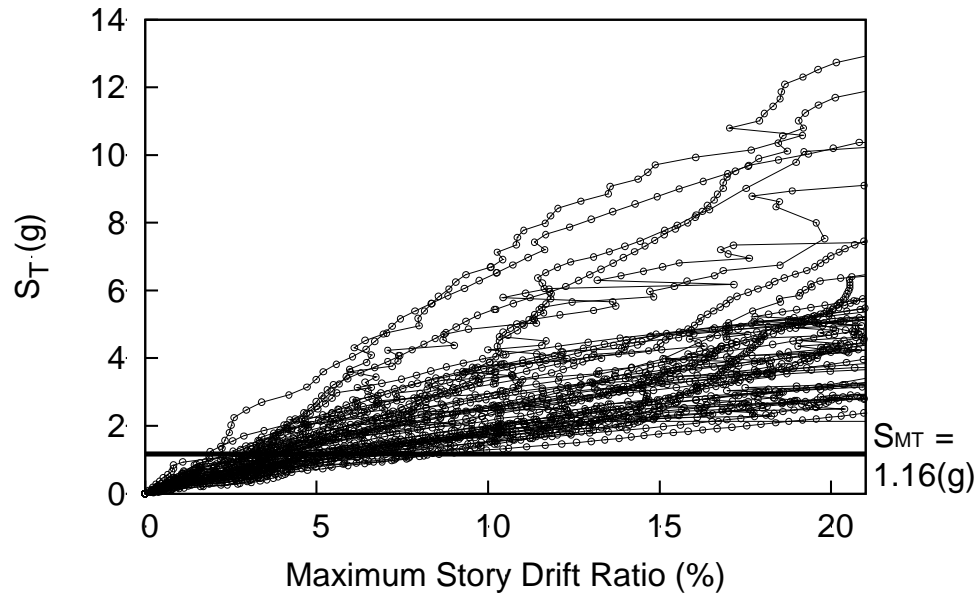


Figure C.19 Archetype 10

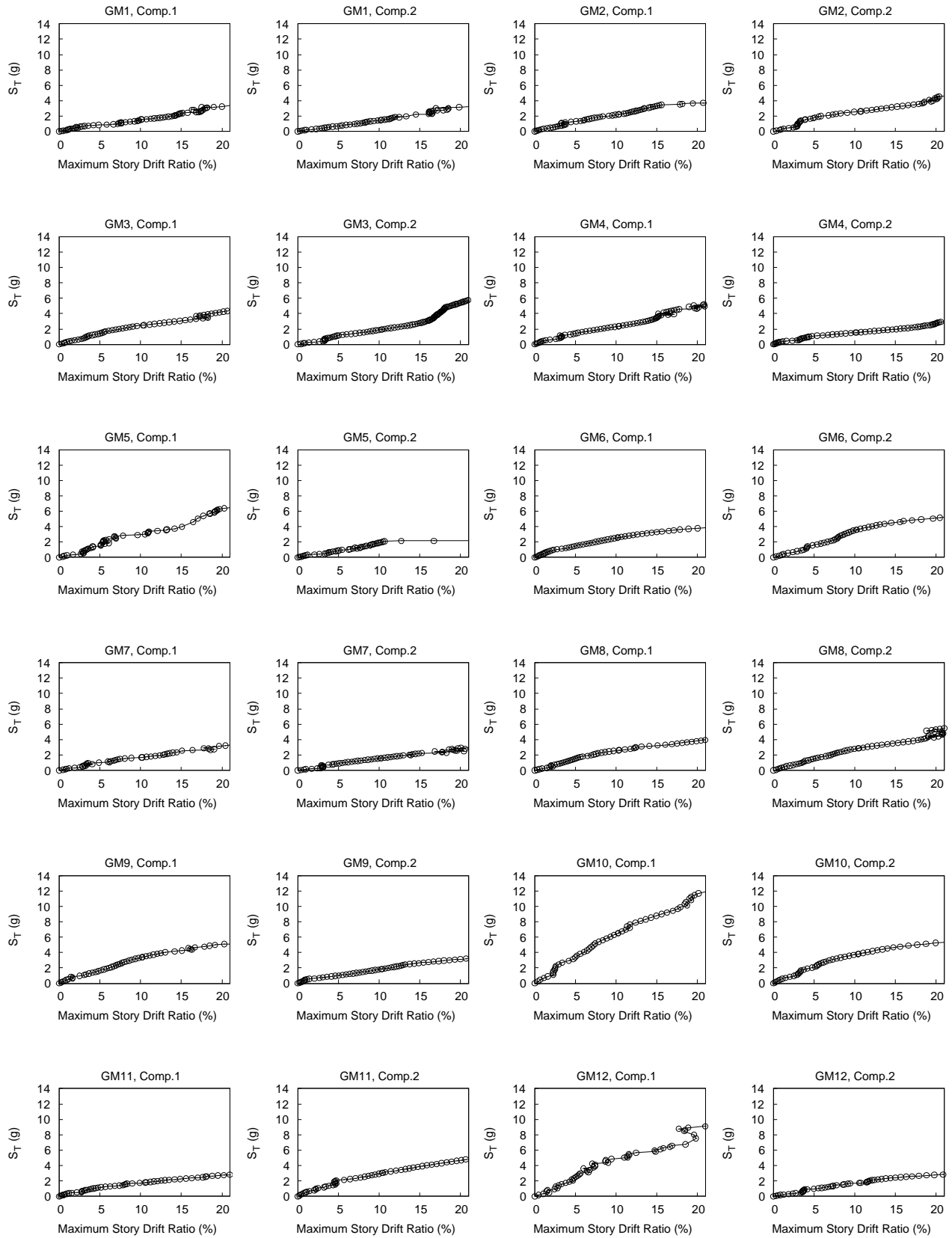


Figure C.20 Archetype 10

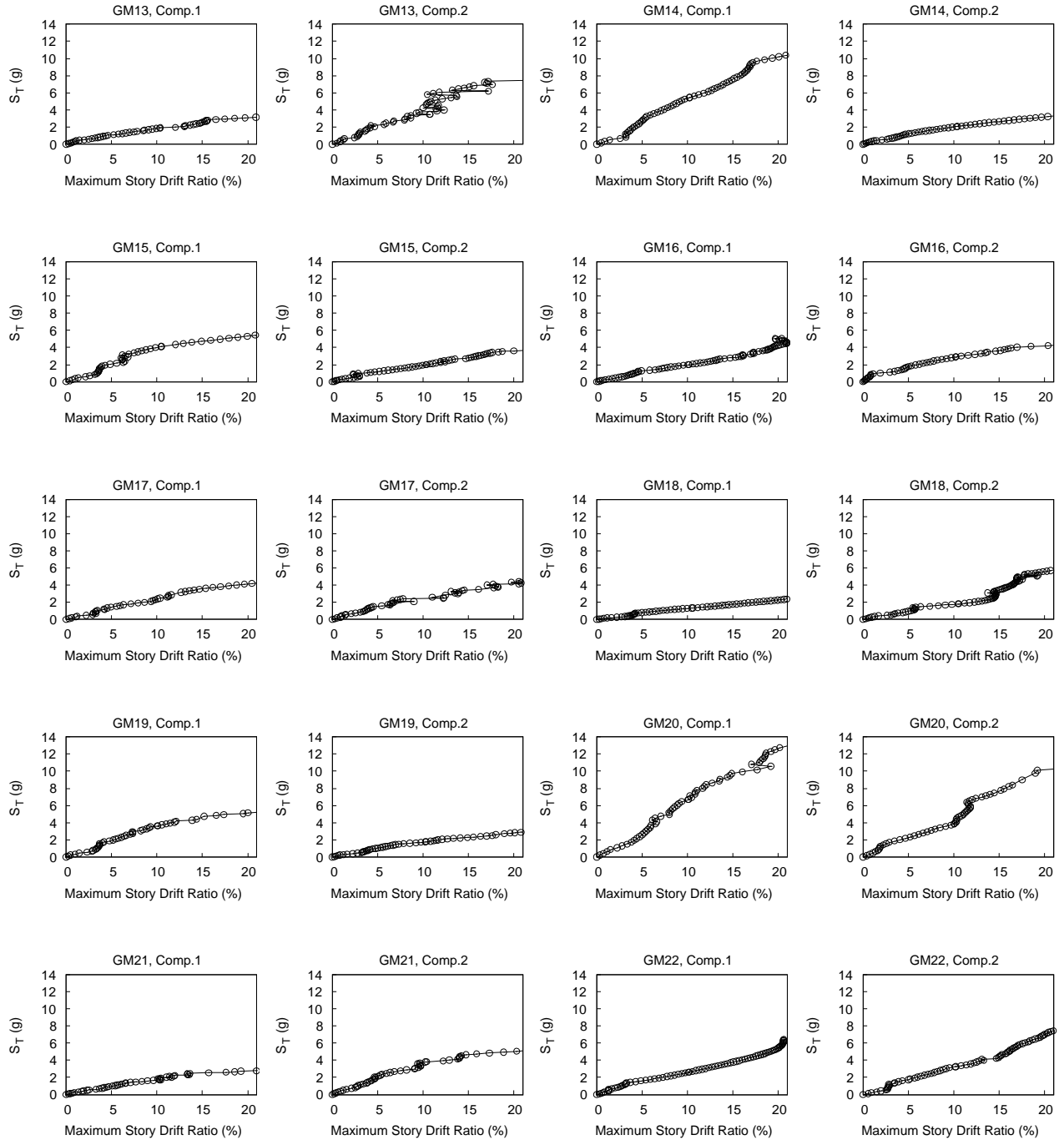
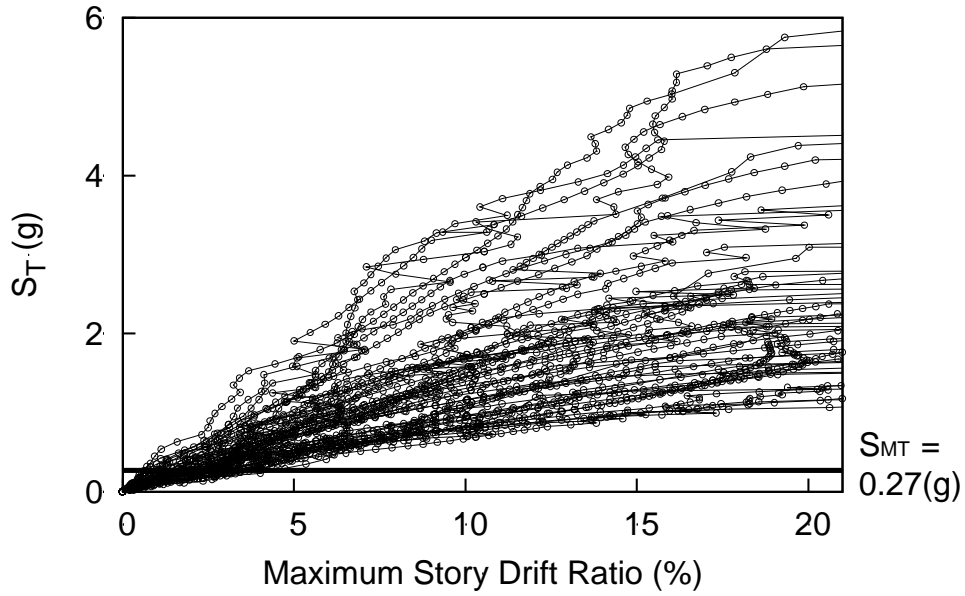
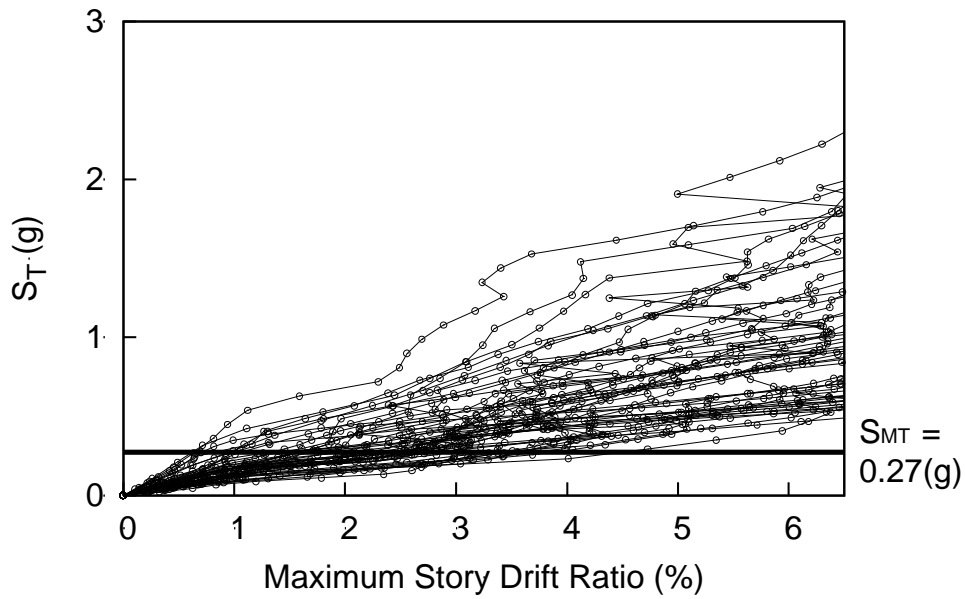


Figure C.20 Archetype 10 (cont.)



(a) Story Drift Ratio up to 20%



(b) Close-up Story Drift Ratio 6%

Figure C.21 Archetype 11

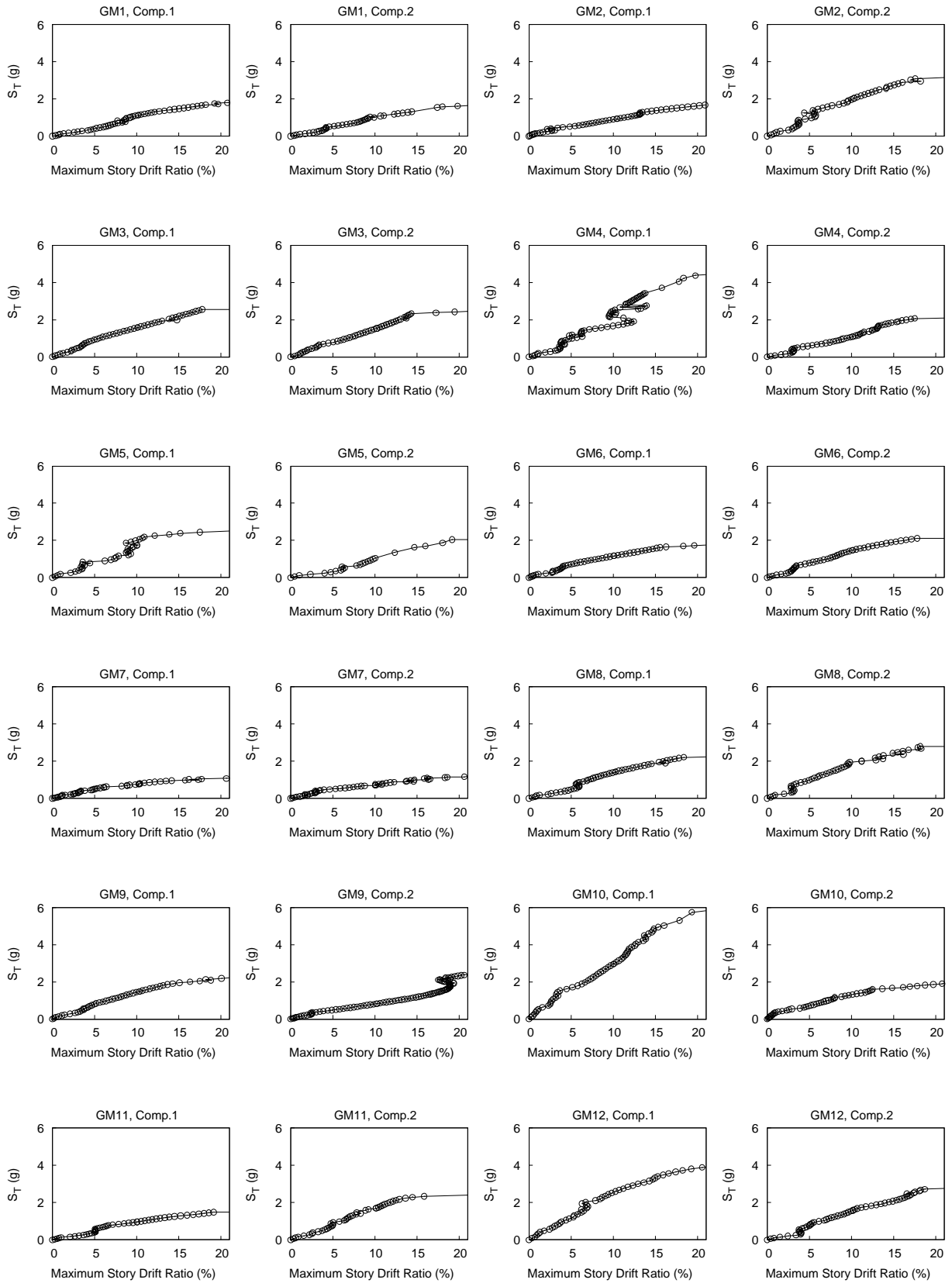


Figure C.22 Archetype 11

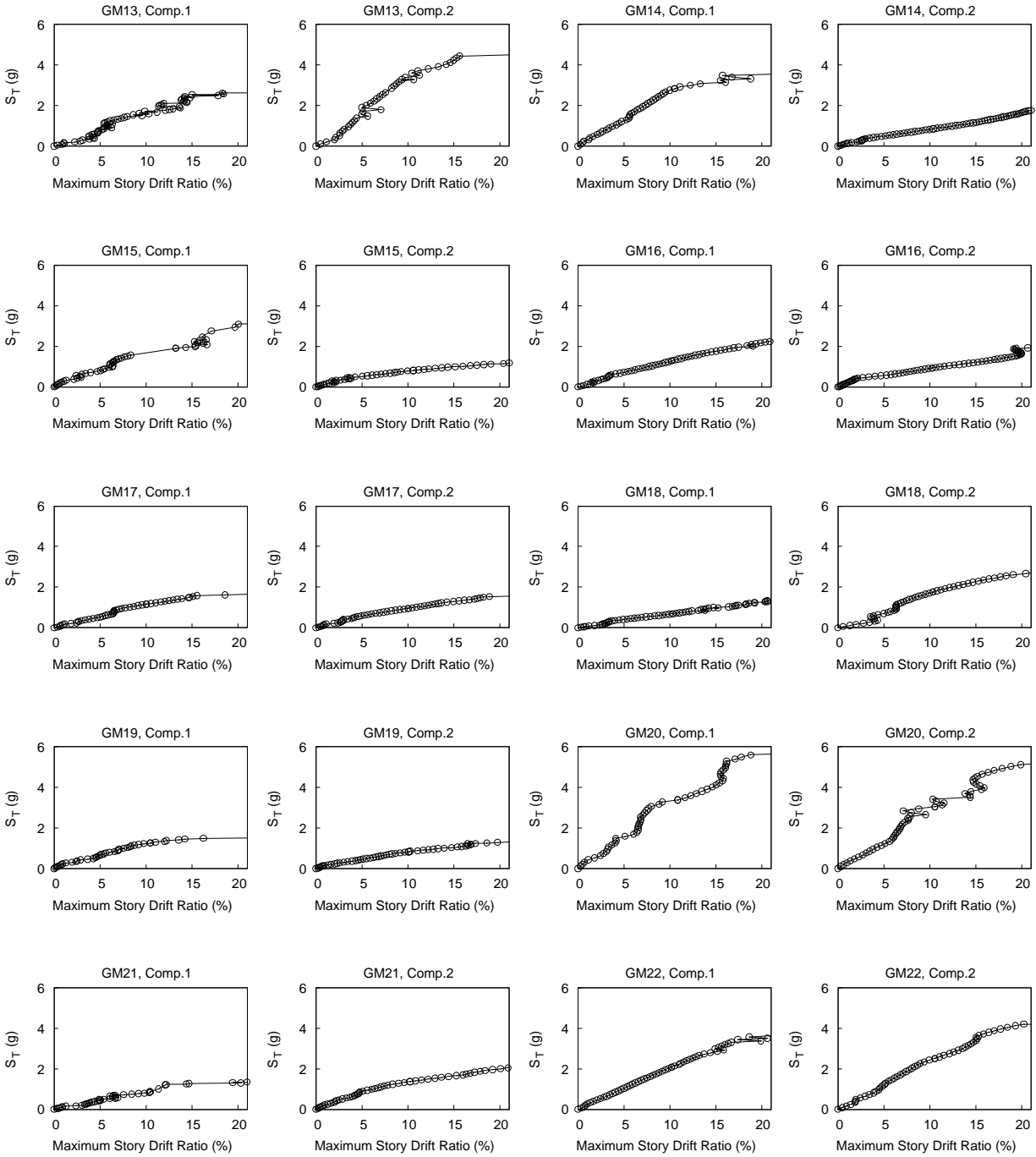
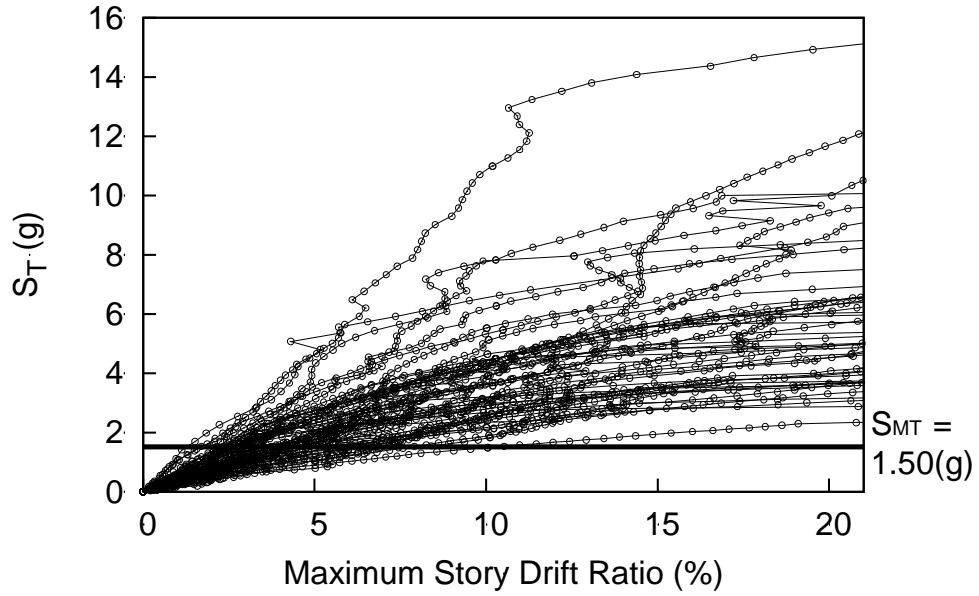
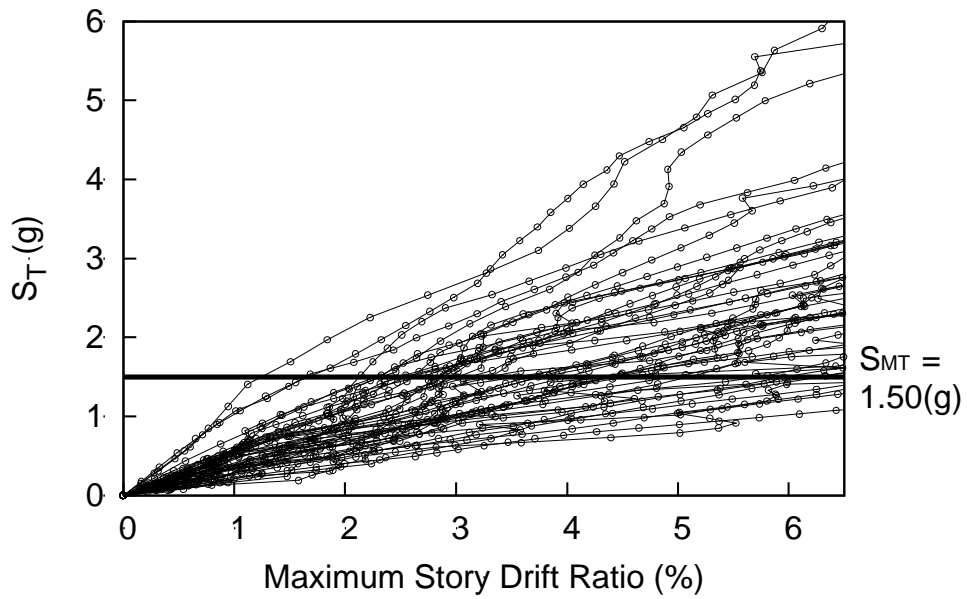


Figure C.22 Archetype 11 (cont.)



(a) Story Drift Ratio up to 20%



(b) Close-up Story Drift Ratio 6%

Figure C.23 Archetype 12

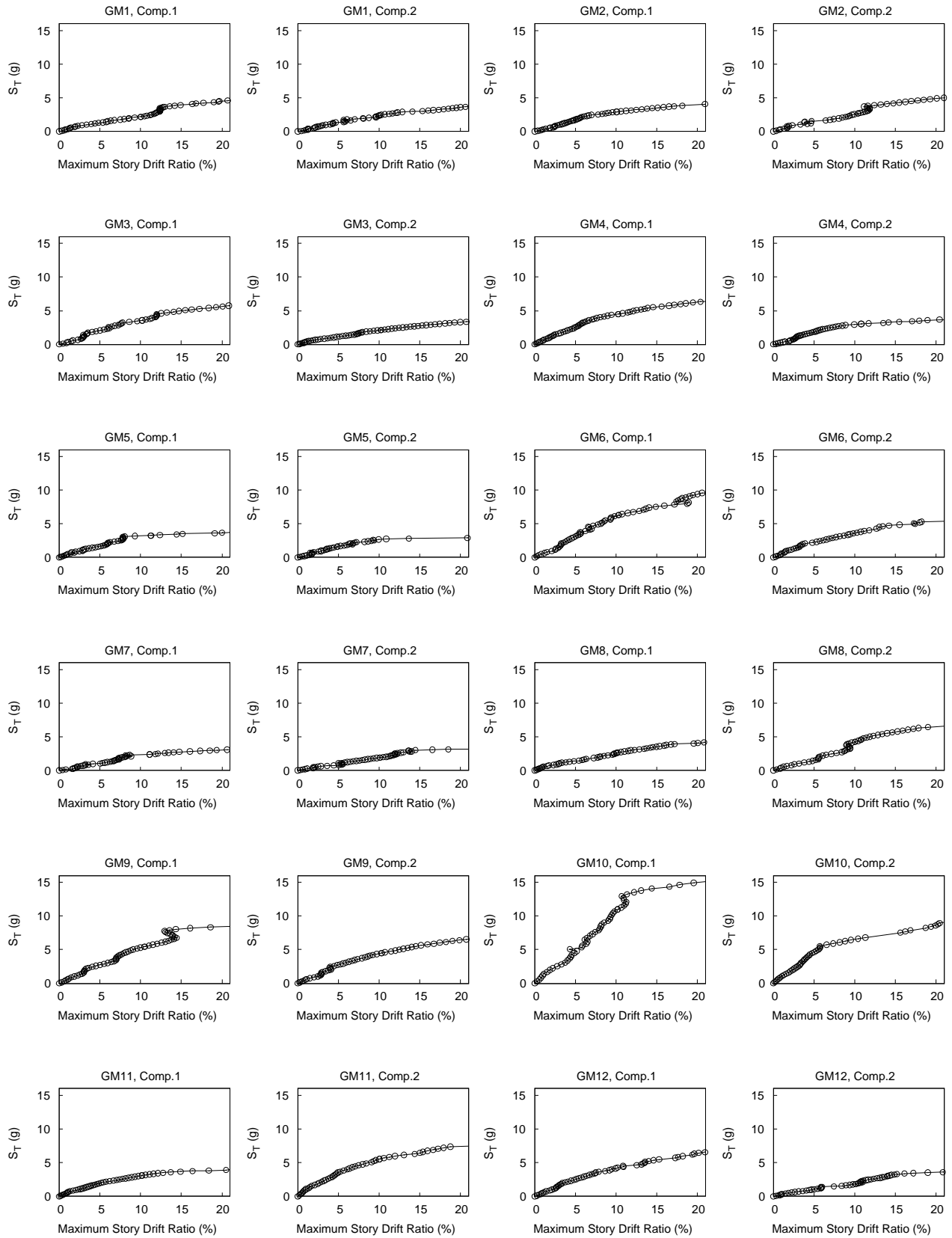


Figure C.24 Archetype 12

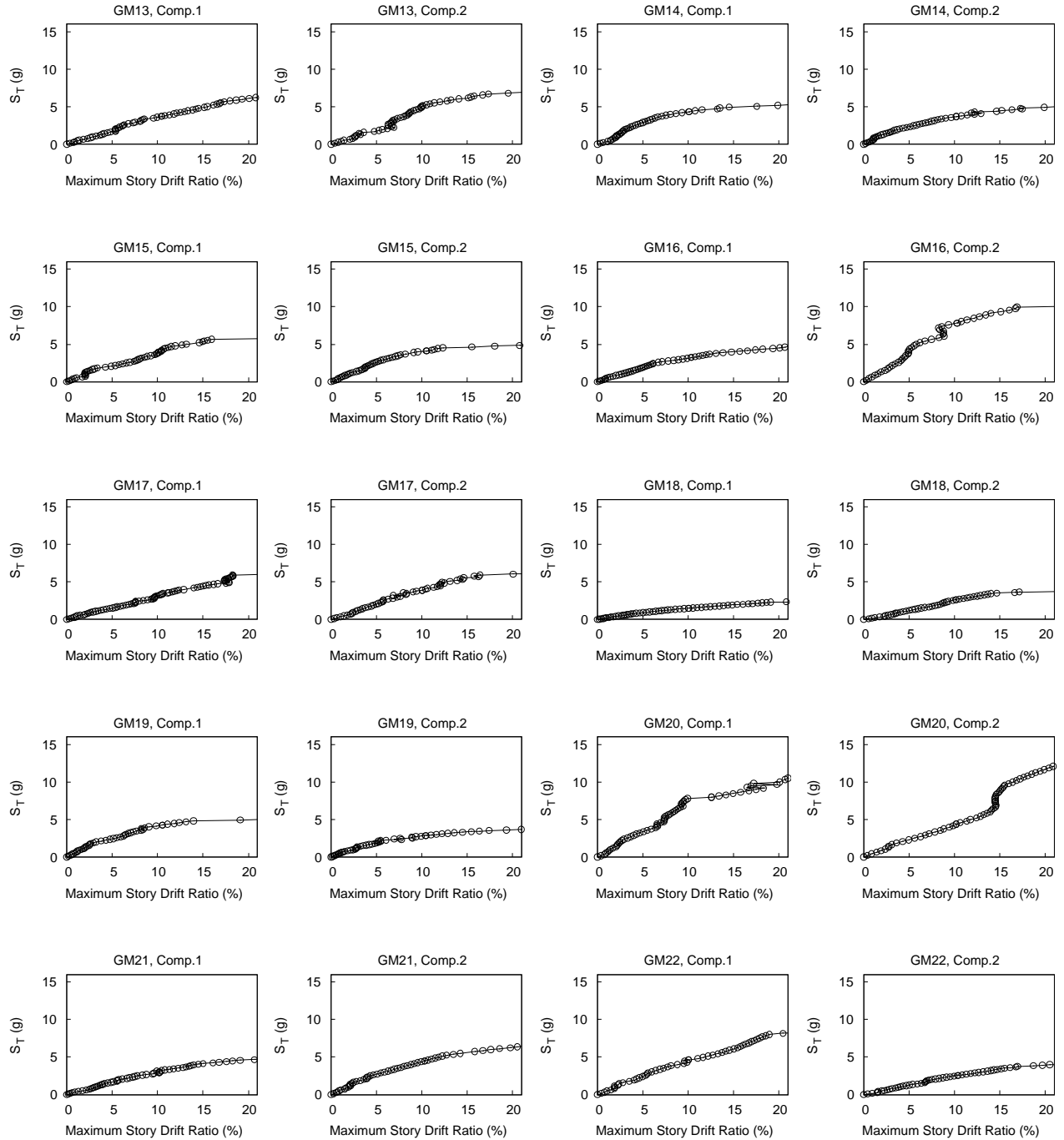
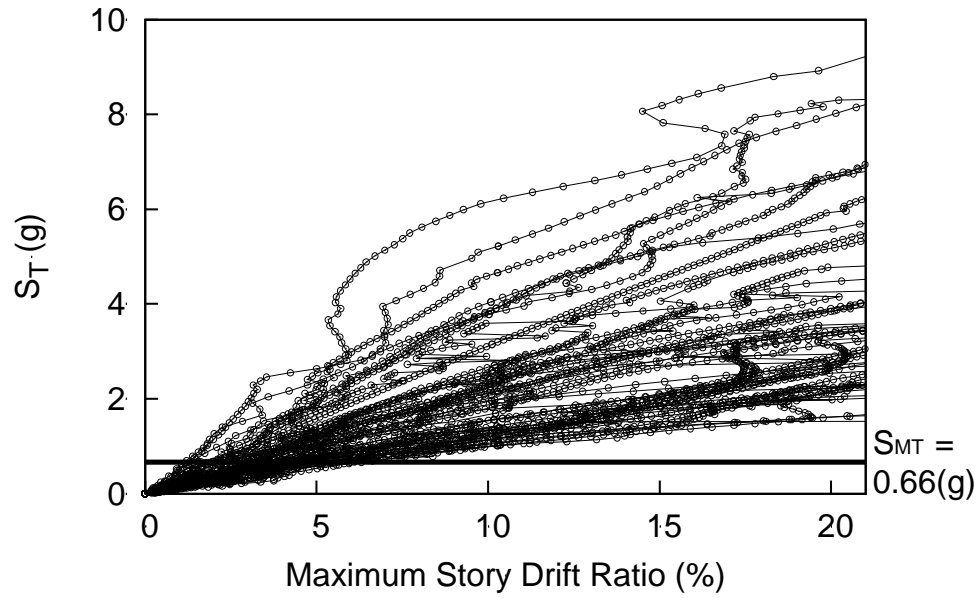
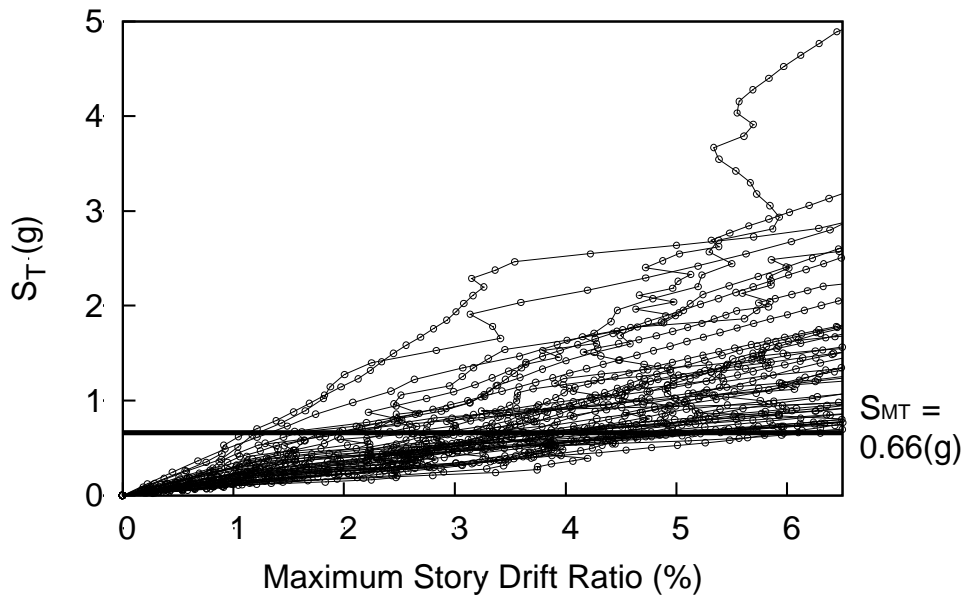


Figure C.24 Archetype 12 (cont.)



(a) Story Drift Ratio up to 20%



(b) Close-up Story Drift Ratio 6%

Figure C.25 Archetype 13

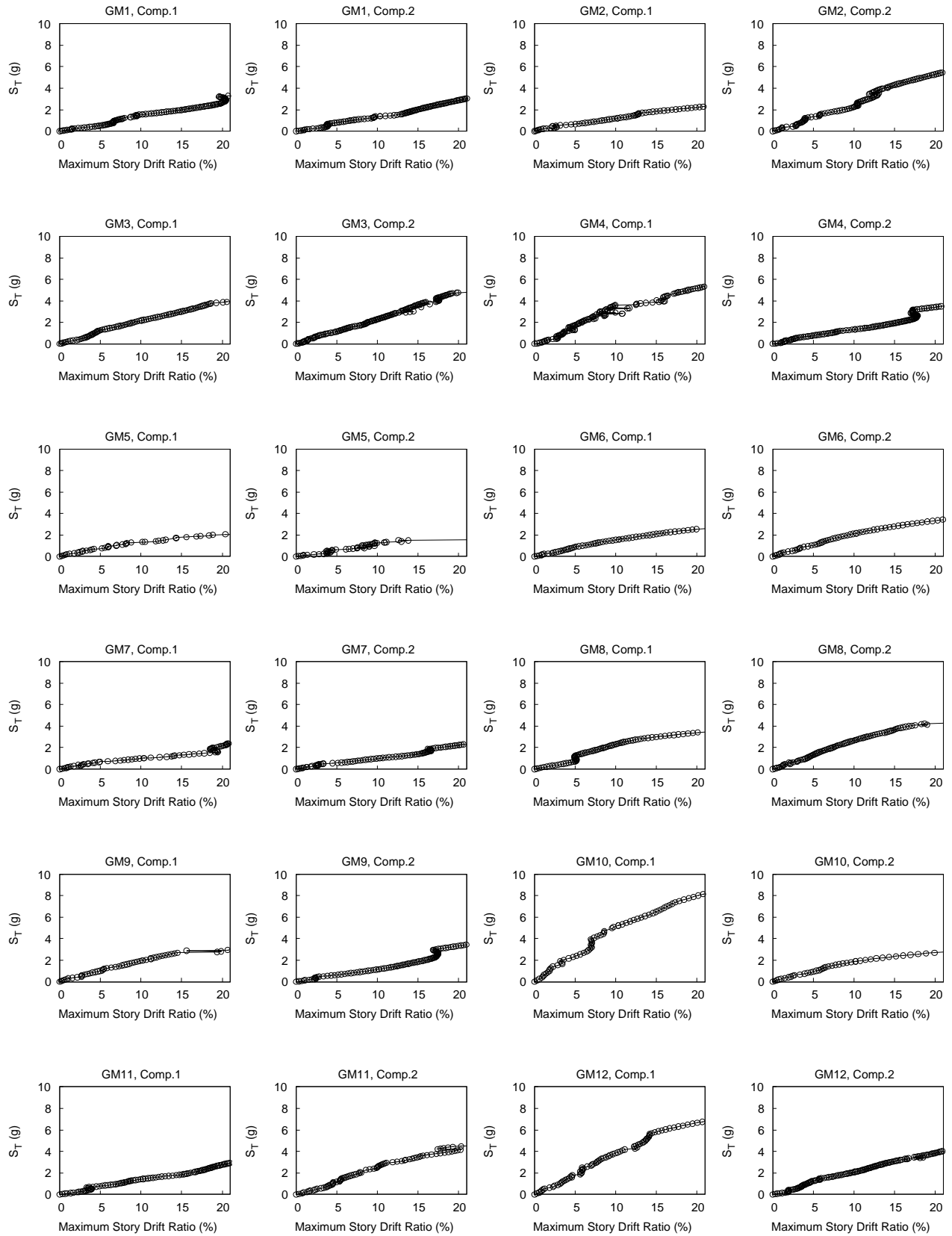


Figure C.26 Archetype 13

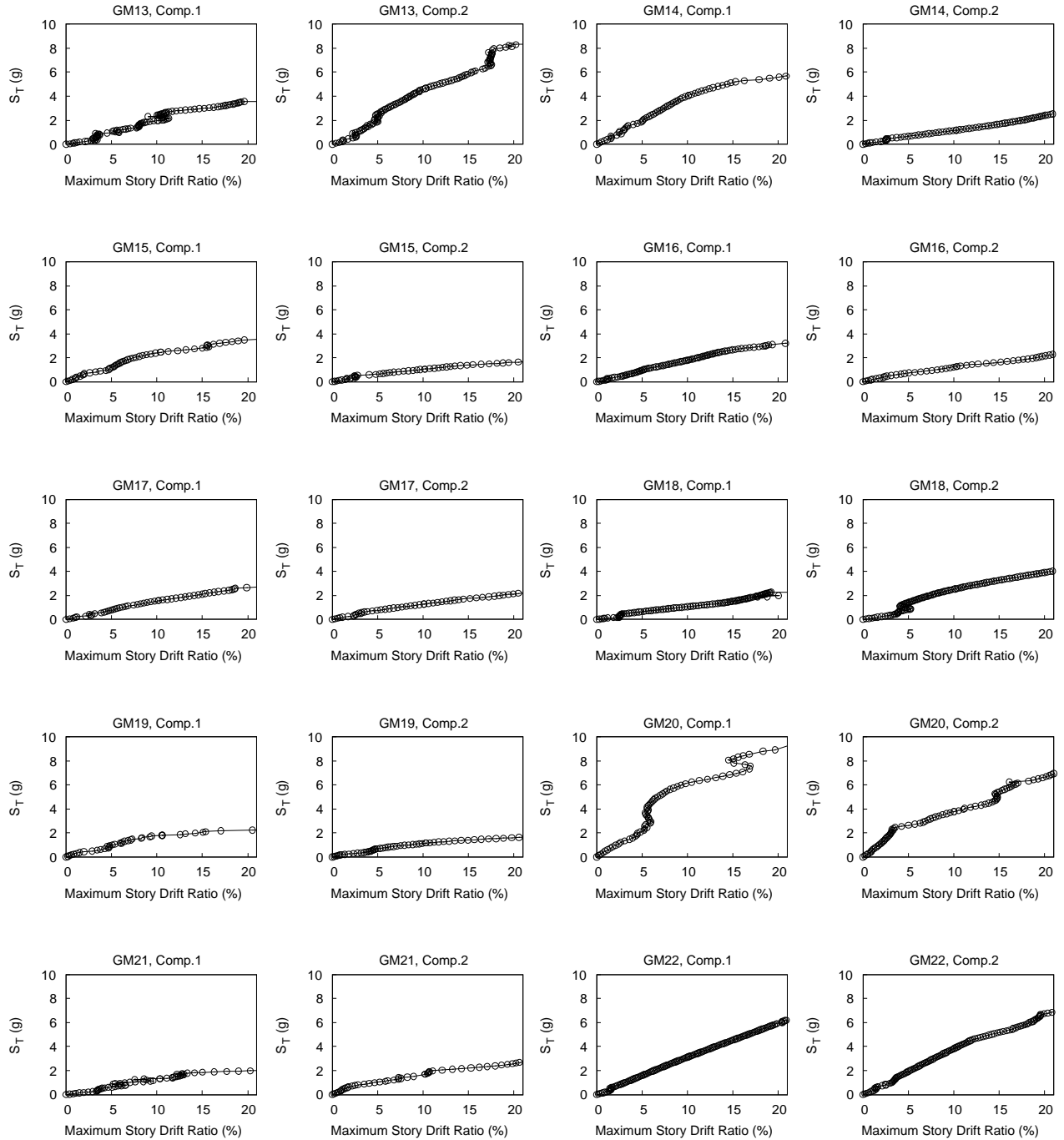
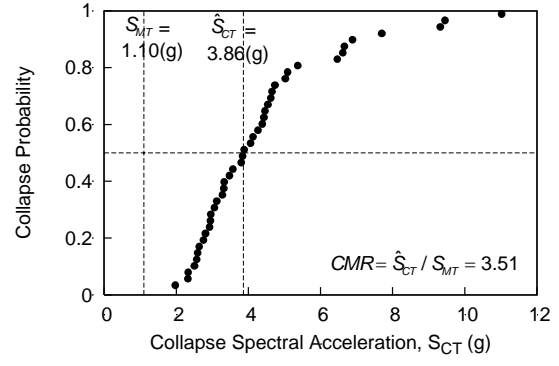
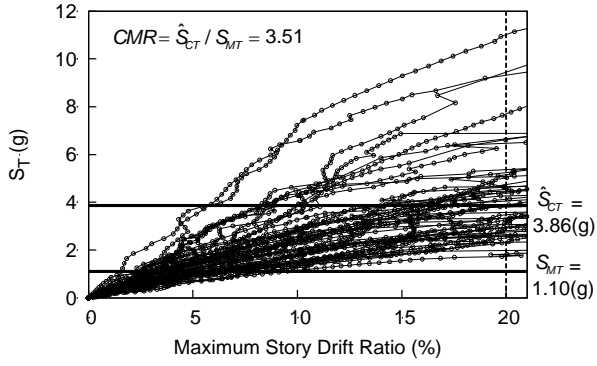
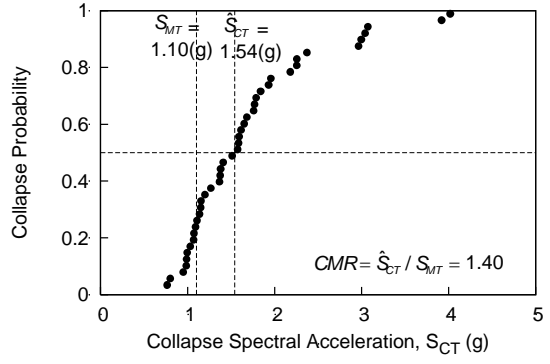
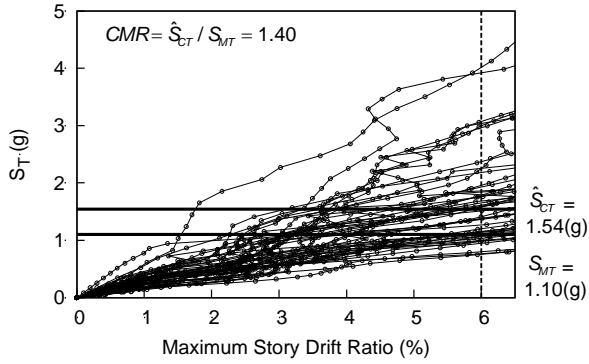


Figure C.26 Archetype 13 (cont.)

APPENDIX D: Collapse Probability

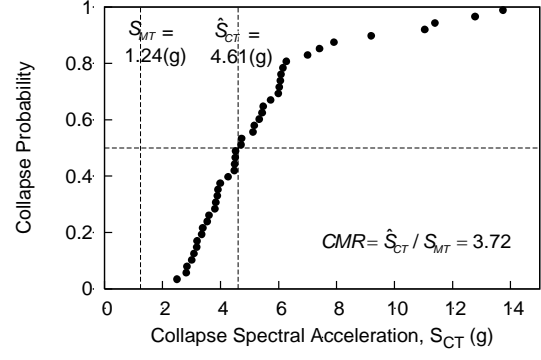
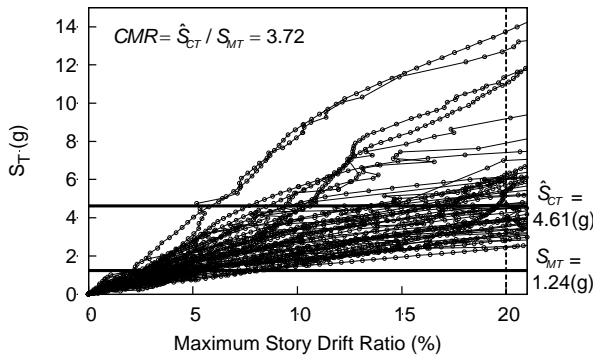


(a) Upper Bound

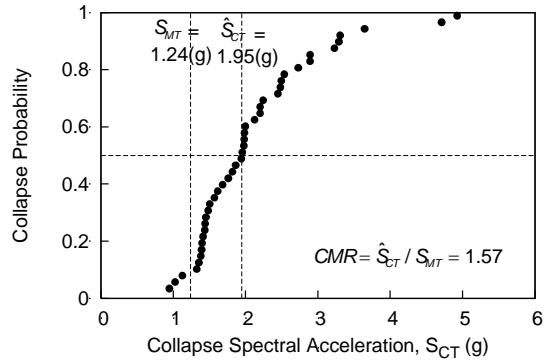
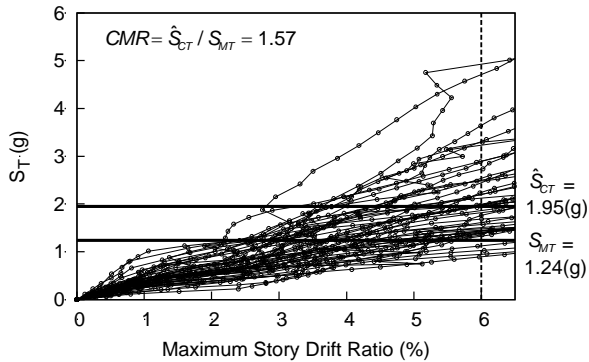


(b) Lower Bound

Figure D.1 Archetype 1

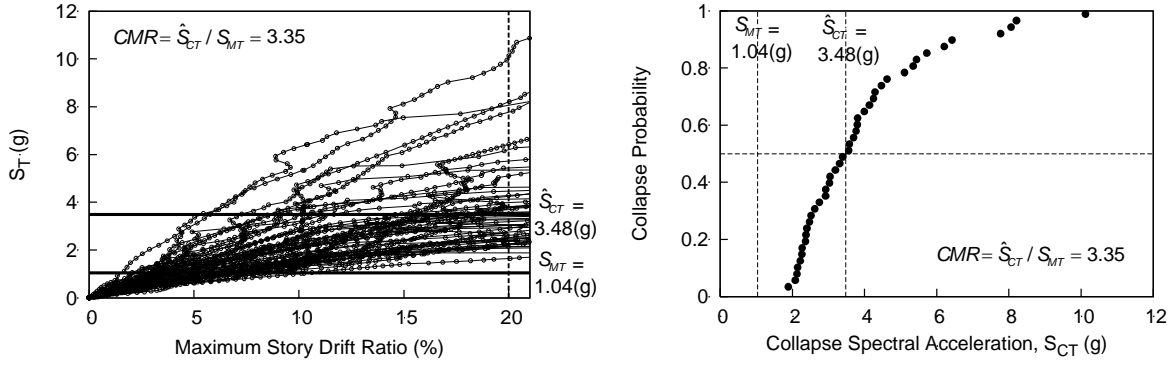


(a) Upper Bound

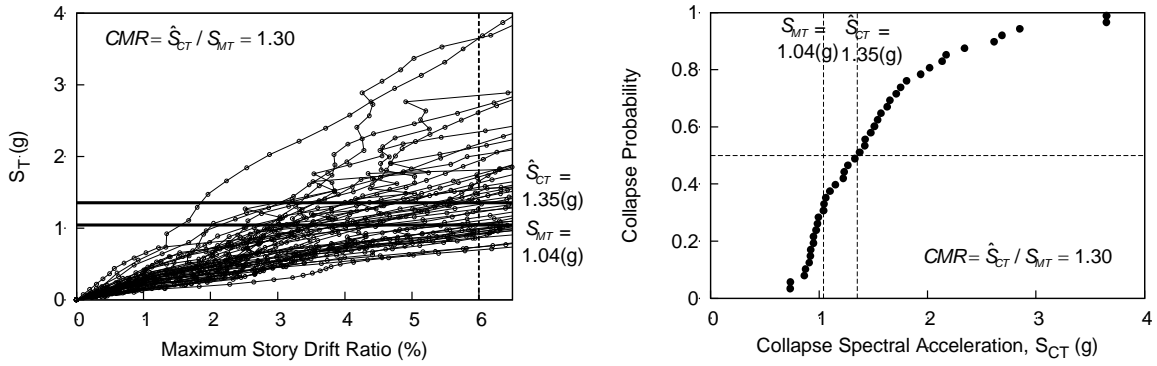


(b) Lower Bound

Figure D.2 Archetype 2

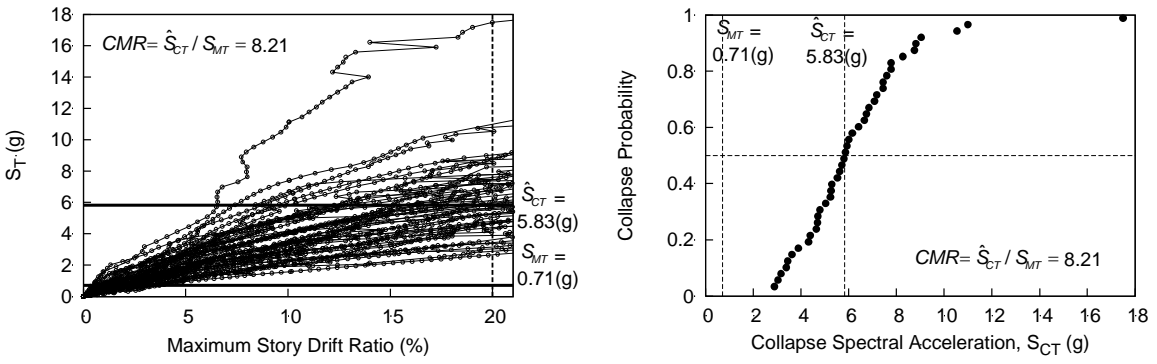


(a) Upper Bound

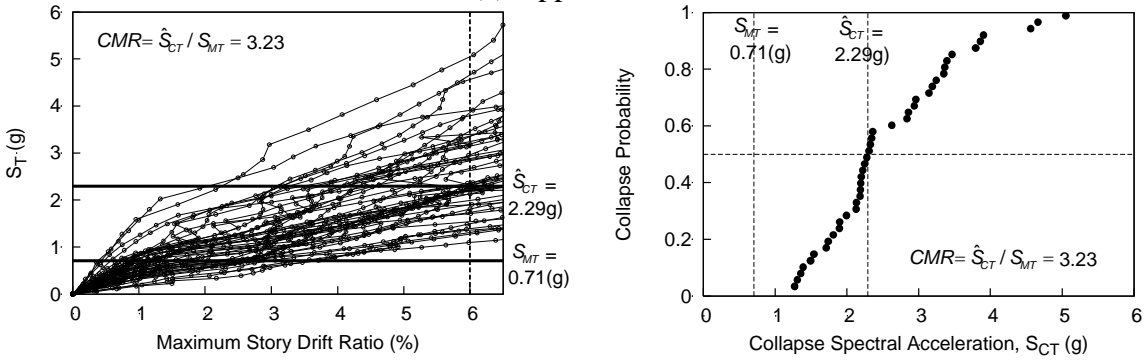


(b) Lower Bound

Figure D.3 Archetype 3

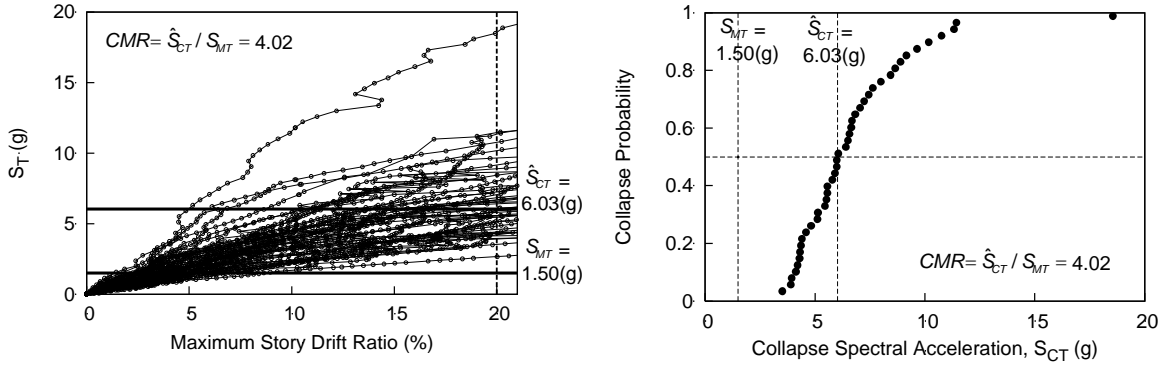


(a) Upper Bound

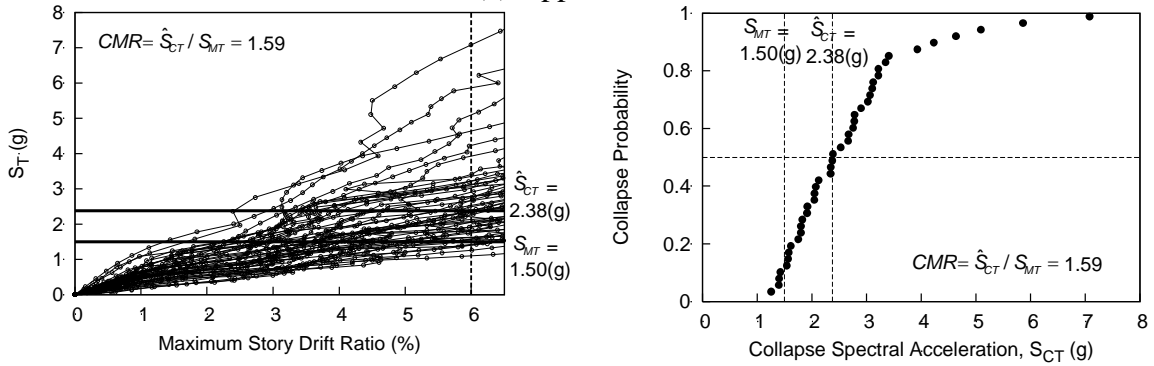


(b) Lower Bound

Figure D.4 Archetype 4

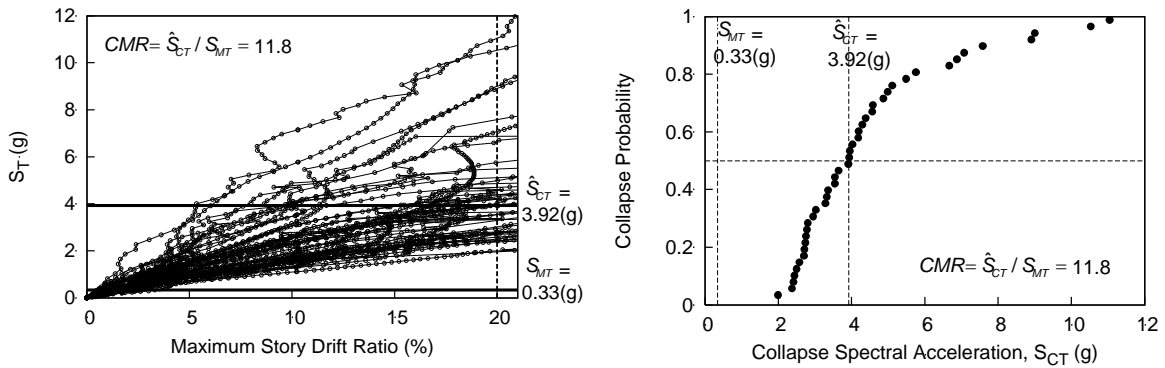


(a) Upper Bound

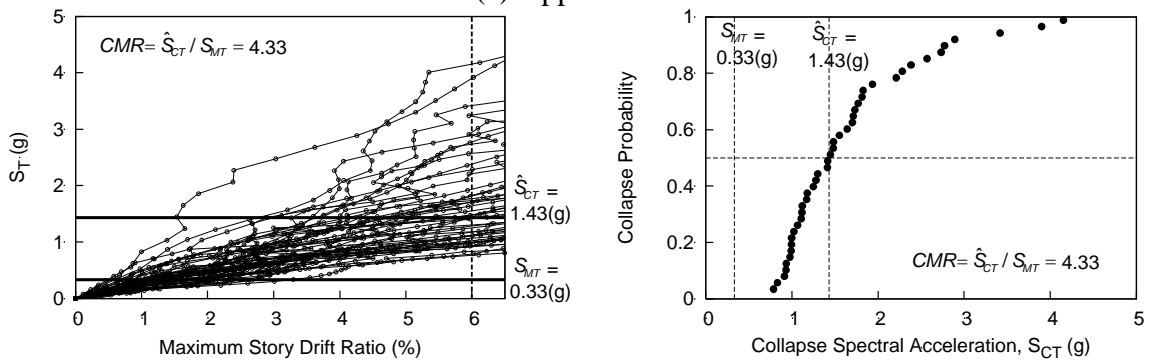


(b) Lower Bound

Figure D.5 Archetype 5

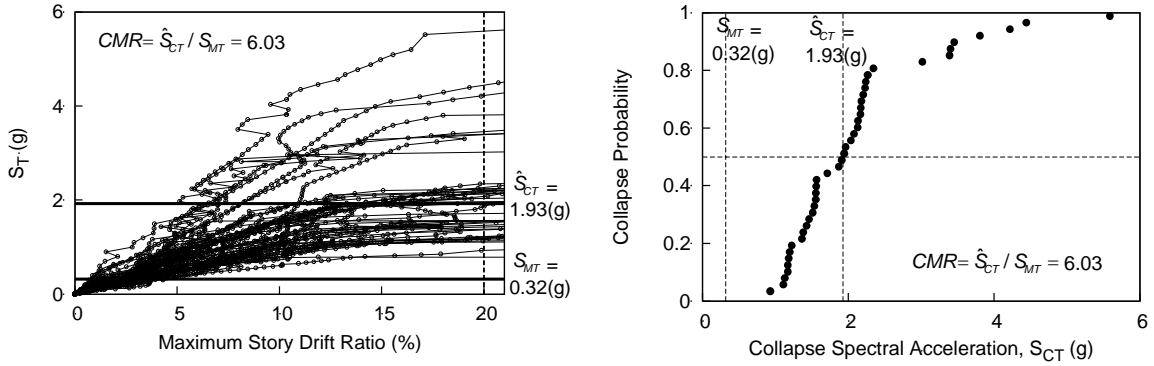


(a) Upper Bound

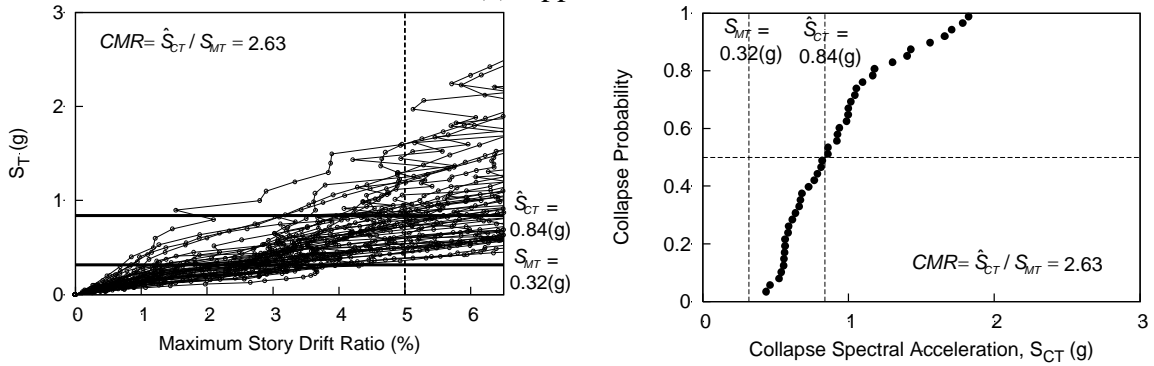


(b) Lower Bound

Figure D.6 Archetype 6

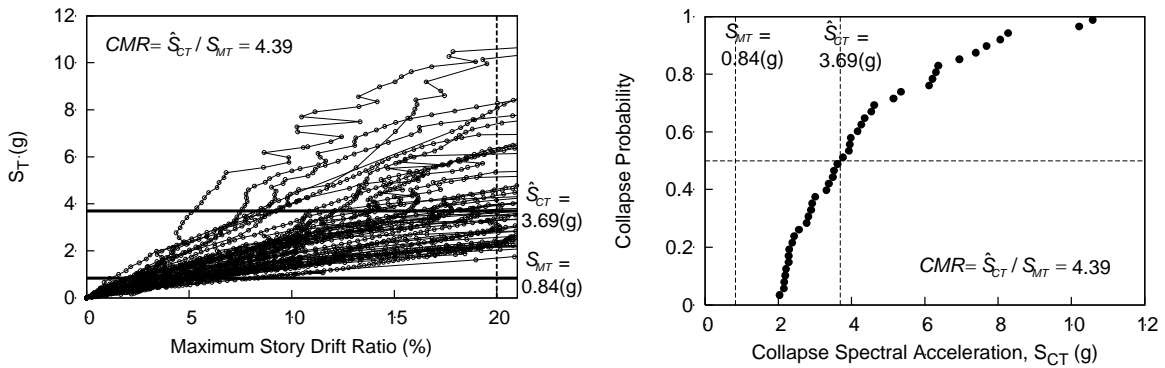


(a) Upper Bound

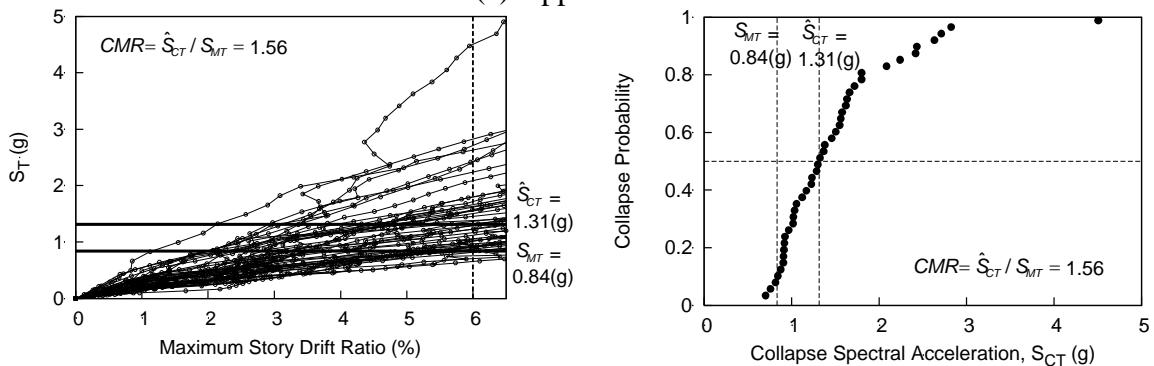


(b) Lower Bound

Figure D.7 Archetype 7

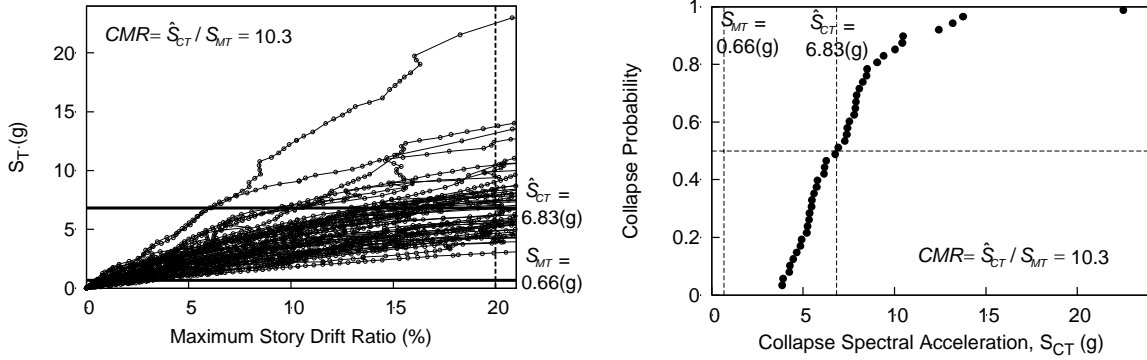


(a) Upper Bound

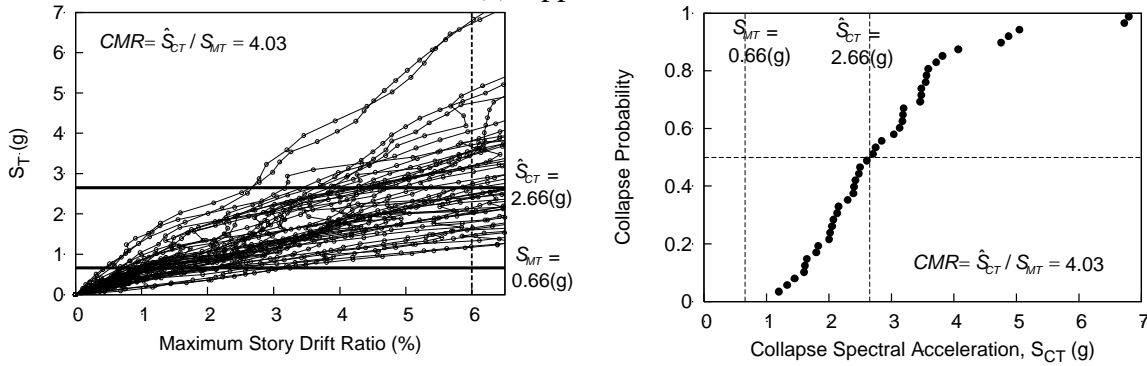


(b) Lower Bound

Figure D.8 Archetype 8

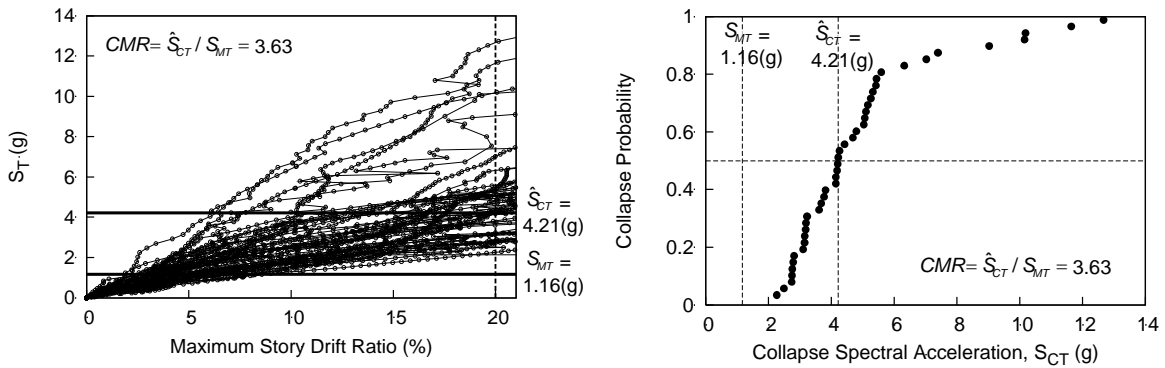


(a) Upper Bound

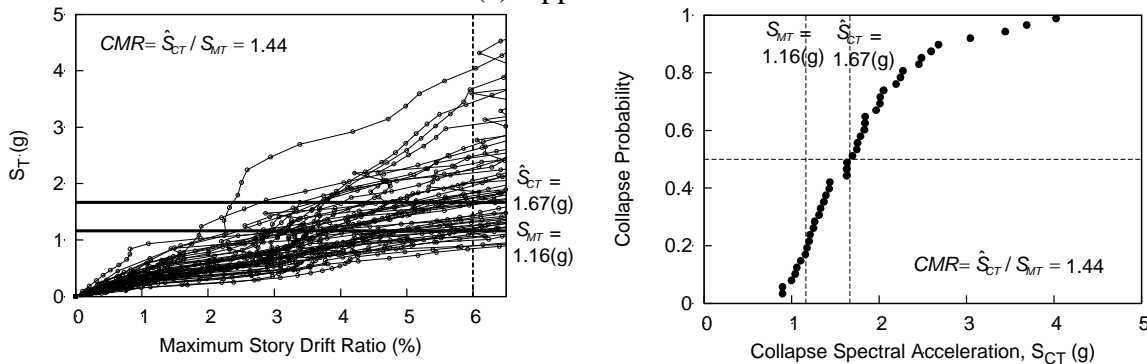


(b) Lower Bound

Figure D.9 Archetype 9

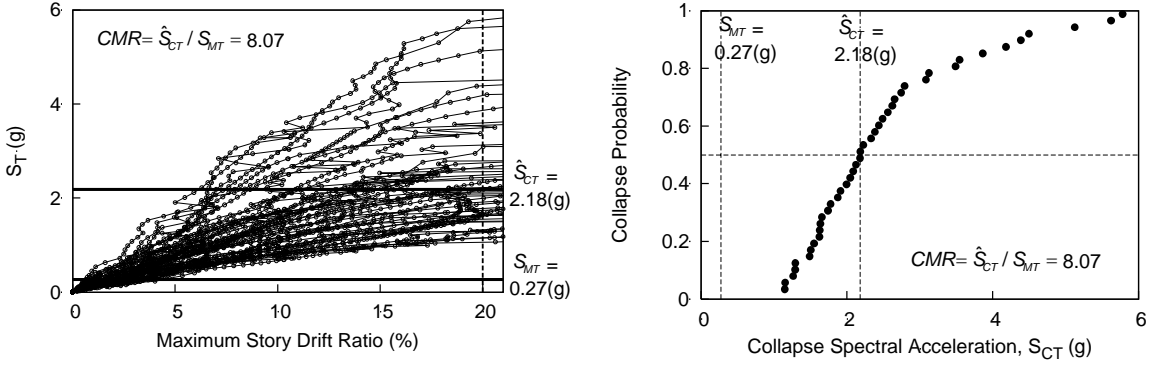


(a) Upper Bound

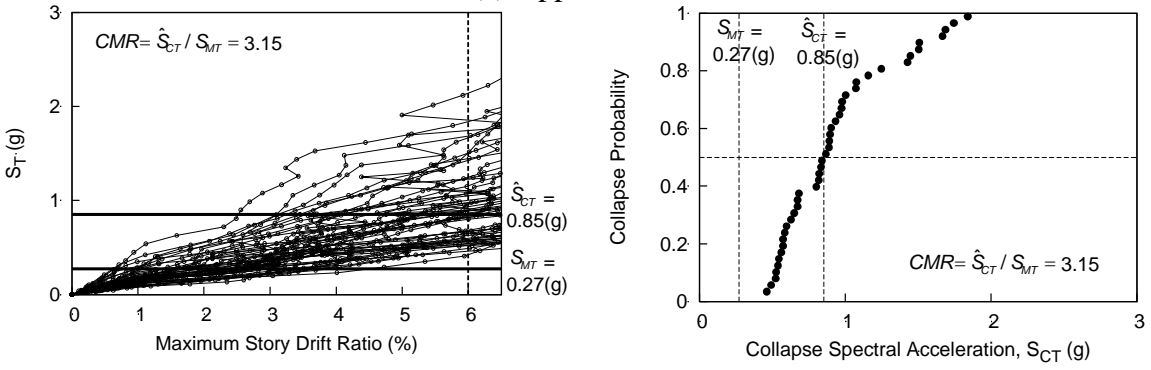


(b) Lower Bound

Figure D.10 Archetype 10

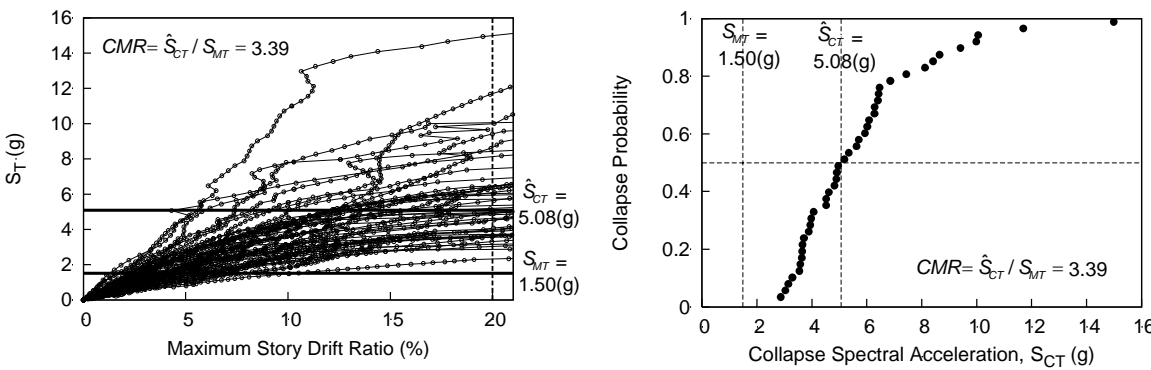


(a) Upper Bound

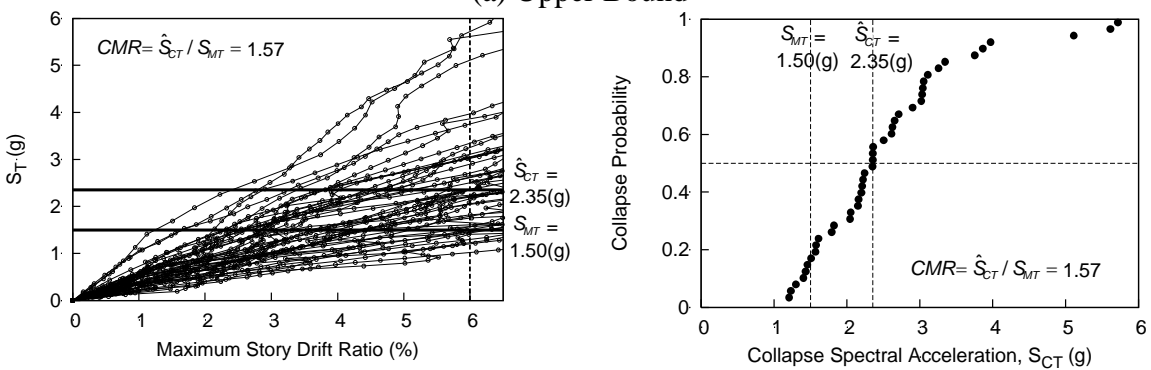


(b) Lower Bound

Figure D.11 Archetype 11

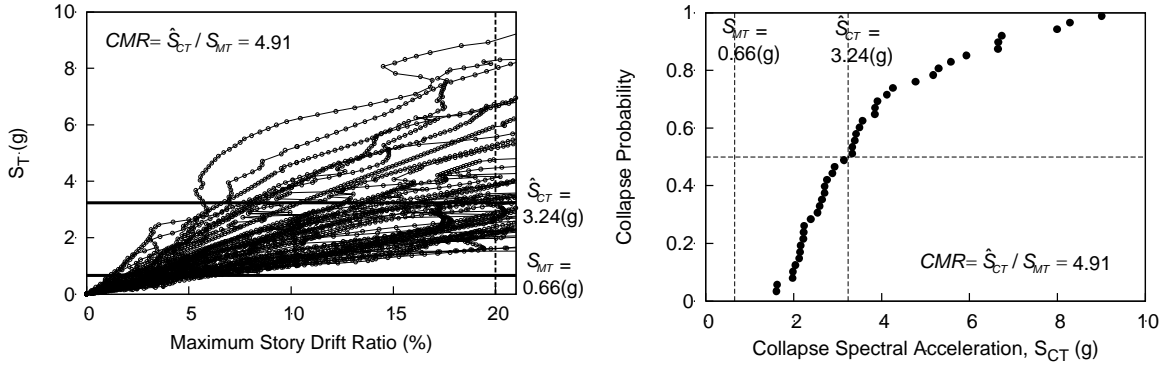


(a) Upper Bound

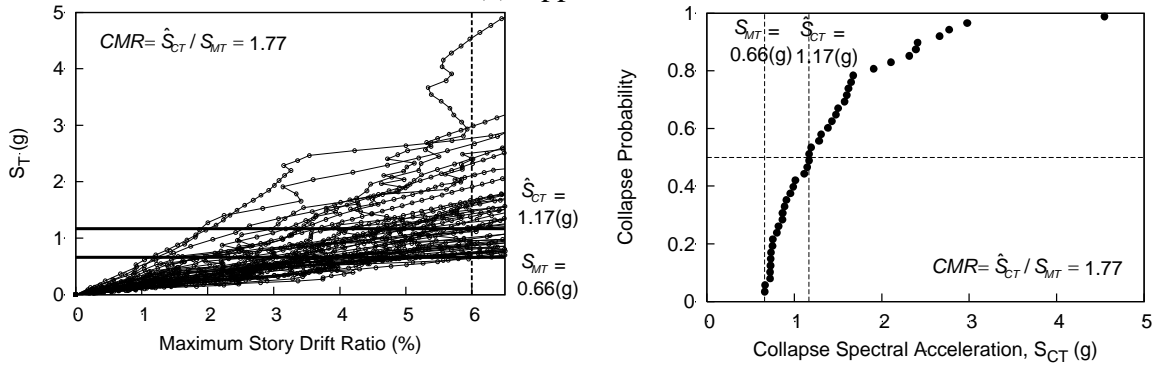


(b) Lower Bound

Figure D.12 Archetype 12



(a) Upper Bound



(b) Lower Bound

Figure D.13 Archetype 13



**American
Iron and Steel
Institute**

1140 Connecticut Avenue, NW
Suite 705
Washington, DC 20036
www.steel.org



Research Report RP-08-8